
Electronic Thesis and Dissertation Repository

7-30-2013 12:00 AM

Reproducibility of Hyperpolarized Xenon-129 Magnetic Resonance Imaging

Nikhil Kanhere
The University of Western Ontario

Supervisor
Dr. Grace Parraga
The University of Western Ontario

Graduate Program in Biomedical Engineering
A thesis submitted in partial fulfillment of the requirements for the degree in Master of Engineering Science
© Nikhil Kanhere 2013

Follow this and additional works at: <https://ir.lib.uwo.ca/etd>



Part of the [Bioimaging and Biomedical Optics Commons](#)

Recommended Citation

Kanhere, Nikhil, "Reproducibility of Hyperpolarized Xenon-129 Magnetic Resonance Imaging" (2013).
Electronic Thesis and Dissertation Repository. 1376.
<https://ir.lib.uwo.ca/etd/1376>

This Dissertation/Thesis is brought to you for free and open access by Scholarship@Western. It has been accepted for inclusion in Electronic Thesis and Dissertation Repository by an authorized administrator of Scholarship@Western. For more information, please contact wlsadmin@uwo.ca.

REPRODUCIBILITY OF HYPERPOLARIZED XENON-129 MAGNETIC RESONANCE IMAGING

(Thesis format: Monograph)

by

Nikhil Kanhere, B.E.

Graduate Program in Biomedical Engineering

A thesis submitted in partial fulfillment
of the requirements for the degree of
Master of Engineering Science

The School of Graduate and Postdoctoral Studies
The University of Western Ontario
London, Ontario, Canada

© Nikhil Kanhere 2013

Abstract

Spirometry and plethysmography provide gold standard measurements of obstructive lung disease, although these are global measurements of lung function made at the mouth, of a highly regionally heterogeneous disease. Hyperpolarized ^{129}Xe magnetic resonance imaging (MRI) is a non-invasive, non-radiation-based imaging tool for visualizing regional lung structure and function. However, the reproducibility of ^{129}Xe MRI measurements has not yet been studied or determined. Hence, in this thesis, we evaluated the reproducibility of ^{129}Xe MRI using quantitative measurements such as ventilation defect percent (VDP). We showed that ^{129}Xe VDP had high intra-observer and inter-observer reproducibility for repeated scans acquired on the same-day and after 1-week and its reproducibility was comparable to that of ^3He VDP. ^{129}Xe VDP showed strong and significant correlations with pulmonary function tests. These results suggested that ^{129}Xe VDP is reproducible over short periods of time and can be a reliable measurement to study pulmonary function in imaging studies.

Keywords: Hyperpolarized, ^{129}Xe , ^3He , magnetic resonance imaging, chronic obstructive pulmonary disease, reproducibility, functional lung imaging, ventilation defects

Co-Authorship Statement

The following thesis contains one manuscript submitted for peer-review to the scientific journal “Academic Radiology” entitled “Reproducibility of Hyperpolarized Xenon-129 Magnetic Resonance Imaging in Healthy Subjects and Chronic Obstructive Pulmonary Disease”. The manuscript was co-authored by Nikhil Kanhere, Khadija Sheikh, Yajur Shukla, Miranda Kirby, David G. McCormack and Grace Parraga.

As the principal author and M.E.Sc candidate, Nikhil Kanhere assisted with the study subject visits including the acquisition of MRI and pulmonary function tests and the polarization of the gas, performed all the data and statistical analysis, led interpretation of results, drafted the manuscript and revised the manuscript for publication in response to reviews. Khadija Sheikh performed data analysis. Dr. Yajur Shukla, Dr. Miranda Kirby and Dr. David G. McCormack provided technical and clinical expertise. Dr. Grace Parraga, as the principal investigator led the study design, helped to determine project objectives, provided mentorship, assisted with interpretation of results, provided editorial assistance and overall guidance.

Pulmonary function data acquisition was performed under the supervision of Sandra Blamires, CCRC. Hyperpolarization of ^{129}Xe and ^3He was performed by Andrew Wheatley, BSc. MRI acquisition was performed by Trevor Szekeres, MRT(MR)(R).

Acknowledgments

First a massive thank you to my supervisor Dr. Grace Parraga, for giving me the opportunity to be part of this magnificent research group. Her guidance and support over the last two years has been invaluable to me. Grace is extremely passionate about her research and inspires her students to be the same way as well. She has created a great work environment in the lab focused on teamwork and productivity. I really appreciate the work ethic that she has instilled in me. I would like to thank her for the numerous opportunities that she has given me to improve myself by making me push myself beyond what I thought was possible. I have learnt a lot from her during my time here in the lab.

I would also like to thank the other members of my advisory committee - Dr. Aaron Fenster, Dr. Nigel Paterson and Dr. Hanif Ladak for their guidance throughout my Masters program. I really appreciated the constructive criticism they provided which gave new directions and ideas for my project. They always challenged me with difficult questions, encouraged me to develop and improve my skills and always showed interest and enthusiasm for my research.

I would like to thank the staff of the Parraga lab: Andrew Wheatley, Sandra Blamires, Trevor Szekeres, Daniel Buchanan and Shayna McKay. To Andrew- I really enjoyed sitting next to you when I moved upstairs. Thank you for being patient with my incessant questions. Thank you for being a wonderful instructor for my polarizer training. To Sandra- thank you for keeping all the patient records so organized and all your help regarding patient data. I really enjoyed our little chats during the oPEP study visits and spending time with you in San Francisco. To Trevor- thank you very much for all the wonderful images and all the assistance with imaging related questions. I always enjoyed your poems the most at the lab outings. To Shayna- thank you for taking care of all the administrative stuff when I started. Although we only had a very brief overlap in the lab, I really enjoyed the time we spent together in the lab.

To all the graduate students: thank you very much for being so wonderful and making these two years really memorable. I will really miss you all and hope we can keep in

touch. I really cherish the friendships that I have made here and would like to wish you all the very best. To Miranda, thank you very much for everything. Thank you very much for being an awesome mentor and all the help over the last two years. I have learnt a lot from you. I really enjoyed the time I spent with you and Sarah in Melbourne and San Francisco. To Sarah- thank you for getting me an awesome place to live when I came here. We struggled through all our classes together and kept each other company on the weekends. Thank you for all your help during my time here. To Dan- thank you very much for making me feel so welcome in the lab. I will really cherish the time we spent together: both in the lab and outside it. To Amir- you taught me to keep smiling no matter what the situation. Thank you very much for all your help with physics related questions. To Steve- thank you for all the epic chats we had about science and life. Thank you for always having answers for all my questions, no matter how stupid they might have been. To Damien- thank you for being an awesome lab-mate and an even better room-mate. I will always remember the laughs we had and the not so happy times we shared. To Khadija- thank you for all the physics chats and more importantly thanks for all the awesome food from back home. To Tamas- thank you for always keeping me company in the dark room. I enjoyed all the stories and laughs we shared in there. To Brian- I got to learn a lot about life from you while you were here. Thank you for that. Finally, I would like to thank all the students on the second floor- Yonathan, Ozkan, Patrick, Kundan, Justin and Krzysztof- for making me feel so comfortable when I moved there.

Finally, I am thankful for the financial support I received during my graduate studies, particularly the Western Graduate Research Scholarship and the Queen Elizabeth II Graduate Scholarship in Science and Technology.

Table of Contents

Abstract	ii
Co-Authorship Statement.....	iii
Acknowledgments.....	iv
Table of Contents	vi
List of Tables	ix
List of Figures	x
List of Appendices	xii
List of Abbreviations	xiii
CHAPTER 1: INTRODUCTION	1
1.1 Burden of Pulmonary Disease	1
1.2 Lung Structure and Function	5
1.2.1 The Conducting Zone	7
1.2.2 Respiratory Zone.....	8
1.3 Obstructive Lung Disease.....	9
1.3.1 Chronic Obstructive Pulmonary Disease	9
1.3.2 Asthma	15
1.4 Established Methods for diagnosis of Obstructive Lung Disease	16
1.4.1 Spirometry.....	16
1.4.2 Plethysmography.....	18
1.4.3 Six minute Walk Test.....	21
1.4.4 St. George's Respiratory Questionnaire	22
1.5 Pulmonary Imaging.....	22
1.5.1 Chest X-Ray.....	22
1.5.2 X-ray Computed Tomography	24

1.5.3 Nuclear Medicine.....	27
1.5.4 Magnetic Resonance Imaging.....	29
1.6 Thesis Hypotheses and Objectives.....	41
1.7 Reference List.....	Error! Bookmark not defined. 42
CHAPTER 2: MATERIALS AND METHODS	53
2.1 Study Subjects.....	53
2.2 Pulmonary Function Tests	54
2.3 Image Acquisition.....	54
2.4 Image Analysis.....	58
2.5 Statistical Methods.....	61
2.6 Reference List	63
CHAPTER 3: RESULTS	64
3.1 Subject Demographics	64
3.2 ^{129}Xe MRI Baseline Measurements	65
3.3 Comparison of reproducibility of ^{129}Xe MRI VDP and ^3He MRI VDP.....	69
3.4 ^{129}Xe MRI Intra-Observer Reproducibility.....	71
3.5 ^{129}Xe MRI Inter-Observer Reproducibility.....	75
3.6 ^{129}Xe MRI VDP relationship to pulmonary function measurements.....	76
3.7 Reference List	78
CHAPTER 4: DISCUSSION AND FUTURE WORK	79
4.1 ^{129}Xe MRI Baseline Measurements	79
4.2 Comparison of reproducibility of ^{129}Xe MRI VDP and ^3He MRI VDP.....	80
4.3 ^{129}Xe MRI Intra-Observer Reproducibility.....	82
4.4 ^{129}Xe MRI Inter-Observer Reproducibility.....	84
4.5 ^{129}Xe MRI VDP relationship to Pulmonary Function Measurements	85

4.6 Study Limitations.....	86
4.7 Future Work.....	86
4.8 Conclusion	87
4.9 Reference List.....	88

List of Tables

Table 1.1 Leading causes of death worldwide 2004 and predicted values in 2030.....	2
Table 1.2 Classification of COPD according to severity of airflow obstruction.....	17
Table 3.1 Subject Demographics	65
Table 3.2 Mean values for VDP for a single observer for healthy volunteers and COPD subjects for ^{129}Xe and ^3He over 5 rounds of analysis of baseline NDW images	67
Table 3.3 Repeated measures ANOVA for ^{129}Xe VDP and ^3He VDP for same day rescan	70
Table 3.4 ICC and COV analysis for ^{129}Xe MRI VDP and ^3He MRI VDP for same day rescan	70
Table 3.5 Repeated measures ANOVA for intra-observer reproducibility: ^{129}Xe VDP same day rescan and 1-week rescan.....	73
Table 3.6 ICC and COV Analysis for intra-observer reproducibility: ^{129}Xe VDP same day rescan and 1-week rescan.....	74
Table 3.7 Repeated Measures ANOVA for inter-observer reproducibility: ^{129}Xe VDP same day rescan and 1-week rescan.....	75
Table 3.8 ICC and COV for inter-observer reproducibility: ^{129}Xe VDP same day rescan and 1-week rescan.....	75

List of Figures

Figure 1.1 Proportion of all deaths for men (A) and women (B) in Canada in 2005	3
Figure 1.2 Total economic burden of respiratory diseases in Canada in 2000	4
Figure 1.3 Schematic of the human airway tree by generation (Image is not to scale)	6
Figure 1.4 Schematic of the human airways and alveoli in healthy volunteers and subjects with COPD.....	13
Figure 1.5 Small Airways Disease and Emphysema in COPD	14
Figure 1.6 Spirometry and Plethysmography	19
Figure 1.7 Sample airflow curves obtained through a plethysmograph	20
Figure 1.8 Chest X-Ray of a 63 year old male COPD Stage III subject.....	23
Figure 1.9 X-ray computed tomography (CT).....	26
Figure 1.10 Conventional proton MRI of the lung	31
Figure 1.11 Hyperpolarized ^3He MRI images	34
Figure 1.12 Hyperpolarized ^{129}Xe MRI images.....	39
Figure 1.13 Hyperpolarized ^{129}Xe ADC maps.....	40
Figure 2.1 FGRE pulse sequences	56
Figure 2.2 Image acquisition procedure.....	57
Figure 2.3 Sequence of scans acquired.....	58
Figure 2.4 Schematic showing the semi-automated segmentation and registration process for ^{129}Xe static ventilation and ^1H images.	61

Figure 3.1 Non Diffusion Weighted (NDW) and static ventilation (SV) center slice images for ^{129}Xe and ^3He MRI for healthy volunteers and COPD subjects	66
Figure 3.2 ^{129}Xe NDW VDP for Healthy Volunteers and COPD subjects.....	67
Figure 3.3 Relationship between pulse sequences for VDP	68
Figure 3.4 Relationship between ^{129}Xe VDP and SNR	69
Figure 3.5 ^{129}Xe NDW images over three time points for three COPD subjects	72
Figure 3.6 Relationship between repeated scans for VDP.....	74
Figure 3.7 Inter-observer correlations for ^{129}Xe VDP	76
Figure 3.8 ^{129}Xe baseline NDW VDP correlations with pulmonary function tests	77

List of Appendices

Appendix A: Health Science Research Ethics Board Approval Notices	90
Appendix B: Copyrighted Material and Permissions	92
Appendix C: Curriculum Vitae	93

List of Abbreviations

2D	Two-Dimensional
3D	Three-Dimensional
6MWT	Six Minute Walk Test
ADC	Apparent Diffusion Coefficient
AHR	Airway Hyper-responsiveness
ANOVA	Analysis of Variance
ASM	Airway Smooth Muscle
ATP	Adenosine triphosphate
BMI	Body Mass Index
CF	Cystic Fibrosis
CO	Carbon Monoxide
COPD	Chronic Obstructive Pulmonary Disease
CT	Computed Tomography
DL _{CO}	Diffusing Capacity of the Lung for Carbon Monoxide
DHS	US Department of Homeland Security
DNA	Deoxyribonucleic Acid
DOE	Department of Energy
DW	Diffusion-Weighted
ERV	Expiratory Reserve Volume
FDG	Fluorodeoxyglucose
FEV ₁	Forced Expiratory Volume in one second
FGRE	Fast Gradient Recalled Echo
FOV	Field of View
FRC	Functional Residual Capacity
FVC	Forced Vital Capacity
G	Gradient Amplitude
GEHC	General Electric Health Care
GOLD	Global Initiative for Chronic Obstructive Lung Disease
¹ H	Proton
³ He	Helium-3
HIPAA	Health Insurance Portability and Accountability Act
HRCT	High Resolution Computed Tomography
HU	Hounsfield Unit
HV	Healthy Volunteer
IRV	Inspiratory Reserve Volume
IC	Inspiratory Capacity
ICC	Intraclass Correlation Coefficient
MAA	Macro-Aggregated Albumin
MR	Magnetic Resonance
MRI	Magnetic Resonance Imaging
NDW	Non-diffusion-weighted
OLD	Obstructive Lung Disease
PA	Posterior-to-Anterior
PET	Positron Emission Tomography

PIPEDA	Personal Information Protection and Electronic Documents Act
PVV	Percent Ventilation Volume
Rb	Rubidium
ROI	Region-of-Interest
RILI	Radiation Induced Lung Injury
RF	Radio-frequency
RV	Residual Volume
SGRQ	St George's Respiratory Questionnaire
SNR	Signal-to-Noise Ratio
SPECT	Single Photon Emission Computed Tomography
SRGA	Seeded Region Growing Algorithm
STP	Standard Conditions for Temperature and Pressure
SV	Static Ventilation
SVC	Slow Vital Capacity
^{99m} Tc	Technetium-99
TE	Echo-Time
TLC	Total Lung Capacity
TR	Repetition-Time
TV	Tidal Volume
UTE	Ultra-short Echo Time
VC	Vital Capacity
VDP	Ventilation Defect Percent
VDV	Ventilation Defect Volume
VV	Ventilation Volume
¹²⁹ Xe	Xenon-129

CHAPTER 1: INTRODUCTION

During the last two decades, hyperpolarized noble gas magnetic resonance imaging (MRI) has emerged as an important tool to study pulmonary diseases like chronic obstructive pulmonary disease (COPD) and asthma. Understanding the anatomy of the lung and the physiological changes that take place after the onset of disease is critical for understanding the mechanism of disease progression and improvements after therapy as well as the implementation of new diagnostic tools. The objective of Chapter 1 is to provide a motivation for the work presented in the following chapters as well as provide an overview of pulmonary anatomy, pathology of obstructive lung disease, the diagnostic tools and the different imaging modalities currently used to evaluate pulmonary disease.

1.1 Burden of Pulmonary Disease

According to the World Health Organizations' global burden of disease 2004 update, respiratory diseases were responsible for 6.8% of all male and 6.9% of all female deaths worldwide.⁶ Chronic obstructive pulmonary disease (COPD) was the 4th leading cause of death worldwide, and accounted for three million or 5.1% of all deaths worldwide while asthma was responsible for another 0.287 million or 0.5% of all deaths worldwide.⁶ It is predicted that by 2030, COPD will be the 3rd leading cause worldwide accounting for 8.6% of all deaths as shown in **Table 1.1**.⁷ It was estimated that the prevalence of COPD was 63.6 million and asthma 234.9 million worldwide in 2004.⁶ Asthma was the leading chronic disease in children in industrialized countries.⁸ COPD and asthma were the 10th and 13th leading causes of moderate and severe disability in 2004 responsible for 26.6 million and 19.4 million disabilities worldwide respectively.⁶

In Canada, respiratory diseases were the 3rd leading cause of death just below cardiovascular disease and cancer in 2005.¹ As shown in **Figure 1.1**, respiratory diseases were responsible for 8.7% of all male deaths and 8.6% of all female deaths in Canada with COPD alone accounting for 4.5% and 4% of deaths respectively.¹ The economic burden of respiratory diseases is enormous, with COPD and asthma accounting for 3% and 1% of all hospitalizations in Canada in 2004-05.¹ As shown in **Figure 1.2**,

respiratory diseases were ranked 8th in terms of the total healthcare costs in Canada accounting for just over 5.6 billion dollars in 2000.¹ In 2010, the cost rose to approximately 12 billion dollars, and in the best case scenario, the number is expected to rise to just over 24 billion dollars in 2030.⁹ Asthma was the number one cause for emergency room visits in Canada in 1994.⁸ There were 3.1 million people suffering from asthma and just over 1.65 million from COPD in Canada in 2010.⁹

Table 1.1 Leading causes of death worldwide 2004 and predicted values in 2030. Adapted from World Health Organization. The global burden of disease: 2004 update⁶ and World Health Organization. World Health Statistics⁷

2004			2030		
Disease	Deaths (%)	Rank	Rank	Deaths (%)	Disease
Ischaemic heart disease	12.2	1	1	14.2	Ischaemic heart disease
Cerebrovascular disease	9.7	2	2	12.1	Cerebrovascular disease
Lower Respiratory Tract infections	7.1	3	3	8.6	COPD
COPD	5.1	4	4	3.8	Lower Respiratory Tract infections

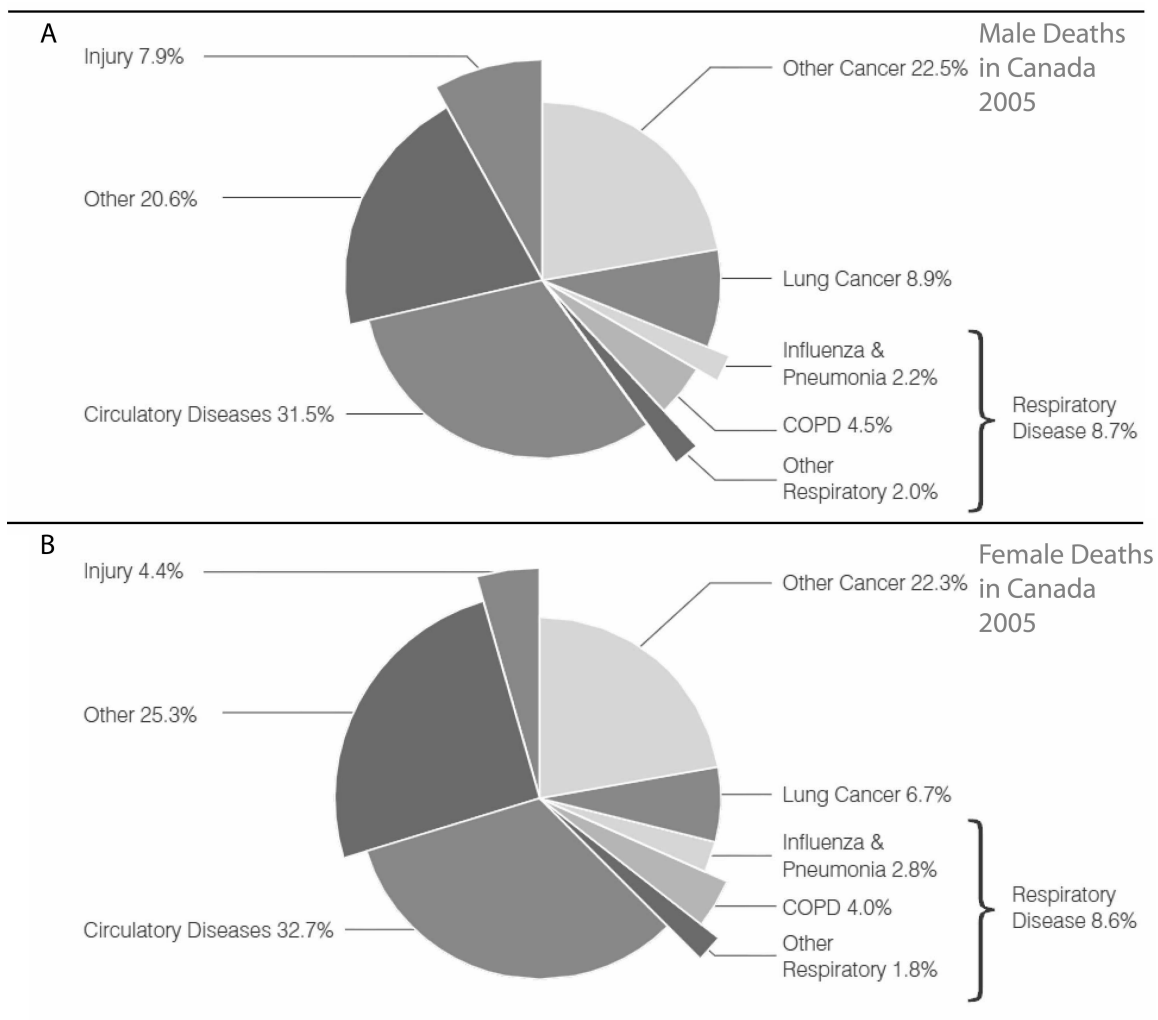


Figure 1.1 Proportion of all deaths for men (A) and women (B) in Canada in 2005
 Reproduced with permission from Life and Breath: Respiratory Disease in Canada¹

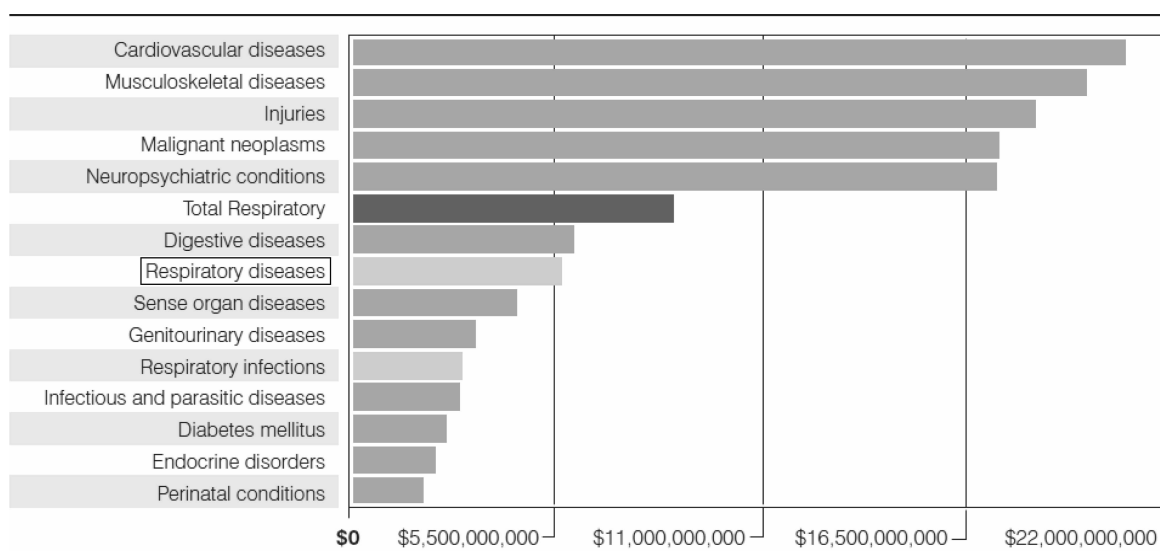


Figure 1.2 Total economic burden of respiratory diseases in Canada in 2000

Reproduced with permission from Life and Breath: Respiratory Disease in Canada¹

Note: Respiratory infections include lower and upper respiratory tract infections, otitis media and tuberculosis. Respiratory disease includes asthma, COPD and other diseases of the respiratory system (excluding lower and upper respiratory tract infections, lung cancer and tuberculosis), Total Respiratory is a sum of Respiratory infections and Respiratory disease (excludes lung cancer)

Recent studies have shown that the prevalence of COPD is actually much greater than previously believed, with a reported 9-10% of adults aged 40 years or higher having COPD worldwide.^{10,11} Studies have also shown that of these individuals who were determined to have COPD, only 19% were previously diagnosed and treated.¹² These studies suggest that COPD is highly under-diagnosed and the majority of patients do not have a diagnosis or a treatment plan for the disease. Reports from 1979 in Canada showed 2.3% of the population suffered from asthma, whereas in 2004, this number jumped to 8.4% of the population.⁸ These results suggest that there is an immediate need to develop new imaging tools for early detection and diagnosis of these respiratory diseases in the future.

In the following sections, I will be describing the anatomy of the lung, the nature of obstructive lung disease as well as the gold standard and imaging modalities currently used for pulmonary disease diagnosis.

1.2 Lung Structure and Function

Human cells obtain most of their cellular energy in the form of adenosine triphosphate (ATP) from glucose through a process called as cellular respiration.^{13,14} Oxygen is required by the cells for respiration and carbon dioxide is formed as a byproduct.^{13,14} Hence there is a need for transfer of oxygen from the external environment into the body and carbon dioxide from the body to the external environment. The main organ responsible for this gas exchange with the external environment is the lung and the respiratory system assists in this process. The respiratory system consists of the oral and nasal cavities, the paranasal sinuses, the pharynx, the larynx, the trachea, the bronchi and their smaller branches, and the lungs, which contain the gas exchange chambers, called the alveoli.¹³ Functionally the respiratory structures are divided into two zones- the conducting and the respiratory zones as shown in **Figure 1.3**.² The conducting zone extends from the top of the trachea to the beginning of the respiratory bronchioles; and has no capacity for gas exchange with the blood as these airways are not lined with alveoli. The respiratory zone extends from the respiratory bronchioles down; it contains alveoli and is the region of the lungs responsible for gas exchange with the blood.¹⁴

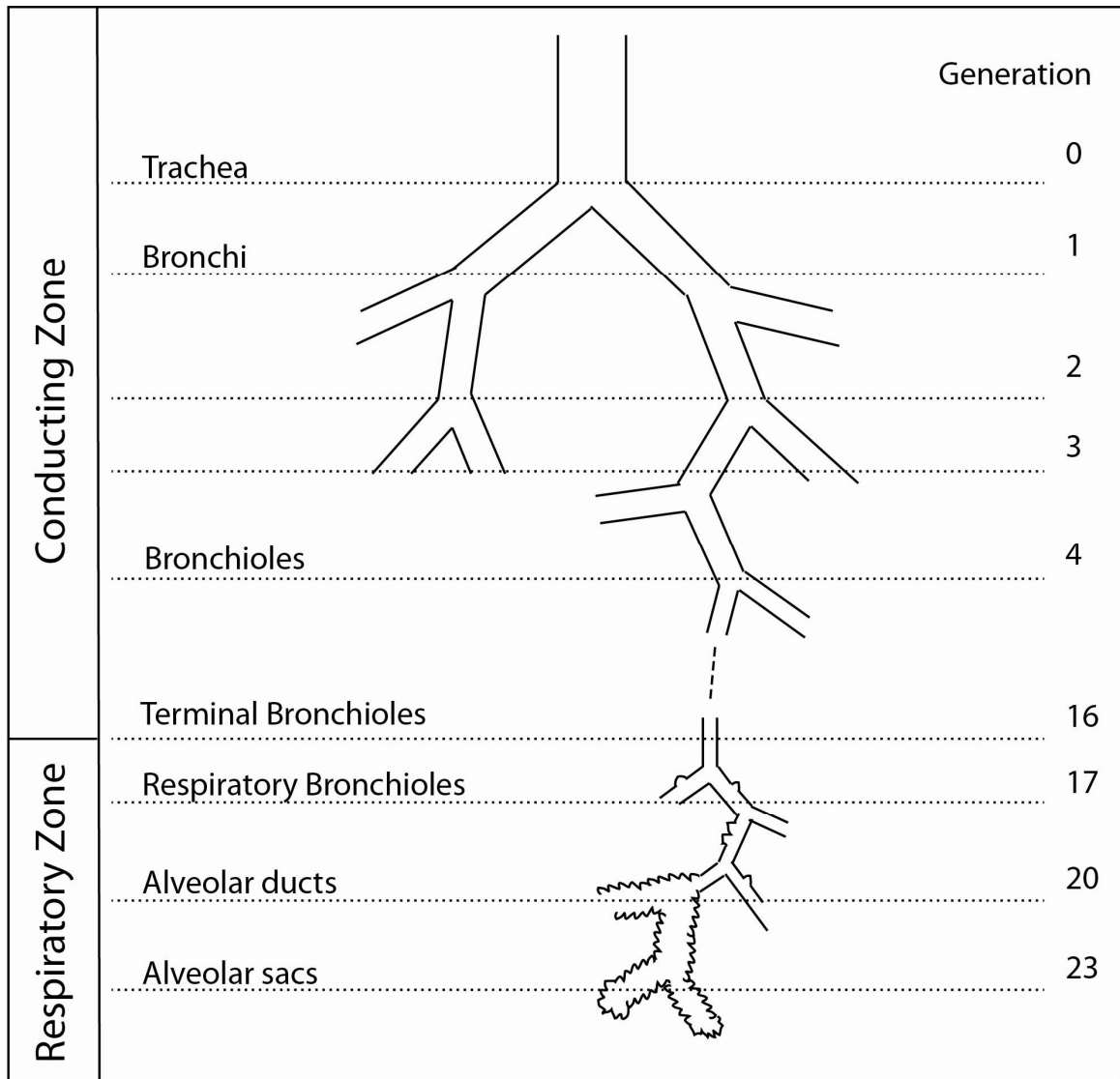


Figure 1.3 Schematic of the human airway tree by generation (Image is not to scale)
Image adapted from West JB, Respiratory Physiology; The Essentials²

1.2.1 The Conducting Zone

The organs that make up the conducting zone filter, humidify and warm the air passing from the external environment to the lungs. As shown in **Figure 1.3**, the airways consist of a series of branching tubes that become shorter, narrower and more numerous through the generations of airways (deeper in the lung). The airways have about 23 generations of dichotomous branching.¹⁵ Generation number zero, or the trachea, divides into the right and left main bronchi, which in turn divide into lobar, followed by segmental bronchi.² This process continues until the terminal bronchioles, which are the smallest airways without alveoli, and the last generation of airways included in the conducting zone.² The airways of conducting zone do not partake in gas exchange as these airways are not lined with alveoli, and hence the volume of gas present in the conducting zone is called the anatomical dead space which is approximately 150 ml in a healthy adult.²

The flexible trachea, or windpipe, descends through the larynx, through the neck and into the mediastinum.¹³ A study by Kamel *et. al* using computed tomography (CT) scans showed that the average tracheal length in males was 105mm while that in females was 98mm with males having an average tracheal volume of 36 cm³ and females 24 cm³.¹⁶ The wall of the trachea contains 16-20 C-shaped rings of hyaline cartilage connected by membranes of fibro-elastic connective tissue, enabling the trachea to be flexible enough to permit bending and elongation during inhalation and exhalation, but preventing it from collapsing due to the changes in pressure during breathing.¹³ All the air moving in and out of the lungs must pass through the trachea which divides into generation one of the airways or the two main bronchi.

The right and left main bronchi originate from the trachea and are also called the primary bronchi. The left and the right main bronchi are responsible for transport of gas from the trachea to their respective lungs. The main bronchi further divides into generation two of the airway tree or the lobar bronchi. The human lungs are divided into several lobes- three on the right and two on the left.¹³ There is one lobar bronchus supplying each lobe, hence a total of five lobar bronchi exist. The lobar bronchi further divide into generation three or the segmental bronchi, which in turn repeatedly divide into smaller bronchi till about 23 generations. The generations smaller than 1mm in diameter

are called bronchioles (“little bronchi”) and the smallest of the bronchioles, known as the terminal bronchioles, are less than 0.5mm in diameter.¹³ The terminal bronchioles are the last generation of airways of the conducting zone and hence the last generation of airways that do not participate in gas exchange and are found around generation 16.² They further divide into the respiratory bronchioles which are the first respiratory zone structures.

1.2.2 Respiratory Zone

The respiratory zone is the last part of the airway tree, distinguished from the conducting zone by the fact that the walls of the airways are lined by the air-exchange chambers called the alveoli. The first generation of airways in the respiratory zone, called the respiratory bronchioles (generations 17-19 of the airway tree) have scattered alveoli protruding from their surface.¹³ The respiratory bronchioles lead into the next generation of airways known as the alveolar ducts. The alveolar ducts are straight ducts whose walls are almost entirely covered with alveoli.¹³ The alveolar ducts lead into terminal clusters of alveoli called alveolar sacs.¹³ The alveolar sacs are a group of alveoli. The opening from an alveolar duct into an alveolar sac is called the atrium or “entrance chamber”.¹³ The alveoli are tiny hollow sacs whose openings are continuous with the lumens of the airways.¹⁴ The alveoli are the location where the actual gas exchange occurs. A study by Ochs *et al.*¹⁷ estimated that the mean alveolar number in human lungs was 480 million and was closely related to total lung volume with larger lungs having significantly more alveoli. The study also reported that the mean size of an alveoli was constant ($4.2 \times 10^6 \mu\text{m}^3$) irrespective of the size of the lungs. In this part of the respiratory zone, the alveolar walls contain capillaries and a very small interstitial space.¹⁴ In many places, this interstitial space is completely absent.¹⁴ Hence, the blood within the alveolar-wall capillary is separated from the air within the alveolus by an extremely thin barrier (0.2 μm , compared with the 7 μm diameter of an average red blood cell).¹⁴ For a healthy individual, the total surface area of the alveoli in contact with the capillaries is roughly the size of a tennis court.¹⁴ The large surface area coupled with the thinness of the barrier allow for the rapid exchange of large quantities of oxygen and carbon dioxide by diffusion. The rate of diffusion of gases across the membrane is described by Fick’s law for diffusion, as shown in equation (1):

$$Diffusion = \frac{A \cdot D \cdot (P_1 - P_2)}{T} \quad (1)$$

where, A is the surface area of the lung for diffusion, D is the diffusion coefficient of gas, $P_1 - P_2$ is the partial pressure difference of the gas across the alveolar capillary membrane, and T is the thickness across the alveolar capillary membrane. The gas diffusion rate is therefore directly proportional to the surface area of the lung, the diffusion coefficient of the gas and the partial pressure difference, and inversely proportional to the thickness across the lung membrane. As the total surface area of all alveoli in an average pair of lungs is 140 square meters¹³, and the thickness of the interstitial space is extremely small ($0.2 \mu\text{m}$)¹⁴, the efficiency of gas exchange is high. The oxygen flows from an area of high partial pressure (inside the alveoli) to an area of low oxygen partial pressure (pulmonary capillaries), hence the oxygen is transported from the external environment to the blood through the respiratory system.

1.3 Obstructive Lung Disease

Obstructive lung disease (OLD) includes several conditions including obstructive chronic bronchitis, emphysema and asthma¹⁸ and is characterized by airway obstruction, inflamed and easily collapsible airways, obstruction to airflow and problems exhaling. Of these, COPD is divided into chronic bronchitis and obstructive emphysema, or a combination of these occurring together.¹⁸ Asthma is an inflammatory disease of the airways, although there is a lot of controversy regarding the best definition of asthma as it is a clinically complex condition.^{19,20}

1.3.1 Chronic Obstructive Pulmonary Disease

COPD is a category of obstructive lung disease, found mainly in smokers, characterized by difficulty in moving air into and out of the lungs, or obstruction to the flow of air. In the Global Initiative for chronic obstructive pulmonary disease guidelines, COPD is defined as “A disease state characterized by progressive development of airflow limitation that is not fully reversible. The airflow limitation is usually progressive and

usually results from an abnormal response of the lungs to noxious particles or gases."²¹ Cigarette smoking, while not the only factor leading to COPD, is the main source of the inhaled noxious particles that leads to its development. Both environmental and genetic factors also contribute to the development of COPD. Although only 10-15% of smokers actually go on to develop obstructive lung disease,²² active, sustained cigarette smoking contributes to the origin of COPD in more than 90% of the subjects.²³ Genetic disorders such as alpha-1 antitrypsin deficiency have been shown to cause emphysema.^{24,25} Although not all smokers develop airflow limitation, studies have shown that cigarette smoking is associated with inflammation in both the large and small airways,^{26,27} as well as the lung parenchyma²⁸ in smokers with normal forced expiratory volume in one second (FEV₁), which is a standard measure for diagnosis of airflow limitation and will be explained in detail in the next part of this chapter. The disease that occurs within the airways is called chronic bronchitis, and that which occurs in the lung parenchyma is called emphysema, which are independent diseases that may manifest together or in isolation. However, the same agents that cause chronic bronchitis- mainly smoking- also cause emphysema, which is why these two diseases frequently occur together.

Chronic bronchitis is one of the conditions associated with COPD and is characterized by excessive mucus production in the bronchi and chronic inflammatory changes in the small airways.¹⁴ So significant is cigarette smoking in the development of chronic bronchitis that this disease would be an insignificant health problem if cigarettes were unavailable. Inhaled irritants (example from cigarette smoking) are responsible for prolonged secretions of excess mucus by the mucosa of the lower respiratory passages, leading to inflammation and fibrosis (formation of scar tissue) of this mucosa. This causes an obstruction in the airways because of an accumulation of mucus in the airways and thickening of the inflamed airways.¹⁴ The obstruction and inflammation severely impair ventilation and gas exchange. **Figure 1.4** shows a normal airway with no inflammation or over-secretion of mucus in the lumen of the airway, as well as an airway inflamed due to chronic bronchitis, with excessive secretion of mucus causing a decrease in the diameter of the airway leading to difficulty in ventilation. Infections also frequently occur in these patients because bacteria and viruses thrive in the stagnant pools of mucus. Coughing is persistent and productive in these patients. Patients with chronic

bronchitis are sometimes called “blue bloaters” because lowered blood oxygenation often results in cyanosis (bluish discoloration of the skin) and other symptoms of right heart failure. However, the degree of dyspnea in patients suffering from chronic bronchitis alone is usually moderate compared to patients suffering from emphysema alone.¹³

From the trachea to the alveolar sacs, as the airway generations increase, the number of airways increases rapidly due to the dichotomous branching pattern.¹⁵ As the total number of airways increases, although they become narrower at each generation, the total cross-sectional area at each generation increases. Although it would be expected that the resistance to the flow of air would increase as the radius of the individual airways decreases according to Poiseuille’s equation (resistance of a single tube is inversely proportional to the 4th power of the radius of the tube), this is not observed because the number of airways and their total cross-section area increases rapidly. Since all the airways are arranged in parallel and the resistance of parallel circuits is added as reciprocals, small airways (<2 mm in diameter) have a very small resistance to the flow of air. This fact was confirmed by Hogg *et. al.*²⁹ who showed that in healthy subjects, the small airways contributed very little to the total airway resistance. They also reported that in subjects with mild and severe emphysema, there was an increase in the resistance of the small airways (<2mm in diameter) with no increase in the total lung resistance. It was shown that the elevated resistance was due to mucus plugging and narrowing and obliteration of the small airways. They defined this condition as “small airways disease” and found that while this condition affected ventilation distribution and gas exchange, it did not change the results of the pulmonary function tests designed to diagnose obstruction in the airways. By the time the total airway resistance elevated to a level recognized by the pulmonary function tests, the obstruction would be much more severe than generally thought. A more recent study by Hogg *et. al.* showed that progression of COPD from Global initiative for chronic Obstructive Lung Disease (GOLD) stage 0 (explained in the next part of the chapter) to GOLD stage 4 was most strongly correlated with thickening of the airway wall caused by a repair or remodelling process.⁴ The degree to which the lumen was filled with mucus and the extent of inflammatory response was more weakly associated with disease progression. **Figure 1.5.A** shows a normal healthy small airway, **Figure 1.5.B** shows a small airway partially filled with

mucus, **Figure 1.5.C** shows an airway with an active inflammatory process, where the exudate extends into the lumen, **Figure 1.5.D** shows an airway that has been narrowed by secretion of mucus in the peribronchiolar space.

Emphysema is characterized by a permanent irreversible enlargement of the alveoli, caused by the deterioration of the alveolar walls¹³ and by the atrophy and collapse of lower airways- those from the terminal bronchioles to the lower generations.¹⁴ The disease is associated with chronic inflammation and increased activity of lung macrophages, whose lysosomal enzymes are responsible for destroying the alveolar walls and breaking down elastin.¹³ Cigarette smoking is the single most important factor in this process as it stimulates the release of proteolytic enzymes and destroys other enzymes that usually protect the lung against these proteolytic enzymes.¹⁴ **Figure 1.5.E** shows normal lung parenchyma in a healthy non-smoker, **Figure 1.5.F** shows moderate emphysema and **Figure 1.5.G** shows severe tissue destruction in severe emphysema. As can be observed from **Figures 1.5.E-G**, as a result of alveolar-wall loss, adjacent alveoli fuse to form fewer but larger alveoli thus reducing the total surface area available for diffusion and hence for gas exchange.¹⁴ Moreover, since the tissue destruction is not consistent throughout the lungs, some areas may receive little amount of air and sufficient amount of blood supply while others show the opposite pattern leading to ventilation-perfusion inequality. Chronic inflammation also leads to fibrosis and the lungs become progressively less elastic, making expiration difficult and exhausting.¹³ In these patients, the bronchioles open during inspiration but collapse during expiration leading to a condition known as “gas trapping” where huge amounts of air get trapped in the alveoli leading to a “barrel chest” appearance due to enlargement of the lungs. Damage to the lung capillaries increases the resistance in the pulmonary vascular circuit, forcing the heart’s right ventricle to enlarge through overwork.¹³ Emphysema is usually divided into two distinct forms: centrilobar and panlobar.²⁴ Centrilobar emphysema is mainly a disease of the upper lobes and the apices within the upper and lower lobes.²⁴ In contrast, panlobar emphysema shows a more homogeneous pattern and is mainly observed in the lower lobes. Studies have shown that there is a relationship between smoking and centrilobular emphysema, but not with panlobar emphysema, which may be associated with genetic disorders such as alpha-1 antitrypsin deficiency.^{24,30,31}

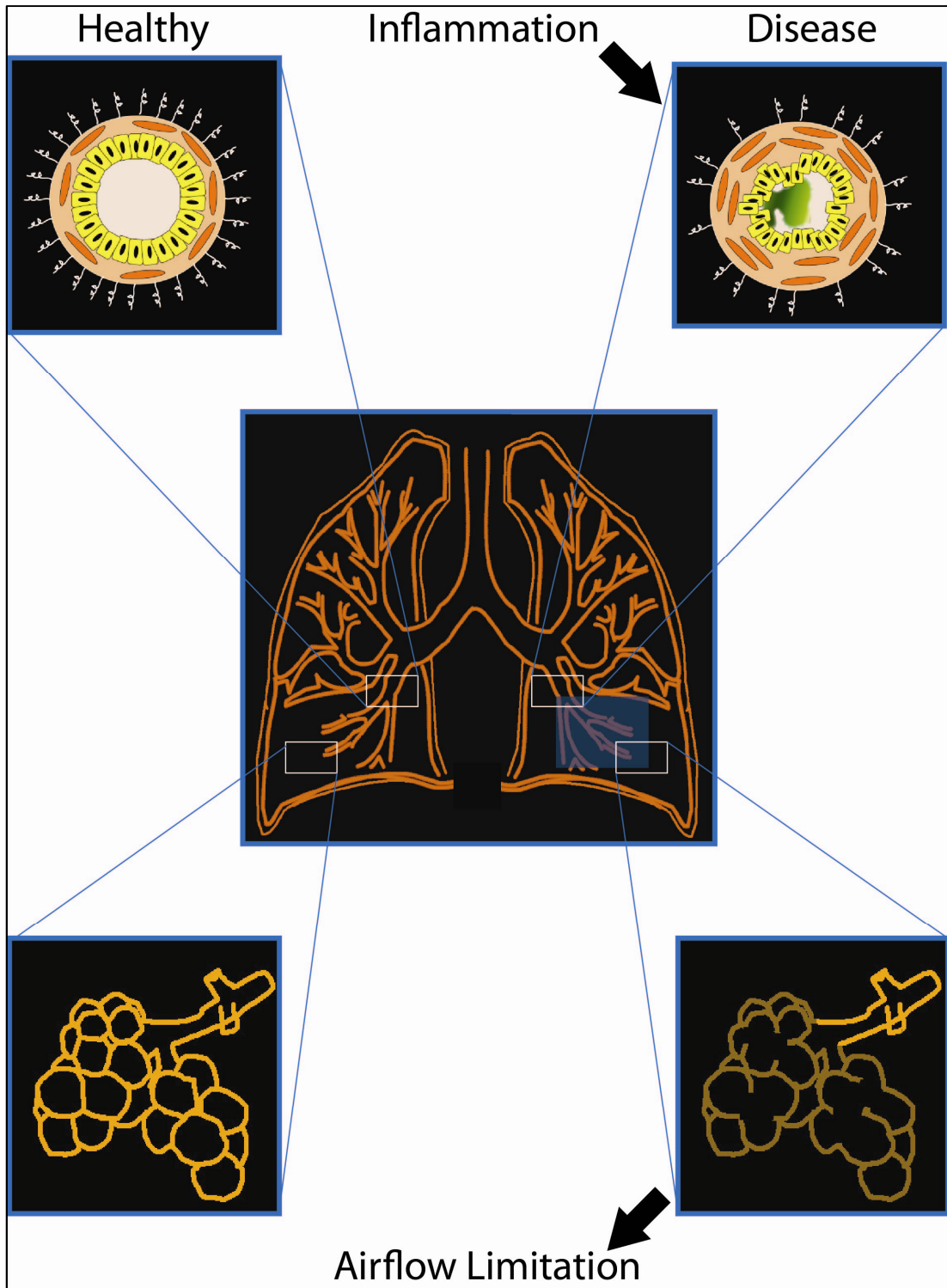


Figure 1.4 Schematic of the human airways and alveoli in healthy volunteers and subjects with COPD.

The airways of the COPD subject on the right shows inflammation and mucus plugging and the alveoli show extensive emphysema

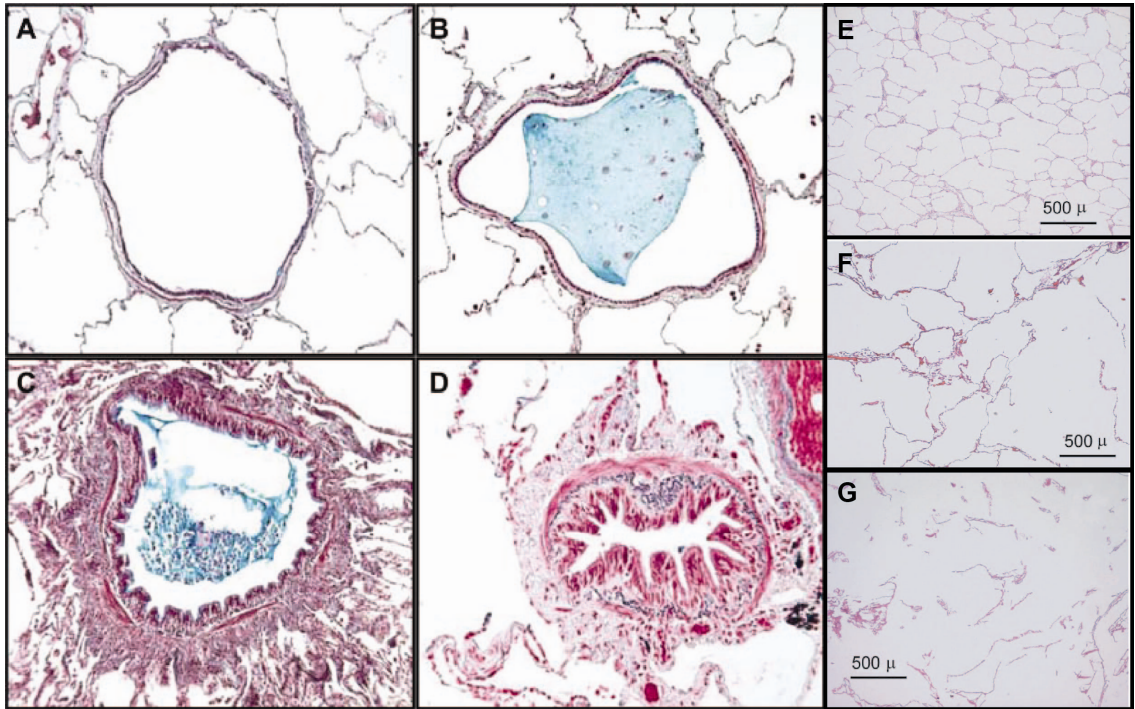


Figure 1.5 Small Airways Disease and Emphysema in COPD

(A) A healthy airway with unobstructed lumen (B) An airway with lumen partially filled with mucus (C) Acutely inflamed airway with lumen filled with an exudates of mucus and epithelial cells (D) An airways with severe inflammation and the lumen has been almost completely obstructed by deposition in the peribronchiolar space (E) Histological slide from a healthy subject showing lack of emphysema (F) Moderate degree of emphysema (G) Severe emphysema sample

Images reproduced with permission from Hogg et al.⁴ and Woods et al.⁵

1.3.2 Asthma

Asthma is predominantly a disease of the airways, characterized by sporadic episodes of strong airway smooth muscle contractions leading to an increase in airway resistance. The causes of asthma vary between individuals and include allergies, viral infections and sensitivity to environmental factors.¹⁴ The basic defect in asthma is chronic inflammation of the airways which makes the airway smooth muscles hyper-responsive and causes them to contract strongly. The trigger for this hyper-responsiveness can be a variety of factors including exercise, exposure to cigarette smoke, pollutants, viruses, allergens and a variety of other substances.¹⁴ An asthma attack starts with an early phase, in which mast cells stimulate both contraction of the bronchial smooth musculature (broncho-constriction) and secretion of mucus in these airways.¹³ Within a few hours, a late phase develops as eosinophils, neutrophils, a certain type of helper T lymphocytes and basophils accumulate in the bronchi and bronchioles, where these leukocytes secrete additional inflammatory chemicals that damage the bronchial mucosa and further increase broncho-constriction and secretion of mucus.¹³ Until recently, it was considered that broncho-constriction was the primary symptom of asthma and quick relief is still provided by drugs that either inhibit smooth-muscle contraction (bronchodilators) or inhibit the parasympathetic stimulation of such contraction (anticholinesterases). Recently it has been discovered that asthma is primarily an inflammatory disease and new treatments using anti-inflammatory drugs (gluco-corticoids and nonsteroidal anti-inflammatory agents) have been developed.¹³ These drugs allow much better long term management of disease, leading to fewer attacks and less damage to the airways. Functionally, asthma can be defined as airway hyper-responsiveness (AHR) leading to areas of airway inflammation and airway obstruction (partial or complete). It might be due to abnormal functioning of the airway smooth muscle (ASM) or an excess of ASM cells. A study by Dunnill and colleagues showed that the percentage of smooth muscle in the segmental bronchial wall was $11.9\% \pm 3.36\%$ in severe asthma compared to only $4.6\% \pm 2.2\%$ in healthy controls.³²

1.4 Established Methods for diagnosis of Obstructive Lung Disease

Currently, the pulmonary function tests provide gold standard measurements of lung function in obstructive lung disease. These are used by physicians for diagnosis of various pulmonary conditions as well as in research studies. They are used to measure lung volumes, bronchial obstruction, gas exchange and lung compliance.³³ Pulmonary function tests are able to identify abnormalities of lung function and can also be used to rule out the possibility of some respiratory disorders such as COPD. These tests are routinely used in the diagnosis of asthma and COPD. Spirometry is the most widely used of these tests.³⁴

1.4.1 Spirometry

Spirometry is used to measure static lung volumes at rest-slow (inspiratory or expiratory) vital capacity (sVC), forced vital capacity (FVC) and dynamic volumes- FEV_1 .³³ The test to measure FEV_1 involves measuring airflow and lung volumes during a forced expiratory maneuver from full inspiration. As shown in **Figure 1.6.A** a hand-held *EasyOne* spirometer (nidd Medizintechnik AG, Zurich, CH) is used for this test. The test begins with the subject putting the spirometer in their mouth and making a tight seal around it with their lips to ensure that there is no leakage of air. They are then instructed to take a couple of normal (tidal) breaths after which they have to inspire fully. Following this they are instructed to exhale as fast as possible and keep going until there is no airflow detected by the spirometer. The volume of gas exhaled by the subject in the first second of the forced maneuver is known as the FEV_1 and the amount of gas exhaled during the entire maneuver is known as FVC as shown in **Figure 1.6.B**.

The American Thoracic Society's guidelines for individual spirometers to be acceptable are if *"they are free from artifacts- cough during first round of exhalation, glottis closure that influences the measurement, early termination or cut-off, effort that is not maximally throughout, leakage of air, obstructed mouthpiece, if they have a good start: extrapolated volume <5% of FVC or 0.15 L, whichever is greater and show satisfactory exhalation: duration ≥ 6 s or a plateau in the volume-time curve or if the subject cannot or should not continue to exhale"*.³⁵ After three acceptable spirometers have been obtained the following conditions have to be met- *"the two largest values of*

FVC must be within 0.150 L of each other and the two largest values of FEV₁ must be within 0.150 L of each other".³⁵ If both the criteria are met, the testing may be concluded, otherwise testing has to be continued until the conditions are met with a maximum of eight tests performed.³⁵ Although the equipment required to perform spirometry is simple and robust, the proper performance of the breathing maneuvers and full cooperation of the patient is critical for getting accurate results. The consistency of the spirometer and the technician conducting the test is essential because large variations can be introduced in the results otherwise. The measurements obtained are highly patient effort dependent and hence the reproducibility of the results might not always be high. These pulmonary function tests (PFT) are also unable to give any regional information about the disease and are insensitive to early pulmonary changes after the onset of disease.

The spirometric measurements of FEV₁ and FVC are used to diagnose diseases like COPD and asthma. The ratio of FEV₁/FVC is used to measure airflow obstruction and a ratio of FEV₁/FVC < 0.7 post bronchodilator confirms the diagnosis of persistent airflow limitation and hence COPD.²¹ As shown in **Table 1.2**, COPD is classified into stages according to the (GOLD) criteria.³⁶

Table 1.2 Classification of COPD according to severity of airflow obstruction. Adapted from the Global strategy for the diagnosis, management, and prevention of chronic obstructive pulmonary disease (Revised 2011), Global Initiative for Chronic Lung Disease³⁶

Severity	GOLD Stage	Post-Bronchodilator FEV ₁ Criteria
Mild	GOLD Stage I	FEV ₁ ≥ 80% predicted
Moderate	GOLD Stage II	50% ≤ FEV ₁ < 80% predicted
Severe	GOLD Stage III	30% ≤ FEV ₁ < 50% predicted
Very Severe	GOLD Stage IV	FEV ₁ < 30% predicted

Specific spirometric cut-off points (e.g., FEV₁/FVC < 0.7, FEV₁ < 80, 50, 30 % predicted) are used for simplicity, but have not been clinically validated.³⁶ These fixed

ratios may result in over-diagnosis of COPD in the elderly, especially in those with mild disease because the process of ageing does affect lung volumes.³⁶ The predicted values are calculated depending on age, sex, height, weight and ethnicity as well as the research study.

Spirometry is also used in the diagnosis of asthma.¹⁹ The two main measurements used are FEV₁ and FVC and the ratio of FEV₁/FVC is often used by respirologists to assess lung function.

1.4.2 Plethysmography

A full body MedGraphics' Elite Series stand-alone body plethysmograph (MedGraphics Corporation. 350 Oak Grove Parkway St. Paul, MN USA), as shown in **Figure 1.6.C**, is a device used to measure lung volumes. The various lung volumes are shown in **Figure 1.7** and their definitions are as follows- tidal volume (TV) is the amount of air inhaled or exhaled in one breath during relaxed, quiet breathing (typical value in an average young adult male-500ml), inspiratory reserve volume (IRV) is the amount of air in excess of tidal inspiration that can be inhaled with maximum effort (typical value in an average young adult male-3000ml), expiratory reserve volume (ERV) is the amount of air in excess of tidal inspiration that can be exhaled with maximum effort (typical value in an average young adult male-1200ml), residual volume (RV) is the amount of air remaining in the lungs after maximum expiration; keeps alveoli inflated between breaths and mixes with fresh air on next inspiration (typical value in an average young adult male-1200ml), vital capacity (VC) is the amount of air that can be exhaled with maximum effort after maximum inspiration ($VC = ERV + TV + IRV$); used to assess strength of thoracic muscles as well as pulmonary function (typical value in an average young adult male-4700ml), inspiratory capacity (IC) is the maximum amount of air that can be inhaled after a normal tidal expiration ($IC = TV + IRV$, typical value in an average young adult male-3500ml), functional residual capacity (FRC) is the amount of air remaining in the lungs after a normal tidal expiration ($FRC = RV + ERV$, typical value in an average young adult male-2400ml), total lung capacity (TLC) is the maximum amount of air the lungs can contain ($TLC = RV + VC$, typical value in an average young adult male-5900ml).¹⁴

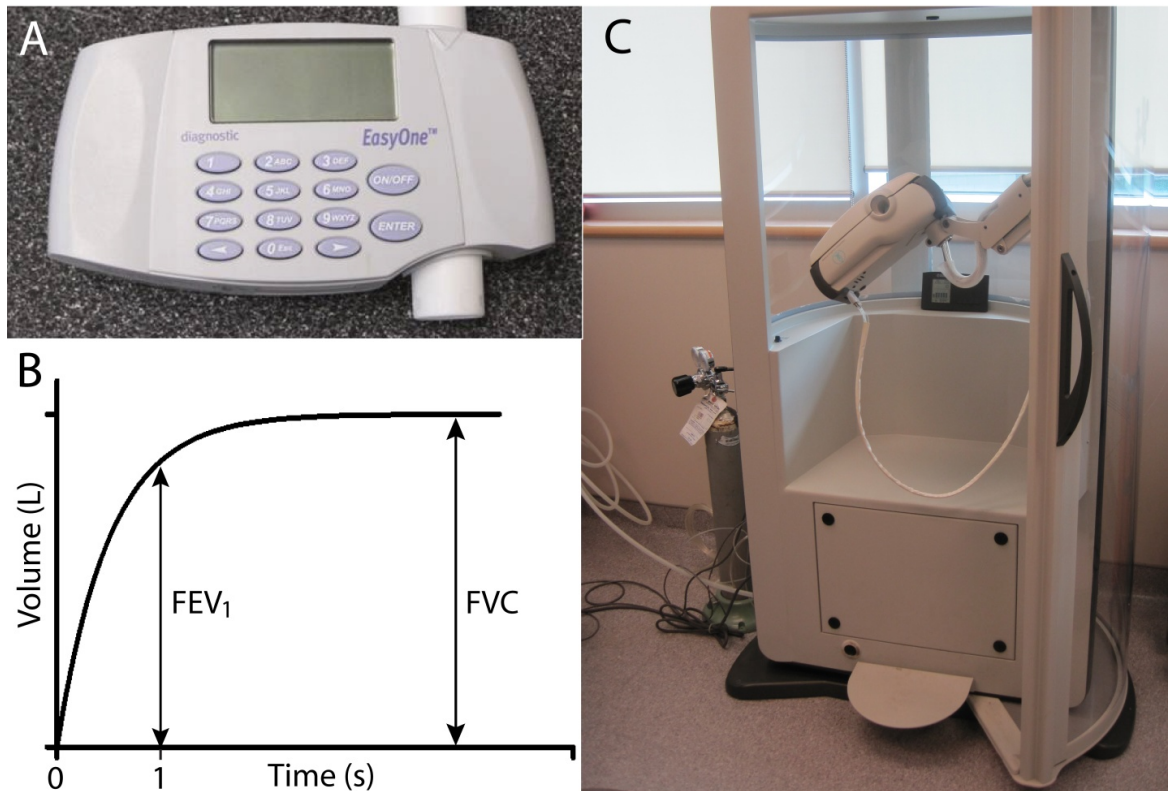


Figure 1.6 Spirometry and Plethysmography

(A) A hand-held spirometer (B) A sample airflow curve obtained from the spirometer used to calculate FEV₁ and FVC (C) A whole body plethysmograph

Measurement of lung volumes requires a method of estimating the volume of gas inside the thorax. The body plethysmograph uses the small fluctuations in pressure inside a sealed box containing the patient during breathing to calculate the volume of gas in the thorax.³⁷ The basic principle behind the body box is Boyle's law (shown in equation 2, which states that for a given mass of gas, the product of pressure and volume remains constant provided that the temperature does not change-

$$P_1 \times V_1 = P_2 \times V_2 \quad (2)$$

Where P_1 and V_1 are the pressure and volume of gas and P_2 and V_2 are the pressure and volume of the same mass of gas after a change in pressure and volume.³⁷ To measure lung volumes, the patient sits inside a sealed body box. Inside the box there are two masses of gas: one in the thorax and one outside the body but inside the chamber. The patient breathes through a mouthpiece with a shutter and performs a series of “pant” (shallow rapid breathing). During these “pant” the shutter closes but the subject continues to pant against the closed shutter. The fluctuations in the box pressure are measured and the volume fluctuations are calculated. At the same time a pressure transducer inside the mouthpiece records the pressure changes within the mouth which can be used as a surrogate for pressure changes inside the lungs. Using these values and Boyle’s law, FRC can be calculated. Measuring airflow through the mouthpiece during tidal breathing, maximum inspiration and maximum expiration allows us to calculate all the other lung volumes.

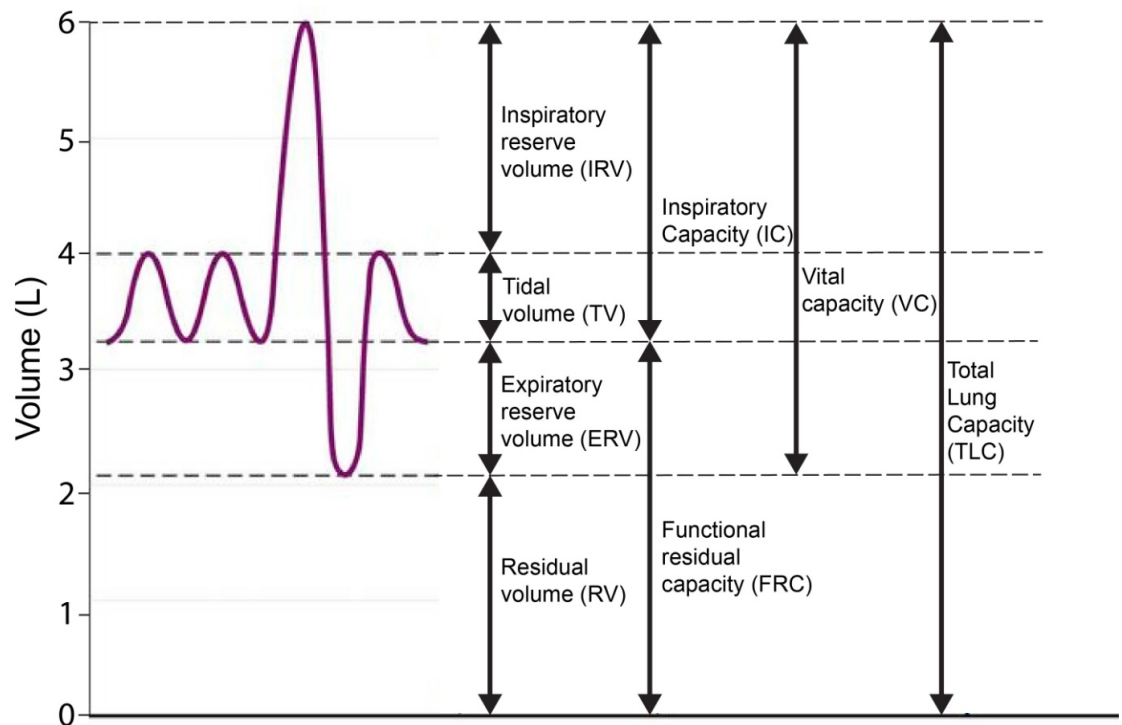


Figure 1.7 Sample airflow curves obtained through a plethysmograph

The body plethysmograph attached to a Medgraphics gas analyzer (MedGraphics Corporation, 350 Oak Grove Parkway St. Paul, MN USA) is also used to measure the diffusing capacity of the lung for carbon monoxide (DL_{CO}) which is a surrogate measurement for diffusion of oxygen across the alveolar membrane into the blood. Carbon monoxide (CO) has similar physical properties as oxygen in terms of its solubility and ability to diffuse across membranes. It also has the added advantage of being very strongly bound to hemoglobin, so that the entire CO transferred across the alveolar wall is retained within the blood and is not exhaled. DL_{CO} is measured by first instructing the subject to exhale to RV and then inhaling to TLC. During this inhalation the subject inhales a known concentration of CO (0.3%) and helium (10%) with air.³⁸ After that the subject holds their breath for 8 seconds before exhalation which gives enough time for the CO to diffuse across the alveolar membrane. The volume of gas is then collected and analyzed. The exhaled concentrations of CO and helium are compared to the inhaled concentrations and after correcting for anatomical dead space, the amount of CO diffusing across the alveolar membrane is calculated. There should be at least two acceptable tests that meet the repeatability criteria of either being within 3 mL CO (STPD). $\text{min}^{-1}.\text{mmHg}^{-1}$ (or $1 \text{ mmol}.\text{min}^{-1}.\text{kPa}^{-1}$) of each other or within 10% of the highest value.³⁸ The average of at least two acceptable tests that meet this repeatability requirement should be reported. Pulmonary conditions such as emphysema reduce the surface area to volume ratio of the alveoli and hence the DL_{CO} reported in subjects suffering from emphysema is often found to be lower than healthy subjects.

1.4.3 Six minute Walk Test

The six minute walk test (6MWT) is safe and easy to administer walk test, and is well tolerated and better reflects activities of daily living than other walk tests (example the shuttle walk test).³⁹ The 6MWT is a self-paced exercise test that measures the total distance the subject can walk on a flat surface in 6 minutes. In severe COPD subjects, the 6MWT has been shown to be a better predictor of mortality than traditional markers (FEV_1 and Body Mass Index) of disease severity.⁴⁰

1.4.4 St. George's Respiratory Questionnaire

The St George's Respiratory Questionnaire (SGRQ) is a well established, self-reported health status questionnaire developed for COPD and asthma.⁴¹ The questionnaire contains three component scores: symptoms, activity and impact on daily life and a total score.⁴² The total score goes from 0 to 100 and higher scores indicate more severe limitation. In both asthma and COPD, SGRQ has been shown to be a valid measure of impaired health in chronic airflow limitation and is repeatable and sensitive.⁴³

1.5 Pulmonary Imaging

There have been tremendous improvements in pulmonary imaging techniques during the last two decades. The advancement of imaging methods has improved our ability to diagnose, characterize and quantify pulmonary pathology. These imaging methods provide a noninvasive method of acquiring functional as well as structural pulmonary information. The technological improvements in computed tomography (CT) and magnetic resonance imaging (MRI) have led to the development of new techniques for pulmonary imaging, and recent advancements in nuclear medicine techniques such as positron emission tomography (PET) have made noninvasive characterization of lesions possible.⁴⁴ New methods of pulmonary imaging using CT and MRI have been used to evaluate pulmonary ventilation and perfusion and to detect small airways disease.⁴⁴ There has been developmental progress made towards transitioning to digital chest radiography, which is starting to replace more traditional methods of acquisition, transmission and viewing of chest radiographs.

1.5.1 Chest X-Ray

X-rays are a form of electromagnetic radiation and on account of their high frequency and energy are able to pass through a patient's body and on a X-ray film thus producing an image.⁴⁵ While passing through a patient's body, the X-ray beam is attenuated by a varying magnitude by different organs depending on the density and atomic number of the tissue. X-rays turn the X-ray film black, and hence the less dense the material, the more X-rays get through and the darker the film. Hence, materials of low density appear darker than objects of high density on the X-ray film. Chest X-rays

are usually the first imaging method used for pulmonary disease diagnosis because they are inexpensive, widely available, have a relatively low radiation dose⁴⁶ and allow for visualization of pulmonary structures like the trachea, carina and major bronchi, mediastinum and hilar regions and the diaphragm as shown in **Figure 1.8**. The most commonly used X-ray techniques for the assessment of the lung are the posterior to anterior (PA) and lateral views taken at TLC.^{46,47} During these scans the scapula should be rotated anteriorly, so that they are project away from the lungs and are out of the field of view (FOV). During a PA scan, the patient stands with their anterior chest wall up against the X-ray film. The X-ray tube lies behind the patient so that the X-rays pass in the PA direction. In the lateral view, the patient is positioned with their side up against the film with their arms over their heads so that the scapula is out of the FOV. On account of the differences in density of the various tissues in the thorax, all the structures appear as different signal intensities. The bone tissue which is dense and attenuates X-rays much more than the lung tissue appears bright whereas the lungs appear dark because the attenuation caused by the lungs is minimal.

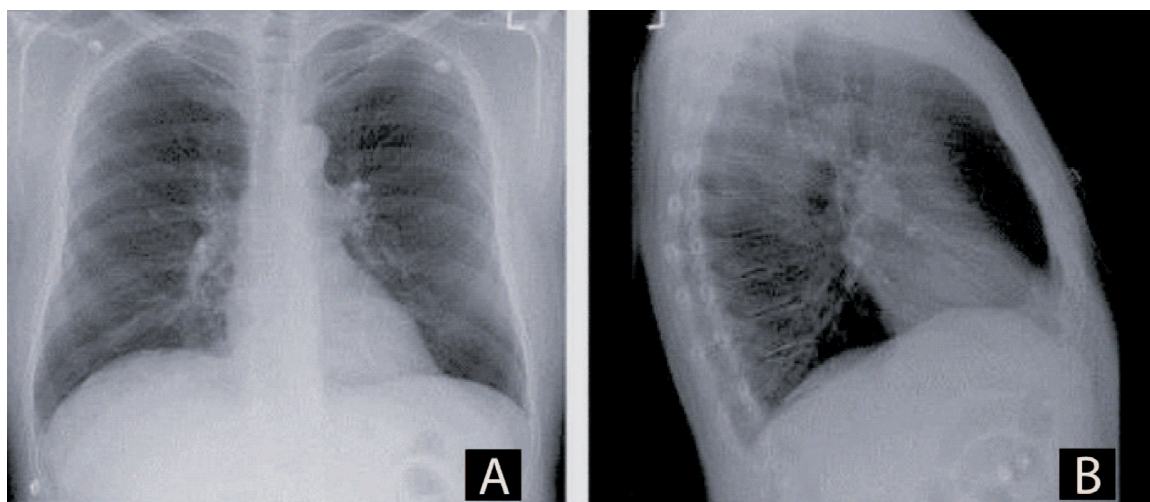


Figure 1.8 Chest X-Ray of a 63 year old male COPD Stage III subject (A) P-A view (B) Lateral View. Adapted from Parraga et. al (2007).³

The average dose from a chest X-ray (single PA film) is 0.02 mSv.⁴⁶ The average natural environmental background radiation is approximately 0.01 mSv/day,⁴⁸ although there are places on earth that have values that are 5-times higher.⁴⁹ Considering the

average environmental exposure of 0.01 mSv/day, the average dose from a PA chest X-ray is equivalent to that a person receives from the environment in about 2 days. Ionizing radiation, such as X-rays, is capable of creating ions by knocking electrons out of their orbits. When biological molecules are exposed to X-rays, these X-rays interact with the water molecules within the body leading to the formation of hydroxyl radicals. These radicals then interact with the nearby Deoxyribonucleic acid (DNA) to cause strand breaks or base damage. X-rays are also capable of ionizing DNA directly. While radiation-induced damage is repaired within the cell, DNA double-strand breaks are more difficult to repair and occasional misrepair can lead to induction of point mutations, chromosomal translocations and gene fusion which are all linked to cancer induction.⁵⁰ Therefore, the low radiation dose, along with quick acquisition time, is a very important advantage of a chest X-rays compared to CT. Various lung structure abnormalities can be identified using a chest X-ray such as flattening and increased translucency of the diaphragm which is commonly associated with gas trapping in respiratory disease. However, in a chest X-ray, all the anatomical structures are super-imposed on top of one another making it difficult to diagnose diseases like COPD, particularly in early disease stages. Hence chest X-rays are used for assessment of more advanced morphological lung changes in COPD.⁵¹

1.5.2 X-ray Computed Tomography

X-ray CT is another major imaging modality used in the evaluation of pulmonary disease. Traditionally, CT images are a two-dimensional representation of a cross-sectional slice through a region of interest in the body.⁴⁷ The third dimension of the image is the slice thickness which could range from 1 to 10mm.⁴⁷ These cross-sectional images are obtained by using X-rays being emitted by an X-ray tube on one side of the gantry with a set of detectors on the other. The patient passes through the gantry that rotates around at the level of interest. Information from the detectors is analyzed by computers and displayed as an image. Owing to the use of computer algorithms, a much greater array of densities can be displayed compared to conventional X-ray films. This allows for differentiation of solid organs from each other and from pathological processes such as tumors and fluid collection. It also makes this imaging modality extremely

sensitive to the presence of minute amounts of fat, calcium or contrast material. As with a chest X-ray, high density objects attenuate the X-rays to a higher magnitude and therefore appear as lighter gray than objects of lower density, which appear darker.⁴⁵ White or light gray objects are therefore called 'high attenuation' whereas dark grey and black objects are called as 'low attenuation'. In a CT scan, image information can be manipulated to highlight the organ of the body being studied. This is called 'altering the window setting'.⁴⁵ For example, in a chest CT where a wide range of tissue densities are present, a good image of the mediastinal structures shows no lung details. However, the lung parenchyma can be observed in full detail by setting a lung window.

The CT image is composed of multiple pixels and images are usually 512 pixels by 512 pixels. The pixel area multiplied by the slice thickness defines the voxel volume. The X-ray attenuation of the structures within a voxel is averaged to produce the attenuation value for the voxel that is recorded to produce an image. Each voxel in a CT image is assigned a Hounsfield unit (HU)⁵² based on its attenuation coefficient relative to that of distilled water at room temperature as shown in equation (3).

$$HU = \frac{\mu_x - \mu_{water}}{\mu_{water}} \times 1000 \quad (3)$$

where μ_x is the linear attenuation coefficient of the object and μ_{water} is the linear attenuation coefficient of water. Based on this, water is assigned a value of 0 HU, while air has a value of -1000 HU and all the tissues with an attenuation coefficient higher than that of water (materials denser than water) are assigned positive HU values.⁵³ Standardization of the units allows for direct comparison between scans acquired on different scanners made by different manufactures.

Emphysema is pathologically defined as the presence of permanent enlargement of air spaces and therefore these air filled regions have HU values closer to that of air than healthy tissue and appear dark in CT scans as shown in **Figure 1.9**. There are two basic patterns of emphysema that can be identified: centrilobular and panlobular. Centrilobular emphysema is typically more pronounced within the upper lobes and in CT images shows up as regions of decreased attenuation, without definable walls that are confined to the center of the secondary lobule.⁴⁷ The changes in lung structure associated with panlobular emphysema are predominantly observed in the mid and lower lungs. On CT images, it is characterized by large regions of low attenuation leading to an apparent simplification of lung architecture.⁴⁷ Emphysema can also be quantitatively measured using CT images by using a HU threshold to quantify the volume of the lung below the threshold.

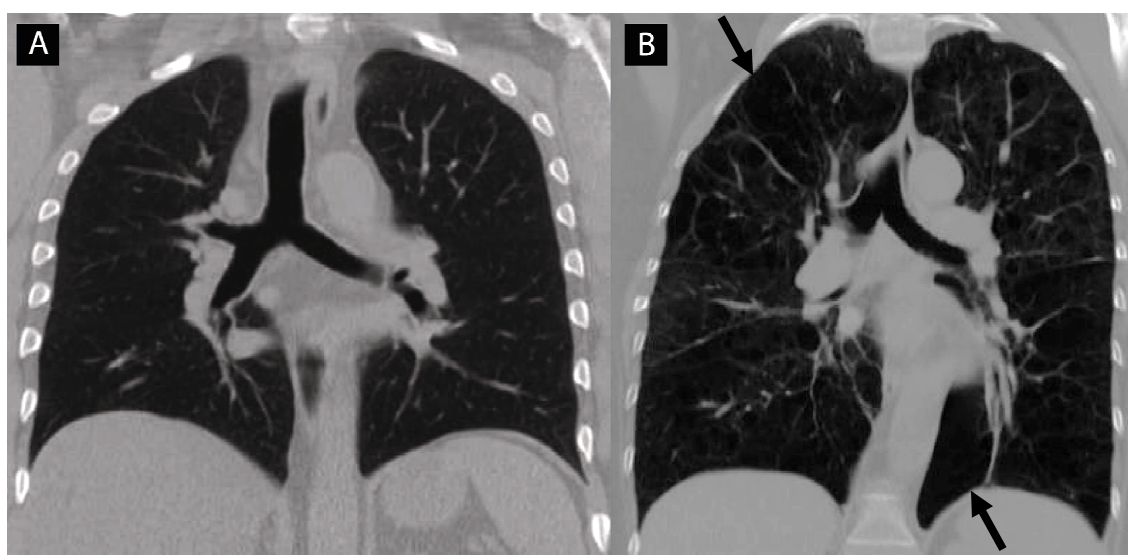


Figure 1.9 X-ray computed tomography (CT)
 (A) CT center slice from a 55 year old male healthy smoker (B) CT center slice from a 60 year old female COPD stage 2 subject

The biggest disadvantage of CT is related to its use of high doses of ionizing radiation, hazards of intravenous contrast, lack of portability of equipment and its relatively high cost. An average abdominal CT scan has a dose of 10 mSv, which is equivalent to 500 chest X-rays or the equivalent to 3 years of background radiation.⁴⁶ In COPD, there is a need for following the patients serially over years for evaluating disease progression and response to treatment which means getting regular CT scans and

exposing the patients to high levels of ionizing radiation. There is a lot of concern about exposing the patients to high amounts of ionizing radiation since there is an increased risk of radiation-induced cancer from cumulative dose related to repeat CT scans.⁵⁴ Assessment of emphysema using CT scans also has certain other limitations like low specificity, low sensitivity in the evaluation of mild disease and considerable inter-observer variability in the interpretation of the findings.⁵⁵

1.5.3 Nuclear Medicine

Nuclear medicine involves the administration of small amounts of compounds labeled with radioactivity (radionuclides) that are used to provide diagnostic information in a wide range of diseases. It involves injecting a compound into the body which is labeled with a gamma-ray-emitting or positron-emitting radionuclide. The radio labeled compound is called a radio-pharmaceutical, or more commonly as tracer or radiotracer. When the radionuclide decays, it emits gamma rays or high-energy photons. These gamma rays or photons have sufficient energy so that they can exit the body without being scattered or attenuated.⁵⁶ Gamma cameras are attached around the bore of the scanner which can detect these rays or photons and form an image of the distribution of the radionuclide.⁵⁶ There are two main classes of nuclear medicine imaging: single photon imaging [which includes scintigraphy and single photon emission computed tomography (SPECT)] and positron imaging [positron emission tomography (PET)].

Scintigraphy uses radionuclides and gamma cameras to form two-dimensional images and can be thought of as being the nuclear medicine equivalent of a chest X-ray. Lung ventilation scintigraphy can be performed using radioactive gases⁵⁷ or labeled aerosols⁵⁸. The radioactive gases most commonly used for lung scintigraphy are xenon and krypton (^{133}Xe , ^{127}Xe and $^{81\text{m}}\text{Kr}$).⁵⁷ The images formed are a two-dimensional projection of the organ being studied. Although planar scintigraphy imaging is still commonly used to study pulmonary ventilation and perfusion, the introduction of the more advanced three-dimensional SPECT about 20 years ago made scintigraphy obsolete in several fields.

SPECT is similar to scintigraphy and can be thought of the CT equivalent of nuclear medicine. Multiple projections (scintigraphs) are acquired at different gamma

camera positions and all the images are reconstructed into a volume which can then be analyzed on a slice by slice basis. This enables cross-sectional images to be reconstructed, providing the depth information missing from planar scintigraphy. Some of the radioactive isotopes used for SPECT are ^{133}Xe , ^{127}Xe , $^{81\text{m}}\text{Kr}$ and a particular aerosol: Technegas, which is called as “pseudo-gas” because of its very small particle size, giving it properties similar to that of a gas.^{59,60} SPECT can be used to analyze ventilation and perfusion in the lungs. Matching of ventilation and perfusion is critical for efficient gas exchange and therefore oxygen supply to the tissue.⁶¹ Ventilation can be studied using various tracer gases like ^{133}Xe or technetium 99m ($^{99\text{m}}\text{Tc}$).^{62,63} Evaluation of wash-in, breath-hold and wash-out phases using a tracer gas can help in detection of functional abnormalities in lung volumes and study ventilation patterns, thus making it sensitive to gas trapping and areas of high resistance within the bronchial tree.^{62,63}

It is critical to study the perfusion pattern along with the ventilation pattern because without perfusion, gas exchange cannot happen even if there is perfect ventilation. The most common radiopharmaceuticals used for perfusion lung imaging are $^{99\text{m}}\text{Tc}$ labeled macro-aggregated albumin (MAA).⁴⁷ Prior to the scan the radio-labeled particles of MAA, marked with $^{99\text{m}}\text{Tc}$ are injected into the peripheral vein.⁵⁷ These particles are 15-100 μm in size and get lodged in the pulmonary capillaries and pre-capillary arterioles as they move along in the blood stream. The particle distribution accurately illustrates regional perfusion. It is critical to account for the number of particles given to the patient. A minimum of 60000 particles are required to obtain an even distribution of activity reflecting regional perfusion.⁶⁴ Normally, about 400,000 labeled particles are injected.⁵⁷ Bearing in mind that there are over 280 billion pulmonary capillaries and 300 million pre-capillary arterioles, the routinely administered particles will result in the blockage of only a small fraction of pulmonary vessels.⁵⁷ MAA is eventually broken down by the body and the obstruction in the arterioles will be removed and normal blood supply will resume. Since $^{99\text{m}}\text{Tc}$ is radioactive,⁶⁵ a radiation dose is given to the subject with each SPECT scan. A ventilation scan with $^{99\text{m}}\text{Tc}$ has an effective dose between 0.1 - 0.6 mSv, depending on the protocol and a perfusion scan has an effective dose of 1.0 mSv.⁶⁶ A single gamma ray is emitted when each of the isotopes

used in the scan undergoes decay which is then detected by the gamma camera and the image is reconstructed.

Similar to SPECT imaging, positron emission tomography (PET) images contain structural and functional information of an organ acquired from decaying nucleotides by emission of photons. PET involves the administration of a radioisotope that decays by emitting a positron. The positron annihilates with an electron producing two 511-keV anti parallel photons.⁵⁷ The two photons have to travel 180 degrees from each other in order to conserve momentum.⁶⁷ Radionucleotides used in PET imaging are ^{11}C , ^{13}N , ^{15}O , ^{18}F , ^{19}Ne and ^{68}Ga .⁶⁸ Fluorodeoxyglucose (^{18}F FDG) is the most widely used PET tracer in clinical practice as it has the longest half life (110 minutes) among all the elements used for PET.⁶⁸ During a scan the patient lies in a supine position in the bore of the scanner which is completely surrounded by gamma cameras. When an annihilation event happens, the emitted photons travel in opposite directions and strike the gamma cameras at the opposite side of the bore. There is usually a difference in the arrival times of these two photons as the distance they have to travel to get to the cameras is not identical, unless the annihilation happens exactly at the bore of the scanner. The difference in arrival times of anti-parallel photons is used to localize the position of the annihilation and spatially identify the areas of annihilation.⁶⁷ Based on all the annihilation data, a computer algorithm can construct the PET image.

1.5.4 Magnetic Resonance Imaging

Magnetic Resonance Imaging (MRI) is a powerful, noninvasive imaging modality that has experienced rapid growth over the last 10-15 years. MRI does not use ionizing radiation to produce images and hence does not give a radiation dose to the patients like CT, SPECT or PET. MRI is based on the fact that when hydrogen nuclei are placed in a magnetic field and stimulated by radio waves of a particular frequency, they emit some of the absorbed energy in the form of radio signals. These signals can be used to create an image.⁶⁹ The advantages of MRI compared to CT are the lack of ionizing radiation; increased soft tissue contrast; the ability to directly image in coronal, sagittal or oblique planes as well as the transverse plane and the intrinsic contrast in the blood vessels as a result of flow phenomenon.

Pulmonary imaging using Conventional Proton (^1H) MRI

The lung is the most difficult organ to image using the conventional ^1H MRI.^{70,71} Problems associated with lung imaging include intrinsically low hydrogen proton density within the lung, local field inhomogeneities and cardiac and respiratory motion.⁷² Approximately 70% of the healthy lung is filled with air, which has minimal hydrogen proton density, making it extremely difficult to acquire any structural and function information using conventional proton MRI.⁷² On account of the vastly different properties between air and tissue, the countless interfaces between air and tissue generate susceptibility artifacts that result in a loss of signal of fine structures such as alveolar septae.⁷² Magnetic susceptibility is the measure of the strength of the magnetic field that the external magnetic field creates in a material. Susceptibility artifacts occur as a result of microscopic gradients or variations in magnetic field strength that occur near the interface of substances of different magnetic susceptibility such as air and tissue. The result is the formation of bright and dark areas with spatial distortion of surrounding anatomy. Cardiac and respiratory motion also causes motion artifacts in the images due to the relatively large image acquisition time.⁷⁰ The motion artifacts in the images can be minimized by acquiring the MRI under breath-hold conditions, although this means severe constraints on the duration of image acquisition. **Figure 1-10** shows a conventional proton MRI center slice of the lung. As can be observed, the lungs appear as two “black holes” on the MRI which makes it difficult to extract functional or structural information about lung anatomy from the images. However, recently there have been developments that have led to the mitigation of these problems.



Figure 1.10 Conventional proton MRI of the lung
Pulse sequence used is fast spoiled gradient-recalled-echo sequence with a 40cm x 40cm FOV

Some of the new techniques developed recently are ultra-short echo time (UTE) MRI,⁷³⁻⁷⁵ oxygen-enhanced MRI^{28,76} and Fourier decomposition methods⁷⁷. In human subjects, ultrashort echo delay (TE) gradient-echo sequence has been shown to increase the lung parenchyma signal intensity.⁷⁸ The problem with conventional MRI is that due to the large magnetic field inhomogeneities, the apparent transverse relaxation time $T2^*$ is very short which makes conventional echo-based pulse sequences inadequate for acquiring signal from the lung parenchyma.⁷⁹ The amount of signal acquired after the TE with conventional gradient-echo (TE=15 msec) or spin-echo (TE= 20 msec) sequences is minimal after the conventional MRI systems begin to operate in receive mode.⁷³ However this problem can be overcome with faster pulse sequences like UTE. It has been shown that lung MRI images with diagnostic quality comparable to that of CT can be acquired in cystic fibrosis (CF) patients using short TE pulse sequences.⁸⁰ Pulse sequences that employ shorter TE generally give higher signal intensity as compared with conventional pulse sequences that use longer TE. In oxygen-enhanced MRI, inhaled molecular oxygen is used as a contrast agent for visualizing the transfer of oxygen across

the alveolus into the pulmonary vasculature. Initial studies with oxygen enhanced MRI in patients with emphysema showed ventilation defects corresponding to bullous changes in the lungs.²⁸ This method has been able to show significant differences between subjects with and without emphysema and has an excellent correlation with FEV₁ and DL_{CO}.^{28,81} Oxygen-enhanced MRI has been able to show differences in regional ventilation in human subjects. Fourier decomposition in proton MRI is another imaging method that has been used for non-contrast-enhanced regional lung perfusion and ventilation studies.⁷⁷ It has also been shown that there is qualitative agreement in the assessment of regional lung ventilation and perfusion between Fourier decomposition proton MR imaging and conventional SPECT/CT in an animal model.⁸² High resolution ventilation distribution maps have been characterized with this method.⁸³ All these methods have undergone rapid development in the past few years and hold promise in the future. Another method that has been extensively used to study the structural and functional pulmonary pathology has been hyperpolarized noble gas MRI.

Hyperpolarized Noble Gas MRI

Hyperpolarized noble gas MRI had been used over the last 2 decades to study lung structure and function. This method was first developed by Albert and colleagues in 1994.⁸⁴ In conventional MRI, the signal intensity of the image depends on the total magnetization in the chosen sample volume element. When a sample containing protons is kept in an external magnetic field, all the protons line up either in the parallel or the anti-parallel direction to the magnetic field. The number of protons lined up with the field is slightly higher than that of protons lined up against the field. The ratio of the number of protons lined up with the field to that of the number of protons lined up against the field is called the polarization and in large magnetic fields, thermal-equilibrium polarizations reach close to 10^{-5} meaning that the probability of excess spins being aligned with the field is about 1 in 100000. But with the massive number of protons in the human body, even this minute probability is enough to get good quality images. However, for inhaled contrast agents, the concentration is not enough to be used in conventional high-speed, high-resolution MR scanners.⁸⁴ In hyperpolarized noble gases, the polarization is boosted before the patient inhales the gas in a process known as

hyperpolarization. This process allows for better signal from the inhaled contrast agent and gives better quality images by increasing the polarization of the gas by four to five orders of magnitude.⁸⁵ The polarization of ^{129}Xe and other spin $\frac{1}{2}$ noble gases can be enormously enhanced through a process known as spin-exchange with an optically pumped alkali metal vapour such as rubidium (Rb). During optically pumping, circularly polarized laser light is directed into a glass cell containing a vapour of Rb and the noble gas. This causes a transfer of angular momentum from the light to the electrons of the Rb and the Rb atoms are said to be polarized. When these Rb atoms collide with the noble gas atoms, there is a transfer of angular momentum from the Rb to the noble gas. The transfer of angular momentum happens from the electron spins of the Rb to the nuclear spins of the noble gas. The wavelength of light required to polarize the electrons in Rb and get the hyperpolarization process started is 794.8 nm.⁸⁵ Although the first experiments in hyperpolarized gas MRI were done using ^{129}Xe gas,⁸⁴ ^3He has been the contrast agent of choice since then due to the nearly 3-fold gyromagnetic ratio of ^3He (^3He :32.4MHz/T, ^{129}Xe : 11.8 MHz/T)⁸⁶ and higher enrichment, both of which lead better signal with ^3He than ^{129}Xe .

Hyperpolarized ^3He MRI has been used to study the structural and functional changes in diseases like COPD,^{3,5,87-91} asthma,⁹²⁻¹⁰⁰, CF¹⁰¹⁻¹⁰³ and radiation induced lung injury (RILI),^{104,105} lung cancer¹⁰⁶ and lung transplant¹⁰⁷⁻¹⁰⁹. The main application of hyperpolarized noble gas lung imaging is to study the structural and functional features of the lung, quantify these measurements and monitor the changes longitudinally. The two main measurements used for these applications are ventilation defect percent (VDP)^{110,111} and apparent diffusion coefficient (ADC)^{3,98,112}. **Figure 1.11** shows hyperpolarized ^3He MRI images for a healthy volunteer (A), subject with COPD (B), asthma (C) and CF (D).

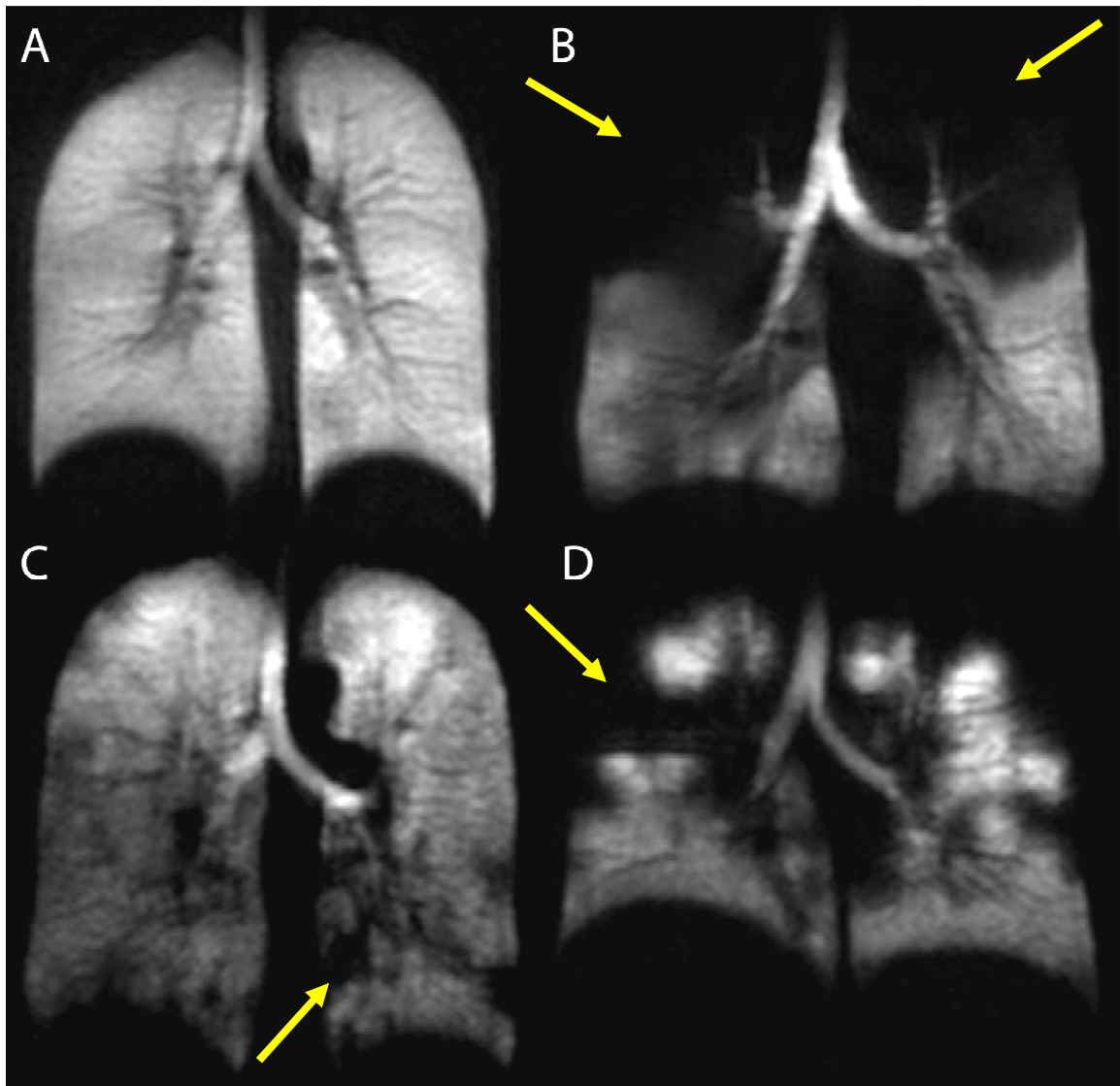


Figure 1.11 Hyperpolarized ^3He MRI images

(A) 26 year old female healthy volunteer with $\text{FEV}_{1\% \text{pred}} = 92$ and $\text{FEV}_1/\text{FVC} = 91$

(B) 77 year old female stage 3 COPD subject with $\text{FEV}_{1\% \text{pred}} = 50$ and $\text{FEV}_1/\text{FVC} = 50$

(C) 50 year old female asthma subject with $\text{FEV}_{1\% \text{pred}} = 71$ and $\text{FEV}_1/\text{FVC} = 68$

(D) 38 year old male CF subject with $\text{FEV}_{1\% \text{pred}} = 49$ and $\text{FEV}_1/\text{FVC} = 55$

The yellow arrows indicate regions of abnormal ventilation called ventilation defects

Ventilation defect percent (VDP) is the measurement of the percentage of the lung that is not being ventilated. “Defects” in the lungs are the areas of the lungs that appear dark in a hyperpolarized noble gas MRI and represent regions of the lungs that are hypo-ventilated or not ventilated at all. These regions have been highlighted using arrows in **Figure 1.11**. The earliest pulmonary imaging study using ^3He MRI studied a single healthy volunteer and showed that ^3He MRI images were able to show a sharp demarcation of the lungs against the diaphragm, heart, chest wall and blood vessels which do not give any signal.¹¹³ This study also showed that the signal intensity within the air spaces was proportional to the concentration of the ^3He gas and hence proportional to the actual ventilation within that region of the lungs.¹¹³ Bachert *et al.* showed that the signal distribution in a healthy volunteer was highly homogeneous within the lungs with a signal void for vascular and cardiac structures.¹¹⁴ This study also suggested that ^3He MRI could be a viable alternative to the established methods for pulmonary imaging all of with used ionizing radiation.¹¹⁴ The first multi-subject study using ^3He MRI was performed by Kauczor *et al.* who studied static ventilation images obtained using ^3He MRI in healthy volunteers as well as subjects with pulmonary diseases.¹¹⁵ Kauczor *et al.* observed that there was homogeneous signal intensity over the lungs and hence uniform ventilation for the healthy volunteers. In subjects with COPD and other lung conditions, they found that the signal intensity was highly heterogeneous with the presence of large wedge-shaped “ventilation defects”. This study demonstrated that it was possible to distinguish between healthy subjects and patients suffering from pulmonary diseases using hyperpolarized noble gas MRI. Subsequently there were studies that found good correlation between ventilation defects observed with hyperpolarized ^3He and xenon-133 scintigraphy.^{116,117} Studies have also shown good correlation between ventilation defect scores assessed using ^3He MRI and $^{81\text{m}}\text{Kr}$ scintigraphy for a group of healthy subjects and COPD patients.¹¹⁸ The defect scores calculated using ^3He MRI were also found to be well correlated with high resolution computed tomography (HRCT) and pulmonary function tests.¹¹⁸ ^3He MRI was shown to be more sensitive than CT at detecting ventilation defects in lung transplant candidates.¹¹⁹ For CF patients, McMahon *et al.* found a strong correlation between ^3He MRI and HRCT measurements and between ^3He MRI measurements and FEV₁ and FVC.¹²⁰

Other studies have also found a good correlation between ^3He MRI measurements and the gold standard for pulmonary imaging- CT as well as ^3He MRI measurements and spirometry.^{91,121,122} The safety profile of hyperpolarized ^3He gas has also been studied and found to be safe for administration to healthy subjects, heavy smokers and those with obstructive lung disease.^{117,123,124}

Mathew *et al.* studied the reproducibility of hyperpolarized ^3He measurements in healthy volunteers and COPD subjects and found the ADC reproducibility to be high for same day as well as 7-day rescan.¹²⁵ Same-day reproducibility for ventilation defect volume (VDV) was also found to be high, and 7-day reproducibility for VDV was moderate.¹²⁵ Niles *et al.* studied the reproducibility of ^3He MRI measurements in subjects with exercise induced bronchoconstriction and found that inter-day and inter-reader reproducibility was generally high when using the same method for image analysis at the two sites involved in the study.⁹⁷ Parraga *et al.* studied the reproducibility of ventilation defects in healthy elderly subjects and found that there was high reproducibility for same day re-scan and moderate to high reproducibility for 7-day rescan.¹²⁶ Diaz *et al.* studied the reproducibility of ^3He MRI ADC measurements in healthy volunteers and patients with emphysema for three visits over 7 days.¹²⁷ They reported high reproducibility in ADC measurements for healthy subjects as well as patients with emphysema over the three visits.¹²⁷ Parraga *et al.* studied the reproducibility of ^3He MRI ADC and ventilation defect measurements in healthy volunteers and COPD patients scanned three times, twice within 10 minutes and again 7 ± 2 days later and reported excellent same-day and 7-day ADC reproducibility as well as excellent reproducibility for same-day ventilation defect scoring and ventilation defect volume (VDV).³ Hence, hyperpolarized ^3He MRI has been shown to be a safe, non-invasive and reproducible method for studying lung structure and function and has the added advantage that it does not use ionizing radiation. However, there are certain problems with ^3He MRI that has made its clinical transition virtually impossible, at least with the technology that is available at this moment.

During the last decade or so the demand for ^3He gas has gone up tremendously and its cost has skyrocketed. The cost of 1 liter of ^3He gas has gone up from \$100 a couple of years ago to more than \$2100 according to a recent report.¹²⁸ There has been a

very high demand for ^3He gas from the US Department of Homeland Security (DHS) and Department of Energy (DOE) which has led to the US inventory of ^3He plunging from 200,000 liters in 2001 to somewhere between 43,000 – 48,000 in 2010.¹²⁸ DOE anticipates that it will have less than 8000 liters per year of ^3He to sell for the next few years while the demand is expected to rise from the 76000 liters in 2009.¹²⁸ In the wake of the 9/11 terrorist attacks, the DHS initiated a program to install more than 1400 radiation monitors at ports and border crossings which need ^3He gas to function.¹²⁹ This huge demand came at the same time that there was a dip in supply of ^3He due to a reduction of nuclear weapons production.¹²⁹ ^3He gas is produced when tritium (used to boost the yield of nuclear weapons) decays and when there was a reduction in nuclear weapons production, naturally there was a dip in tritium decay and hence production of ^3He .¹²⁹ By early 2009, the total demand for ^3He in the United States was over 213,000 liters and the supply was 45,000 liters.¹²⁹ Although theoretically tritium could be manufactured in commercial reactors to help meet the ^3He demand, the cost would be enormous- more than \$20,000 per liter by one estimate and would take more than 20 years to yield sufficient quantities of ^3He .¹²⁸ The increasing price and the lack of availability of ^3He has forced the hyperpolarized noble gas pulmonary imaging field to look for alternatives to ^3He as a contrast agent and ^{129}Xe has emerged as a good prospect.

^{129}Xe is much more abundant as compared to ^3He and is much cheaper as well. After the first study of hyperpolarized noble gas pulmonary imaging was reported using ^{129}Xe ,⁸⁴ the field transitioned to using ^3He as a contrast agent as it had a simpler and more mature polarization technology,⁸⁵ a larger magnetic moment and absence of physiological effects.¹³⁰ However, recently there has been a resurgence in ^{129}Xe MRI research leading to development of methods to improve the volume of polarized gas required for research and clinical studies as well as the polarization of the gas itself.¹³⁰⁻¹³⁴ Xenon has had a long history of being a safe contrast agent in CT studies.¹³⁵ The safety profile of ^{129}Xe MRI has also been studied and found to be safe in healthy volunteers as well as obstructive and restrictive pulmonary disease subjects.^{130,136} Recently there have been studies undertaken to compare ^3He MRI measurements with ^{129}Xe MRI measurements.¹³⁷⁻¹³⁹ Results have shown that although there are differences in the physical properties of ^3He and ^{129}Xe , ^{129}Xe is potentially an excellent alternative for ^3He

in pulmonary imaging studies. There have also been other studies to investigate pulmonary diseases using ^{129}Xe as a contrast agent.^{131,140-143} However, there have not been any studies to investigate the reproducibility of hyperpolarized ^{129}Xe MRI measurements over short periods of time.

Studying the reproducibility of ^{129}Xe measurements over short periods of time is critical in clinical study design. For example, in longitudinal clinical studies that aim to use ^{129}Xe MRI measurements of disease, it will be critical to understand variability that can be attributed to 1) image acquisition methods, including those related to the scanner (field strength, coils used) and subject compliance (breath-hold, motion), 2) image analysis methods that are observer-dependent or computationally driven, 3) site specific methodologies including hyperpolarization of the gas and the gas delivery methods, 4) potential physiological and radiological changes that occur over short periods of time. In order to be confident about the physiological differences being observed in pulmonary diseases, we first have to be confident about the reproducibility of the measurement being used to study these physiological changes.

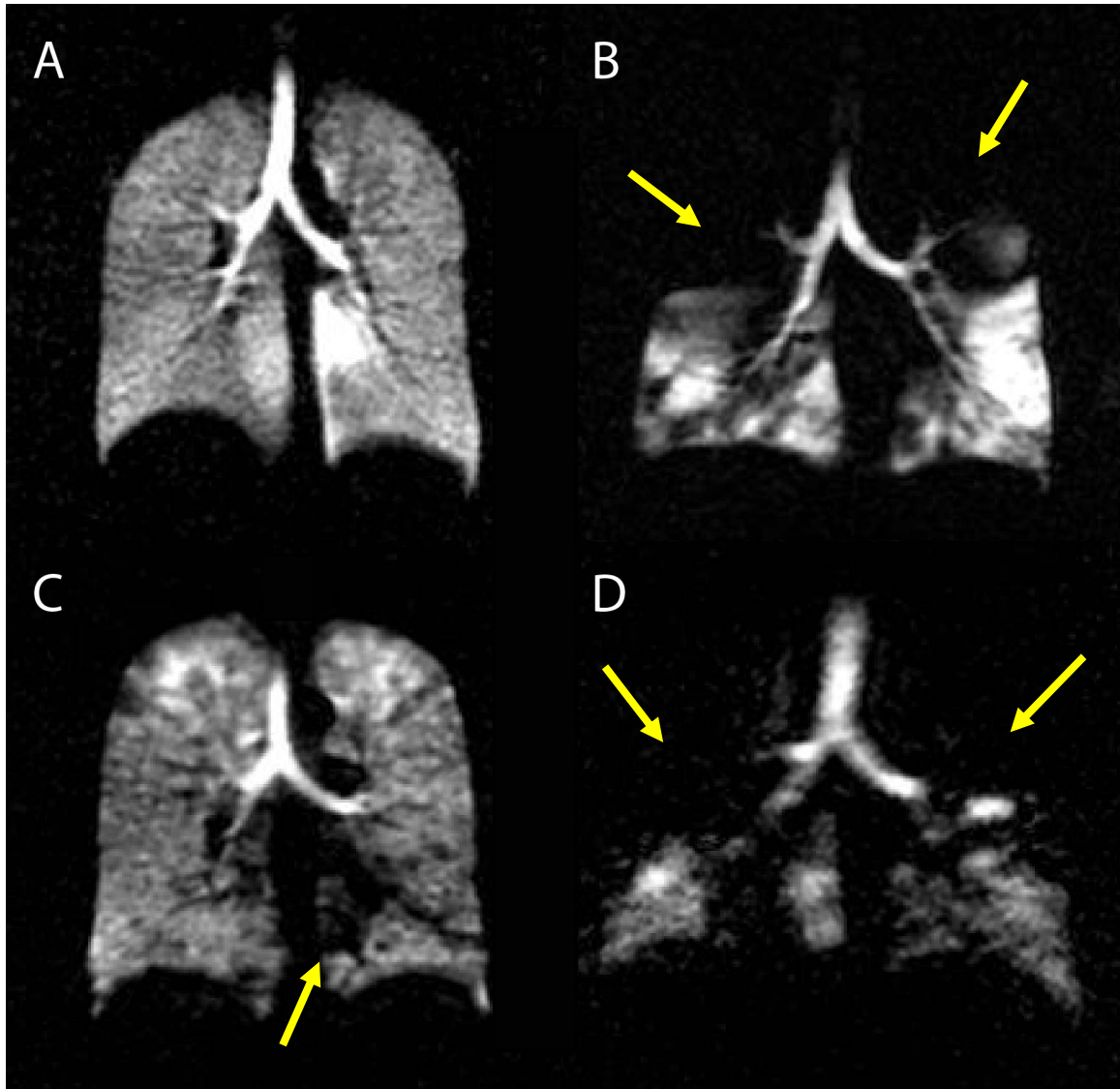


Figure 1.12 Hyperpolarized ^{129}Xe MRI images

(A) 26 year old female healthy volunteer with $\text{FEV}_{1\% \text{pred}} = 92$ and $\text{FEV}_1/\text{FVC} = 91$

(B) 77 year old female stage 3 COPD subject with $\text{FEV}_{1\% \text{pred}} = 50$ and $\text{FEV}_1/\text{FVC} = 50$

(C) 50 year old female asthma subject with $\text{FEV}_{1\% \text{pred}} = 71$ and $\text{FEV}_1/\text{FVC} = 68$

(D) 38 year old male CF subject with $\text{FEV}_{1\% \text{pred}} = 49$ and $\text{FEV}_1/\text{FVC} = 55$

The yellow arrows indicate regions of abnormal ventilation called ventilation defects

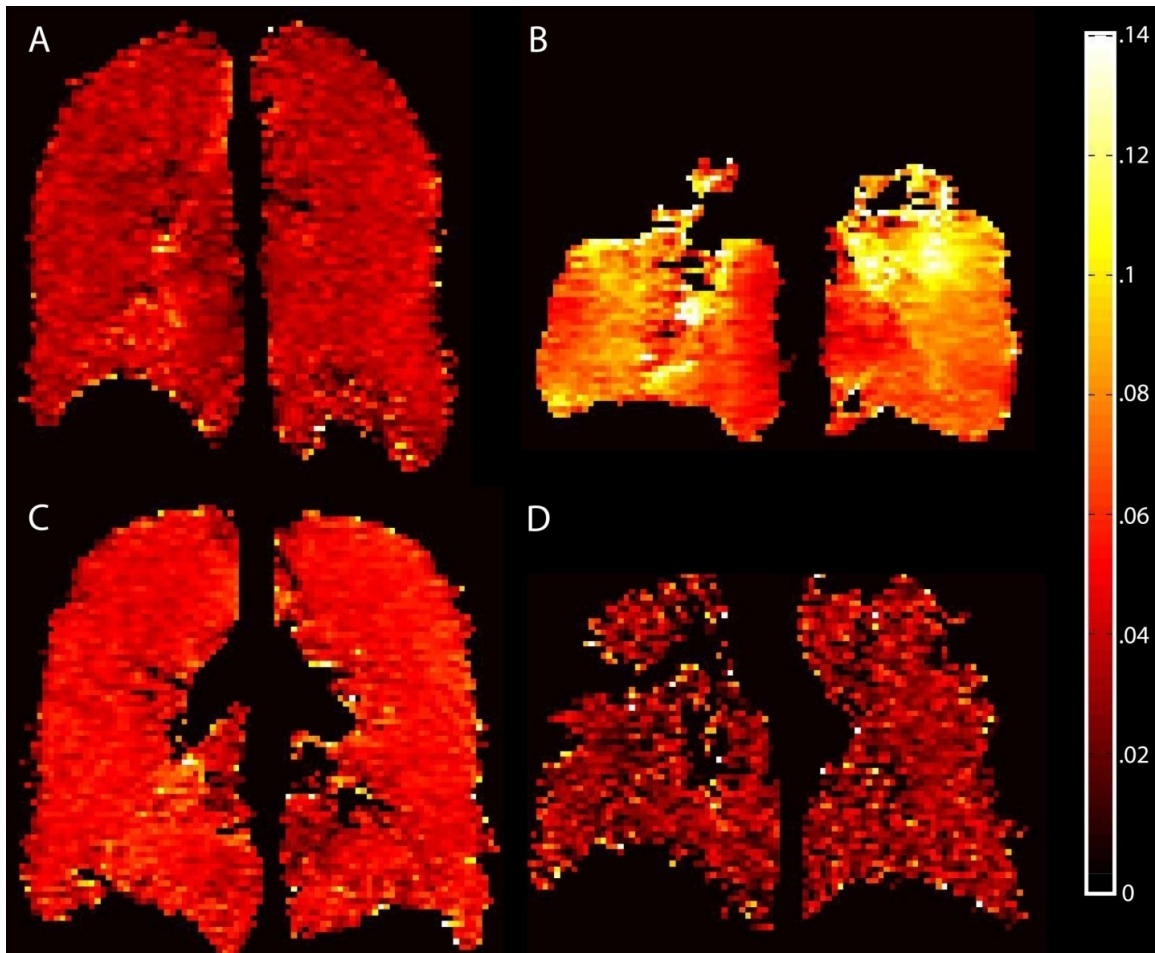


Figure 1.13 Hyperpolarized ^{129}Xe ADC maps

- (A) 26 year old female healthy volunteer with $\text{FEV}_{1\% \text{pred}} = 92$ and $\text{FEV}_1/\text{FVC} = 91$
- (B) 77 year old female stage 3 COPD subject with $\text{FEV}_{1\% \text{pred}} = 50$ and $\text{FEV}_1/\text{FVC} = 50$
- (C) 50 year old female asthma subject with $\text{FEV}_{1\% \text{pred}} = 71$ and $\text{FEV}_1/\text{FVC} = 68$
- (D) 38 year old male CF subject with $\text{FEV}_{1\% \text{pred}} = 49$ and $\text{FEV}_1/\text{FVC} = 55$

1.6 Thesis Hypotheses and Objectives

Hyperpolarized noble gas lung imaging allows us to acquire high temporal and spatial resolution structural and functional images of healthy volunteers and subjects with obstructive and restrictive pulmonary diseases. These images allow us to visualize the ventilation pattern in the lungs and identify regions of no ventilation known as “ventilation defects”. The lung microstructure can also be studied using the apparent diffusion coefficient measurement. Since the first pulmonary images using hyperpolarized noble gas were acquired in 1994, there have been significant improvements in the quality of the images acquired. There has also been development of various measurements to study the structural and functional changes taking place in the lungs after the onset of disease. However, while there have been multiple studies investigating the reproducibility of hyperpolarized ^3He MRI measurements; there have not been any to investigate the reproducibility of ^{129}Xe measurements. Hence the overarching aim of this thesis was to investigate the intra-observer and inter-observer reproducibility of hyperpolarized ^{129}Xe MRI measurements. We wanted to study the reproducibility of the VDP measurement for healthy volunteers and subjects with COPD for same day rescan and 1-week rescan. We also wanted to investigate the differences between two-dimensional (2D) and three-dimensional (3D) image acquisition methods for ^{129}Xe static ventilation images. We hypothesize that the ^{129}Xe MRI VDP will be reproducible for repeated scans over short periods of time when no physiological change is expected to occur in the lungs. We also hypothesize that there will not be any differences observed in the measurements obtained from 2D or 3D image acquisition.

Chapter 2 describes the materials and methods used for this study. Chapter 3 outlines the results of the reproducibility analysis and chapter 4 presents the discussion and conclusion for the work and also includes the study limitations and directions for future work in the study of the reproducibility of the ^{129}Xe MRI measurements.

1.7 Reference List

1. Life and Breath: Respiratory Disease in Canada. 2005.
Ref Type: Report
2. West J B *Respiratory Physiology; The Essentials*. Lippincott, Williams and Wilkins, (2008).
3. Parraga G, Ouriadov A, Evans A *et al*. Hyperpolarized ³He ventilation defects and apparent diffusion coefficients in chronic obstructive pulmonary disease: preliminary results at 3.0 Tesla. *Invest Radiol*. **42**, 384-391 (2007).
4. Hogg JC, Chu F, Utokaparch S *et al*. The nature of small-airway obstruction in chronic obstructive pulmonary disease. *N. Engl. J. Med*. **350**, 2645-2653 (2004).
5. Woods JC, Choong CK, Yablonskiy DA *et al*. Hyperpolarized ³He diffusion MRI and histology in pulmonary emphysema. *Magn Reson. Med*. **56**, 1293-1300 (2006).
6. World Health Organization. The global burden of disease: 2004 update. 2008.
Ref Type: Report
7. World Health Organization. World Health Statistics. 2008.
Ref Type: Report
8. Asthma: A Resource for Canadian Journalists. 2005.
Ref Type: Report
9. The Conference Board of Canada: Insights you can count on. 2012.
Ref Type: Report
10. Buist AS, McBurnie MA, Vollmer WM *et al*. International variation in the prevalence of COPD (the BOLD Study): a population-based prevalence study. *Lancet* **370**, 741-750 (2007).
11. Halbert RJ, Natoli JL, Gano A *et al*. Global burden of COPD: systematic review and meta-analysis. *Eur. Respir. J*. **28**, 523-532 (2006).
12. Bednarek M, Maciejewski J, Wozniak M, Kuca P & Zielinski J Prevalence, severity and underdiagnosis of COPD in the primary care setting. *Thorax* **63**, 402-407 (2008).
13. Marieb, R. N., Mallatt, J. & Wilhelm, P. B. *Human Anatomy*. Pearson Benjamin Cummings, (2004).
14. Widmaier, E. P., Raff, H. & Strang, K. T. *Vander's Human Physiology: The Mechanism of Body Function*. McGraw Hill, (2006).

15. Weibel ER & Gomez DM Architecture of the human lung. Use of quantitative methods establishes fundamental relations between size and number of lung structures. *Science* **137**, 577-585 (1962).
16. Kamel KS, Lau G & Stringer MD In vivo and in vitro morphometry of the human trachea. *Clin. Anat.* **22**, 571-579 (2009).
17. Ochs M, Nyengaard JR, Jung A *et al.* The number of alveoli in the human lung. *Am. J. Respir. Crit Care Med.* **169**, 120-124 (2004).
18. Mannino DM, Gagnon RC, Petty TL & Lydick E Obstructive lung disease and low lung function in adults in the United States: data from the National Health and Nutrition Examination Survey, 1988-1994. *Arch. Intern. Med.* **160**, 1683-1689 (2000).
19. Celli BR The importance of spirometry in COPD and asthma: effect on approach to management. *Chest* **117**, 15S-19S (2000).
20. Jeffery PK Pathology of asthma. *Br. Med. Bull.* **48**, 23-39 (1992).
21. Global Initiative for Chronic Obstructive Lung Disease: Global Strategy for the diagnosis, management, and prevention of chronic obstructive pulmonary disease. 2013.
Ref Type: Report
22. Buist, A. S. *Asthma and COPD: Basic Mechanisms and Clinical Management.* Barnes, P. J., Drazen, J., Rennard, S. & Thomson, N. (eds.), pp. 4-7 (Academic Press,2002).
23. British Thoracic Society Guidelines for the management of chronic obstructive pulmonary disease. *Thorax* **52**, 1-28 (1997).
24. Anderson AE, Jr. & Foraker AG Centrilobular emphysema and panlobular emphysema: two different diseases. *Thorax* **28**, 547-550 (1973).
25. Kim WD, Eidelman DH, Izquierdo JL *et al.* Centrilobular and panlobular emphysema in smokers. Two distinct morphologic and functional entities. *Am. Rev. Respir. Dis.* **144**, 1385-1390 (1991).
26. Mullen JB, Wright JL, Wiggs BR, Pare PD & Hogg JC Reassessment of inflammation of airways in chronic bronchitis. *Br. Med. J. (Clin. Res. Ed)* **291**, 1235-1239 (1985).
27. Niewoehner DE, Kleinerman J & Rice DB Pathologic changes in the peripheral airways of young cigarette smokers. *N. Engl. J. Med.* **291**, 755-758 (1974).

28. Eidelman D, Saetta MP, Ghezzi H *et al.* Cellularity of the alveolar walls in smokers and its relation to alveolar destruction. Functional implications. *Am. Rev. Respir. Dis.* **141**, 1547-1552 (1990).
29. Hogg JC, Macklem PT & Thurlbeck WM Site and nature of airway obstruction in chronic obstructive lung disease. *N. Engl. J. Med.* **278**, 1355-1360 (1968).
30. Anderson AE, Jr., HERNANDEZ JA, ECKERT P & Foraker AG Emphysema In Lung Macrosections Correlated With Smoking Habits. *Science* **144**, 1025-1026 (1964).
31. Kim WD, Eidelman DH, Izquierdo JL *et al.* Centrilobular and panlobular emphysema in smokers. Two distinct morphologic and functional entities. *Am. Rev. Respir. Dis.* **144**, 1385-1390 (1991).
32. Dunnill MS, Massarella GR & Anderson JA A comparison of the quantitative anatomy of the bronchi in normal subjects, in status asthmaticus, in chronic bronchitis, and in emphysema. *Thorax* **24**, 176-179 (1969).
33. Behr J & Furst DE Pulmonary function tests. *Rheumatology. (Oxford)* **47 Suppl 5**, v65-v67 (2008).
34. Crapo RO Pulmonary-function testing. *N. Engl. J. Med.* **331**, 25-30 (1994).
35. Miller MR, Hankinson J, Brusasco V *et al.* Standardisation of spirometry. *Eur. Respir. J.* **26**, 319-338 (2005).
36. Rabe KF, Hurd S, Anzueto A *et al.* Global strategy for the diagnosis, management, and prevention of chronic obstructive pulmonary disease: GOLD executive summary. *Am. J. Respir. Crit Care Med.* **176**, 532-555 (2007).
37. Hancox, B. & Whyte, K. *Pocket Guide to Lung Function Tests*. McGraw-Hill, (2006).
38. Macintyre N, Crapo RO, Viegi G *et al.* Standardisation of the single-breath determination of carbon monoxide uptake in the lung. *Eur. Respir. J.* **26**, 720-735 (2005).
39. Enright PL The six-minute walk test. *Respir. Care* **48**, 783-785 (2003).
40. Pinto-Plata VM, Cote C, Cabral H, Taylor J & Celli BR The 6-min walk distance: change over time and value as a predictor of survival in severe COPD. *Eur. Respir. J.* **23**, 28-33 (2004).
41. Jones PW St. George's Respiratory Questionnaire: MCID. *COPD.* **2**, 75-79 (2005).

42. Jones PW, Quirk FH & Baveystock CM The St George's Respiratory Questionnaire. *Respir. Med.* **85 Suppl B**, 25-31 (1991).
43. Jones PW, Quirk FH, Baveystock CM & Littlejohns P A self-complete measure of health status for chronic airflow limitation. The St. George's Respiratory Questionnaire. *Am. Rev. Respir. Dis.* **145**, 1321-1327 (1992).
44. Maki DD, Gefter WB & Alavi A Recent advances in pulmonary imaging. *Chest* **116**, 1388-1402 (1999).
45. Lisle, D. A. *Imaging for Students*. Arnold, (2001).
46. Jacob, K., Vivian, G. & Steel, J. R. *X-ray dose training: are we exposed to enough?* Elsevier, (2004).
47. Desai, S. R., Franquet, T., Hartman, T. E. & Wells, A. U. *Contributions to Key Clinical Questions: Pulmonary Imaging*. informa healthcare, (2007).
48. Bonner WM Low-dose radiation: thresholds, bystander effects, and adaptive responses. *Proc. Natl. Acad. Sci. U. S. A* **100**, 4973-4975 (2003).
49. Wei LX, Zha YR, Tao ZF *et al.* Epidemiological investigation of radiological effects in high background radiation areas of Yangjiang, China. *J. Radiat. Res.* **31**, 119-136 (1990).
50. Brenner DJ & Hall EJ Computed tomography--an increasing source of radiation exposure. *N. Engl. J. Med.* **357**, 2277-2284 (2007).
51. Reich SB, Weinshelbaum A & Yee J Correlation of radiographic measurements and pulmonary function tests in chronic obstructive pulmonary disease. *AJR Am. J. Roentgenol.* **144**, 695-699 (1985).
52. Buzug, T. M. *Computed Tomography: From Photon Statistics to modern Cone-Beam CT*. Springer, (2008).
53. Fullerton GD & Blanco E. Fundamentals of computerized tomography (CT) tissue characterization of the brain. SPIE. Application of Optical Instrumentation in Medicine IX 273, 256-266. 1981.
Ref Type: Conference Proceeding
54. Brenner DJ, Elliston CD, Hall EJ & Berdon WE Estimates of the cancer risks from pediatric CT radiation are not merely theoretical: comment on "point/counterpoint: in x-ray computed tomography, technique factors should be selected appropriate to patient size. against the proposition". *Med. Phys.* **28**, 2387-2388 (2001).
55. Litmanovich D, Boiselle PM & Bankier AA CT of pulmonary emphysema--current status, challenges, and future directions. *Eur. Radiol.* **19**, 537-551 (2009).

56. Cherry, S. R., Sorenson, J. A. & Phelps, M. E. *Physics in Nuclear Medicine*. Elsevier Health Sciences, (2012).
57. Bajc, M. & Jonson, B. *Clinical Nuclear Medicine*. (Springer,2007).
58. Taplin GV, Poe ND, Isawa T & Dore EK Radioaerosol and xenon gas inhalation and lung perfusion scintigraphy. *Scand. J. Respir. Dis. Suppl* **85**, 144-158 (1974).
59. Burch WM, Tetley IJ & Gras JL Technetium-99m 'pseudogas' for diagnostic studies in the lung. *Clin. Phys. Physiol Meas.* **5**, 79-85 (1984).
60. Burch WM, Sullivan PJ & McLaren CJ Technegas--a new ventilation agent for lung scanning. *Nucl. Med. Commun.* **7**, 865-871 (1986).
61. Fazio F & Wollmer P Clinical ventilation-perfusion scintigraphy. *Clin. Physiol* **1**, 323-337 (1981).
62. King GG, Eberl S, Salome CM, Meikle SR & Woolcock AJ Airway closure measured by a technegas bolus and SPECT. *Am. J. Respir. Crit Care Med.* **155**, 682-688 (1997).
63. Pellegrino R, Biggi A, Papaleo A *et al.* Regional expiratory flow limitation studied with Technegas in asthma. *J. Appl. Physiol* **91**, 2190-2198 (2001).
64. Heck LL & Duley JW, Jr. Statistical considerations in lung imaging with 99mTc albumin particles. *Radiology* **113**, 675-679 (1974).
65. Till JE, Hoffman FO & Dunning DE, Jr. A new look at 99 Tc releases to the atmosphere. *Health Phys.* **36**, 21-30 (1979).
66. Gray, H. W. *Practical Nuclear Medicine.*, pp. 179-204 (Springer,2005).
67. Macovski, A. *Medical Imaging Systems*. Englewood Cliffs, (1983).
68. Harris RS & Schuster DP Visualizing lung function with positron emission tomography. *J. Appl. Physiol* **102**, 448-458 (2007).
69. Cutillo, A. G. *Application of Magnetic Resonance to the Study of Lung*. Futura Publishing Company, Armonk, NY (1996).
70. Kauczor HU & Kreitner KF MRI of the pulmonary parenchyma. *Eur. Radiol.* **9**, 1755-1764 (1999).
71. Puderbach M, Hintze C, Ley S *et al.* MR imaging of the chest: a practical approach at 1.5T. *Eur. J. Radiol.* **64**, 345-355 (2007).
72. Kauczor HU, Ley-Zaporozhan J & Ley S Imaging of pulmonary pathologies: focus on magnetic resonance imaging. *Proc. Am. Thorac. Soc.* **6**, 458-463 (2009).

73. Mayo JR, MacKay A & Muller NL MR imaging of the lungs: value of short TE spin-echo pulse sequences. *AJR Am. J. Roentgenol.* **159**, 951-956 (1992).
74. Takahashi M, Togao O, Obara M *et al.* Ultra-short echo time (UTE) MR imaging of the lung: comparison between normal and emphysematous lungs in mutant mice. *J. Magn Reson. Imaging* **32**, 326-333 (2010).
75. Togao O, Tsuji R, Ohno Y, Dimitrov I & Takahashi M Ultrashort echo time (UTE) MRI of the lung: assessment of tissue density in the lung parenchyma. *Magn Reson. Med.* **64**, 1491-1498 (2010).
76. Ohno Y, Sugimura K & Hatabu H Clinical oxygen-enhanced magnetic resonance imaging of the lung. *Top. Magn Reson. Imaging* **14**, 237-243 (2003).
77. Bauman G, Puderbach M, Deimling M *et al.* Non-contrast-enhanced perfusion and ventilation assessment of the human lung by means of fourier decomposition in proton MRI. *Magn Reson. Med.* **62**, 656-664 (2009).
78. Bergin CJ, Pauly JM & Macovski A Lung parenchyma: projection reconstruction MR imaging. *Radiology* **179**, 777-781 (1991).
79. Tyler DJ, Robson MD, Henkelman RM, Young IR & Bydder GM Magnetic resonance imaging with ultrashort TE (UTE) PULSE sequences: technical considerations. *J. Magn Reson. Imaging* **25**, 279-289 (2007).
80. Failo R, Wielopolski PA, Tiddens HA *et al.* Lung morphology assessment using MRI: a robust ultra-short TR/TE 2D steady state free precession sequence used in cystic fibrosis patients. *Magn Reson. Med.* **61**, 299-306 (2009).
81. Ohno Y, Hatabu H, Takenaka D *et al.* Oxygen-enhanced MR ventilation imaging of the lung: preliminary clinical experience in 25 subjects. *AJR Am. J. Roentgenol.* **177**, 185-194 (2001).
82. Bauman G, Lutzen U, Ullrich M *et al.* Pulmonary functional imaging: qualitative comparison of Fourier decomposition MR imaging with SPECT/CT in porcine lung. *Radiology* **260**, 551-559 (2011).
83. Deimling M, Jellus V, Geiger B & Chafd'hotel C. Time Resolved Lung Ventilation Imaging by Fourier Decomposition. International Society for Magnetic Resonance in Medicine, 2639. 2008. Ref Type: Abstract
84. Albert MS, Cates GD, Driehuys B *et al.* Biological magnetic resonance imaging using laser-polarized ¹²⁹Xe. *Nature* **370**, 199-201 (1994).
85. Moller HE, Chen XJ, Saam B *et al.* MRI of the lungs using hyperpolarized noble gases. *Magn Reson. Med.* **47**, 1029-1051 (2002).

86. Albert MS & Balamore D Development of hyperpolarized noble gas MRI. *Nucl. Instrum. Methods Phys. Res. A* **402**, 441-453 (1998).
87. Kirby M, Mathew L, Wheatley A *et al.* Chronic obstructive pulmonary disease: longitudinal hyperpolarized (3)He MR imaging. *Radiology* **256**, 280-289 (2010).
88. Marshall H, Deppe MH, Parra-Robles J *et al.* Direct visualisation of collateral ventilation in COPD with hyperpolarised gas MRI. *Thorax* **67**, 613-617 (2012).
89. Mathew L, Kirby M, Etemad-Rezai R *et al.* Hyperpolarized (3)He magnetic resonance imaging: preliminary evaluation of phenotyping potential in chronic obstructive pulmonary disease. *Eur. J. Radiol.* **79**, 140-146 (2011).
90. Swift AJ, Wild JM, Fichelle S *et al.* Emphysematous changes and normal variation in smokers and COPD patients using diffusion 3He MRI. *Eur. J. Radiol.* **54**, 352-358 (2005).
91. Van Beek EJ, Dahmen AM, Stavngaard T *et al.* Hyperpolarised 3He MRI versus HRCT in COPD and normal volunteers: PHIL trial. *Eur. Respir. J.* **34**, 1311-1321 (2009).
92. Cadman RV, Lemanske RF, Jr., Evans MD *et al.* Pulmonary 3He magnetic resonance imaging of childhood asthma. *J. Allergy Clin. Immunol.* **131**, 369-376 (2013).
93. Costella S, Kirby M, Maksym GN *et al.* Regional pulmonary response to a methacholine challenge using hyperpolarized (3)He magnetic resonance imaging. *Respirology*. **17**, 1237-1246 (2012).
94. de Lange EE, Altes TA, Patrie JT *et al.* Evaluation of asthma with hyperpolarized helium-3 MRI: correlation with clinical severity and spirometry. *Chest* **130**, 1055-1062 (2006).
95. de Lange EE, Altes TA, Patrie JT *et al.* The variability of regional airflow obstruction within the lungs of patients with asthma: assessment with hyperpolarized helium-3 magnetic resonance imaging. *J. Allergy Clin. Immunol.* **119**, 1072-1078 (2007).
96. Fain SB, Gonzalez-Fernandez G, Peterson ET *et al.* Evaluation of structure-function relationships in asthma using multidetector CT and hyperpolarized He-3 MRI. *Acad. Radiol.* **15**, 753-762 (2008).
97. Niles DJ, Kruger SJ, Dardzinski BJ *et al.* Exercise-induced bronchoconstriction: reproducibility of hyperpolarized 3He MR imaging. *Radiology* **266**, 618-625 (2013).
98. Salerno M, Altes TA, Brookeman JR, de Lange EE & Mugler JP, III Rapid hyperpolarized 3He diffusion MRI of healthy and emphysematous human lungs

- using an optimized interleaved-spiral pulse sequence. *J. Magn Reson. Imaging* **17**, 581-588 (2003).
99. Tustison NJ, Altes TA, Song G *et al.* Feature analysis of hyperpolarized helium-3 pulmonary MRI: a study of asthmatics versus nonasthmatics. *Magn Reson. Med.* **63**, 1448-1455 (2010).
 100. Wang C, Altes TA, Mugler JP, III *et al.* Assessment of the lung microstructure in patients with asthma using hyperpolarized ³He diffusion MRI at two time scales: comparison with healthy subjects and patients with COPD. *J. Magn Reson. Imaging* **28**, 80-88 (2008).
 101. Kirby M, Svenningsen S, Ahmed H *et al.* Quantitative evaluation of hyperpolarized helium-3 magnetic resonance imaging of lung function variability in cystic fibrosis. *Acad. Radiol.* **18**, 1006-1013 (2011).
 102. Mentore K, Froh DK, de Lange EE *et al.* Hyperpolarized HHe 3 MRI of the lung in cystic fibrosis: assessment at baseline and after bronchodilator and airway clearance treatment. *Acad. Radiol.* **12**, 1423-1429 (2005).
 103. Sun Y, O'Sullivan BP, Roche JP *et al.* Using hyperpolarized ³He MRI to evaluate treatment efficacy in cystic fibrosis patients. *J. Magn Reson. Imaging* **34**, 1206-1211 (2011).
 104. Mathew L, Gaede S, Wheatley A *et al.* Detection of longitudinal lung structural and functional changes after diagnosis of radiation-induced lung injury using hyperpolarized ³He magnetic resonance imaging. *Med. Phys.* **37**, 22-31 (2010).
 105. Mathew L, Vandyk J, Etemad-Rezai R, Rodrigues G & Parraga G Hyperpolarized (³He) pulmonary functional magnetic resonance imaging prior to radiation therapy. *Med. Phys.* **39**, 4284-4290 (2012).
 106. Mathew L, Wheatley A, Castillo R *et al.* Hyperpolarized (³He) magnetic resonance imaging: comparison with four-dimensional x-ray computed tomography imaging in lung cancer. *Acad. Radiol.* **19**, 1546-1553 (2012).
 107. Bink A, Hanisch G, Karg A *et al.* Clinical aspects of the apparent diffusion coefficient in ³He MRI: results in healthy volunteers and patients after lung transplantation. *J. Magn Reson. Imaging* **25**, 1152-1158 (2007).
 108. Gast KK, Zaporozhan J, Ley S *et al.* (³He)-MRI in follow-up of lung transplant recipients. *Eur. Radiol.* **14**, 78-85 (2004).
 109. Zaporozhan J, Ley S, Gast KK *et al.* Functional analysis in single-lung transplant recipients: a comparative study of high-resolution CT, ³He-MRI, and pulmonary function tests. *Chest* **125**, 173-181 (2004).

110. Kirby M, Heydarian M, Svenningsen S *et al.* Hyperpolarized ^3He magnetic resonance functional imaging semiautomated segmentation. *Acad. Radiol.* **19**, 141-152 (2012).
111. Woodhouse N, Wild JM, Paley MN *et al.* Combined helium-3/proton magnetic resonance imaging measurement of ventilated lung volumes in smokers compared to never-smokers. *J. Magn Reson. Imaging* **21**, 365-369 (2005).
112. Saam BT, Yablonskiy DA, Kodibagkar VD *et al.* MR imaging of diffusion of (^3He) gas in healthy and diseased lungs. *Magn Reson. Med.* **44**, 174-179 (2000).
113. Ebert M, Grossmann T, Heil W *et al.* Nuclear magnetic resonance imaging with hyperpolarised helium-3. *Lancet* **347**, 1297-1299 (1996).
114. Bachert P, Schad LR, Bock M *et al.* Nuclear magnetic resonance imaging of airways in humans with use of hyperpolarized ^3He . *Magn Reson. Med.* **36**, 192-196 (1996).
115. Kauczor HU, Ebert M, Kreitner KF *et al.* Imaging of the lungs using ^3He MRI: preliminary clinical experience in 18 patients with and without lung disease. *J. Magn Reson. Imaging* **7**, 538-543 (1997).
116. Altes TA, Rehm PK, Harrell F *et al.* Ventilation imaging of the lung: comparison of hyperpolarized helium-3 MR imaging with Xe-133 scintigraphy. *Acad. Radiol.* **11**, 729-734 (2004).
117. de Lange EE, Mugler JP, III, Brookeman JR *et al.* Lung air spaces: MR imaging evaluation with hyperpolarized ^3He gas. *Radiology* **210**, 851-857 (1999).
118. Stavngaard T, Sogaard LV, Mortensen J *et al.* Hyperpolarized ^3He MRI and ^{81}mKr SPECT in chronic obstructive pulmonary disease. *Eur. J. Nucl. Med. Mol. Imaging* **32**, 448-457 (2005).
119. Gast KK, Viallon M, Eberle B *et al.* MRI in lung transplant recipients using hyperpolarized ^3He : comparison with CT. *J. Magn Reson. Imaging* **15**, 268-274 (2002).
120. McMahan CJ, Dodd JD, Hill C *et al.* Hyperpolarized ^3He magnetic resonance ventilation imaging of the lung in cystic fibrosis: comparison with high resolution CT and spirometry. *Eur. Radiol.* **16**, 2483-2490 (2006).
121. Ley S, Zaporozhan J, Morbach A *et al.* Functional evaluation of emphysema using diffusion-weighted ^3He -magnetic resonance imaging, high-resolution computed tomography, and lung function tests. *Invest Radiol.* **39**, 427-434 (2004).
122. Zaporozhan J, Ley S, Gast KK *et al.* Functional analysis in single-lung transplant recipients: a comparative study of high-resolution CT, ^3He -MRI, and pulmonary function tests. *Chest* **125**, 173-181 (2004).

123. Leawoods, J. C., Yablonskiy, D. A., Saam, B., Gierada, D. S. & Conradi, M. S. *Concepts in Magnetic Resonance.*, pp. 277-293 (John Wiley & Sons, Inc.,2001).
124. Lutey BA, Lefrak SS, Woods JC *et al.* Hyperpolarized ^3He MR imaging: physiologic monitoring observations and safety considerations in 100 consecutive subjects. *Radiology* **248**, 655-661 (2008).
125. Mathew L, Evans A, Ouriadov A *et al.* Hyperpolarized ^3He magnetic resonance imaging of chronic obstructive pulmonary disease: reproducibility at 3.0 tesla. *Acad. Radiol.* **15**, 1298-1311 (2008).
126. Parraga G, Mathew L, Etemad-Rezai R, McCormack DG & Santyr GE Hyperpolarized ^3He magnetic resonance imaging of ventilation defects in healthy elderly volunteers: initial findings at 3.0 Tesla. *Acad. Radiol.* **15**, 776-785 (2008).
127. Diaz S, Casselbrant I, Piitulainen E *et al.* Hyperpolarized ^3He apparent diffusion coefficient MRI of the lung: reproducibility and volume dependency in healthy volunteers and patients with emphysema. *J. Magn Reson. Imaging* **27**, 763-770 (2008).
128. Kramer D. DOE begins rationing helium-3. 22-24. 2010. physicstoday. Ref Type: Report
129. Caught by Surprise: Causes and Consequences of the Helium -3 Supply Crisis. 2010. Washington DC, US Government Printing Office. Ref Type: Report
130. Driehuys B, Martinez-Jimenez S, Cleveland ZI *et al.* Chronic obstructive pulmonary disease: safety and tolerability of hyperpolarized ^{129}Xe MR imaging in healthy volunteers and patients. *Radiology* **262**, 279-289 (2012).
131. Cleveland ZI, Cofer GP, Metz G *et al.* Hyperpolarized Xe MR imaging of alveolar gas uptake in humans. *PLoS. One.* **5**, e12192 (2010).
132. Hersman FW, Ruset IC, Ketel S *et al.* Large production system for hyperpolarized ^{129}Xe for human lung imaging studies. *Acad. Radiol.* **15**, 683-692 (2008).
133. Mugler JP, III, Altes TA, Ruset IC *et al.* Simultaneous magnetic resonance imaging of ventilation distribution and gas uptake in the human lung using hyperpolarized xenon-129. *Proc. Natl. Acad. Sci. U. S. A* **107**, 21707-21712 (2010).
134. Ruset IC, Ketel S & Hersman FW Optical pumping system design for large production of hyperpolarized. *Phys. Rev. Lett.* **96**, 053002 (2006).
135. Latchaw RE, Yonas H, Pentheny SL & Gur D Adverse reactions to xenon-enhanced CT cerebral blood flow determination. *Radiology* **163**, 251-254 (1987).

136. Shukla Y, Wheatley A, Kirby M *et al.* Hyperpolarized ^{129}Xe magnetic resonance imaging: tolerability in healthy volunteers and subjects with pulmonary disease. *Acad. Radiol.* **19**, 941-951 (2012).
137. Kirby M, Svenningsen S, Owrangi A *et al.* Hyperpolarized ^3He and ^{129}Xe MR imaging in healthy volunteers and patients with chronic obstructive pulmonary disease. *Radiology* **265**, 600-610 (2012).
138. Kirby M, Svenningsen S, Kanhere N *et al.* Pulmonary ventilation visualized using hyperpolarized helium-3 and xenon-129 magnetic resonance imaging: differences in COPD and relationship to emphysema. *J. Appl. Physiol* **114**, 707-715 (2013).
139. Svenningsen S, Kirby M, Starr D *et al.* Hyperpolarized He and Xe MRI: Differences in asthma before bronchodilation. *J. Magn Reson. Imaging* (2013).
140. Dregely I, Mugler JP, III, Ruset IC *et al.* Hyperpolarized Xenon-129 gas-exchange imaging of lung microstructure: first case studies in subjects with obstructive lung disease. *J. Magn Reson. Imaging* **33**, 1052-1062 (2011).
141. Kaushik SS, Cleveland ZI, Cofer GP *et al.* Diffusion-weighted hyperpolarized ^{129}Xe MRI in healthy volunteers and subjects with chronic obstructive pulmonary disease. *Magn Reson. Med.* **65**, 1154-1165 (2011).
142. Mugler JP, III & Altes TA Hyperpolarized ^{129}Xe MRI of the human lung. *J. Magn Reson. Imaging* **37**, 313-331 (2013).
143. Virgincar RS, Cleveland ZI, Sivaram KS *et al.* Quantitative analysis of hyperpolarized (^{129}Xe) ventilation imaging in healthy volunteers and subjects with chronic obstructive pulmonary disease. *NMR Biomed.* (2012).

CHAPTER 2: MATERIALS AND METHODS

Chapter 2 provides details about the study design and the study subjects. Details about the pulmonary function tests as well as image acquisition and data analysis methods are provided to help the reader better understand how the results presented in chapter 3 were acquired and analyzed.

2.1 Study Subjects

Five healthy volunteers (HV) and ten COPD subjects were enrolled from the general population and a local tertiary health care center. All subjects provided informed written consent to the study protocol approved by the local research ethics board and Health Canada, and the study was compliant with the Personal Information Protection and Electronics Documents Act (PIPEDA, Canada) and the Health Insurance Portability and Accountability Act (HIPAA, USA). COPD subjects required a disease diagnosis of at least 1 year, having had a smoking history of at least 10 pack-years and fewer than three COPD exacerbations within the previous 12 months. COPD subjects were categorized according to the GOLD criteria.¹ HV were included if they had no history of chronic respiratory disease, less than one pack-year smoking history, FEV₁ greater than 80% predicted, FEV₁ divided by the FVC or FEV₁/FVC greater than 70%, and no current diagnosis or history of unstable cardiovascular disease.

Throughout the course of the study, COPD subjects were withdrawn from the study if they had experienced a COPD exacerbation or if they experienced a drop in arterial blood oxygen levels below 80% for 15 continuous seconds during MRI procedures as monitored using pulse oximetry. After providing informed written consent, the subjects underwent physical examination and their vital signs were recorded followed by spirometry and plethysmography. All subjects were screened for MRI safety and coil compatibility before the MRI session and at all times during the MR scan, an expert was present in the MRI suite with the subject to administer the gas to the subject and coach their breathing maneuvers. The subjects breathed in 1L of gas from FRC to ensure uniformity in lung volume for all the scans. This was useful in eliminating errors

in measurements due to differences in lung volume for the same subject due to differences in the volume of inhaled gas.

2.2 Pulmonary Function Tests

Spirometry was performed using an *ndd EasyOne* spirometer (ndd Medizintechnik AG, Zurich, CH) (**Figure 1.6.A**) measuring FEV₁ and FVC with a minimum of three acceptable spirometry maneuvers with the best FEV₁ and FVC selected for analysis according to American Thoracic Society (ATS) guidelines² (**Figure 1.6.B**). Whole body plethysmography was performed using a MedGraphics' Elite Series stand-alone body plethysmograph (MedGraphics Corporation. 350 Oak Grove Parkway St. Paul, MN, USA) (**Figure 1.6.C**) for the measurement of total lung capacity (TLC), inspiratory capacity (IC), residual volume (RV) and functional residual capacity (FRC). A body plethysmograph attached to the Medgraphics gas analyzer was used to measure the DL_{CO}.

2.3 Image Acquisition

¹²⁹Xe MRI was performed on a whole body 3.0 Tesla Discovery 750 MR system (General Electric Health Care (GEHC), Milwaukee WI) with broadband imaging capability as previously described.³ Hyperpolarized ¹²⁹Xe MRI was acquired using a custom-made, unshielded quadrature-asymmetric bird-cage coil tuned to 35.34MHz, as previously described.^{4,5}

¹²⁹Xe gas (86% enriched) was polarized to 10-60% using a turn-key polarizer (XeBox-E10, Xemed LLC, New Hampshire, USA). Doses of hyperpolarized ¹²⁹Xe gas were dispensed directly into the pre-rinsed 1.0L Tedlar[®] bags pre-filled with ⁴He to generate a 50/50 mixture of ⁴He gas and hyperpolarized ¹²⁹Xe gas. Polarization of the diluted dose was measured using a Polarimeter (GEHC, Durham, NC).

During the scanning visits, diffusion-weighted (DW) and non-diffusion-weighted (NDW) images were acquired during a breath-hold of a 1L ¹²⁹Xe/⁴He mixture inhaled from FRC. NDW images were obtained using a two-dimensional fast gradient recalled echo (2D FGRE) sequence with centric phase-encoding ordering as shown in **Figure 2.1.A**. Two interleaved images (16s total data acquisition, TE/TR/flip angle = 10

ms/13.5 ms/9°, bandwidth = 31.25 kHz, FOV = 40 x 40 cm, matrix 128 x 80, 7 slices, 30 mm slice thickness, 0 gap), with and without additional diffusion sensitization (G = 2.90 G/cm, gradient rise and fall time = 0.5 ms, gradient separation = 2 ms, gradient duration = 2.0 ms, diffusion time = 5 ms) were acquired.

During the same visit, ^{129}Xe MRI coronal static ventilation (SV) images were also acquired during a breath-hold of a 1L $^{129}\text{Xe}/^4\text{He}$ mixture inhaled from FRC (14s data acquisition, TE/TR/flip angle = 1.50 ms/6.7 ms/1°, bandwidth = 15.63 kHz, FOV = 40 × 40 cm, matrix 128 × 128, 14 slices, 15 mm slice thickness, 0 gap) using a three-dimensional fast gradient recalled echo 3D FGRE sequence as shown in **Figure 2.1.B**.

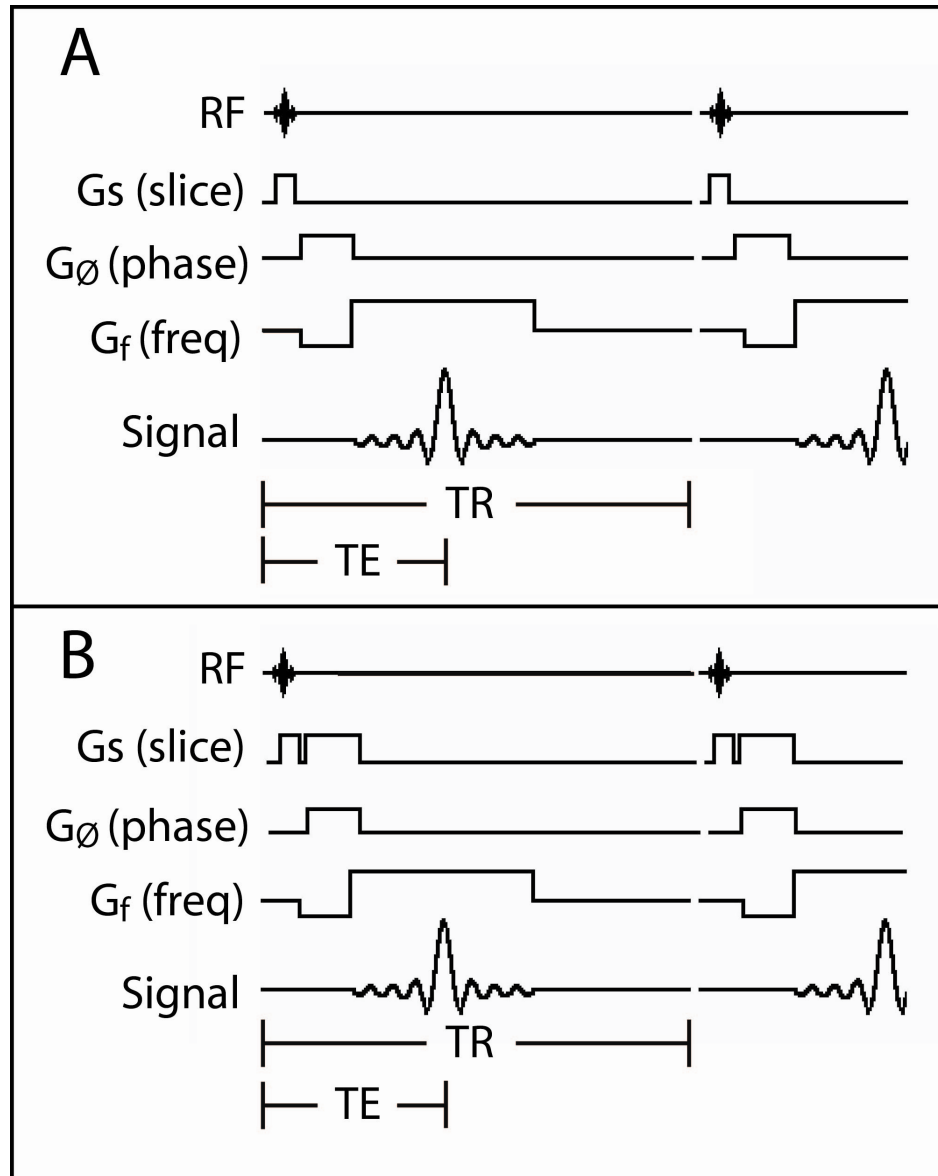


Figure 2.1 FGRE pulse sequences

(A) 2D FGRE, (B) 3D FGRE, G_s = slice select gradient, G_ϕ = phase encode gradient, G_f = frequency encode gradient, TR= repetition time, TE= echo time. Adapted from Hornak, J.P, The Basics of MRI¹⁰

The NDW images were used to assess the ^{129}Xe static ventilation reproducibility between the repeated scans. The NDW images were acquired at multiple time-points and hence were used to study the reproducibility of ^{129}Xe VDP over multiple time-points. Subjects were instructed to perform normal tidal breathing from room air before inhaling

the entire contents of the 1L dose bag mixture from FRC and perform a breath hold of 8-15 seconds. This training was important to minimize the potential for differences in the levels of inspired gas between the breath-hold scans for each subject. The entire process of acquiring the xenon static ventilation images is illustrated in **Figure 2.2**. The time frame between ^{129}Xe scans was within 2 ± 1 minute for all subjects for the same day rescan and 7 days for the three COPD subjects who returned one week later for another visit. The 3 subjects who returned for the 1-week rescan had two NDW scans done within 2 ± 1 minute of each other at the second visit. A 1-week period between scanning sessions was selected to minimize subject inconvenience and to model typical sources of variability stemming from the acquisition of the images over a short period of time because of coil positioning, subject motion and positioning changes and potential short-term physiological changes. Repeat spirometry at the second MRI visit was performed to screen for exacerbations or global disease changes that may have occurred during the 1-week scanning period.

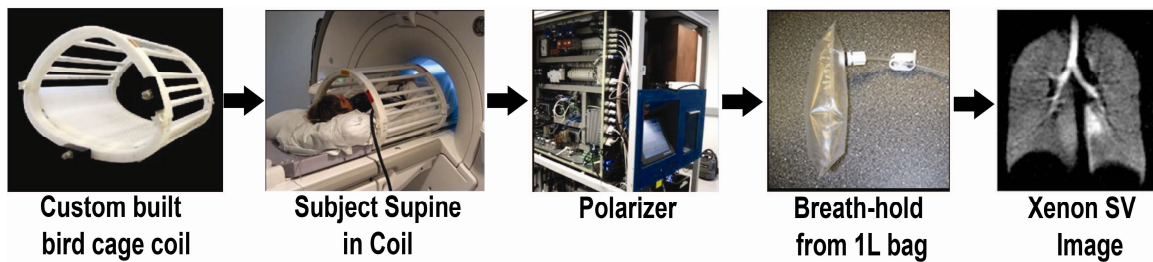


Figure 2.2 Image acquisition procedure

Subjects were instructed to lay supine in the custom built ^{129}Xe bird cage coil which was positioned inside the bore of the MRI. The ^{129}Xe gas was hyperpolarized using the polarizer and images were acquired during a breath-hold after the subjects inhale the entire contents of the bag.

For all the subjects, ^{129}Xe gas breath-holds followed standard full inspiration breath-hold ^1H MRI with subjects scanned during a 1L breath-hold of medical grade nitrogen (N_2) (Spectra Gases, Alpha, NJ) using the whole body radiofrequency (RF) coil and ^1H fast spoiled gradient-recalled-echo sequence as previously described.³

Hyperpolarized ^3He MRI was enabled using a linear bird-cage transmit/receive chest coil (RAPID Biomedical GmbH, Wuerzburg Germany). A turnkey system (HeliSpin™) was used to polarize ^3He gas to 30-40% and doses (5mL/kg body weight)

were administered in 1.0L Tedlar[®] bags diluted with N₂. Hyperpolarized ³He MRI coronal SV images and NDW images were acquired during breath-hold of a 1L ³He/N₂ mixture as previously described.³ **Figure 2.3** shows the sequence in which the scans were acquired and time-period between the scans. The time-period between the consecutive scans acquired on the same day was 2±1 minutes. The time-period between the two visits was exactly 1-week for all the 3 subjects who returned for the second visit.

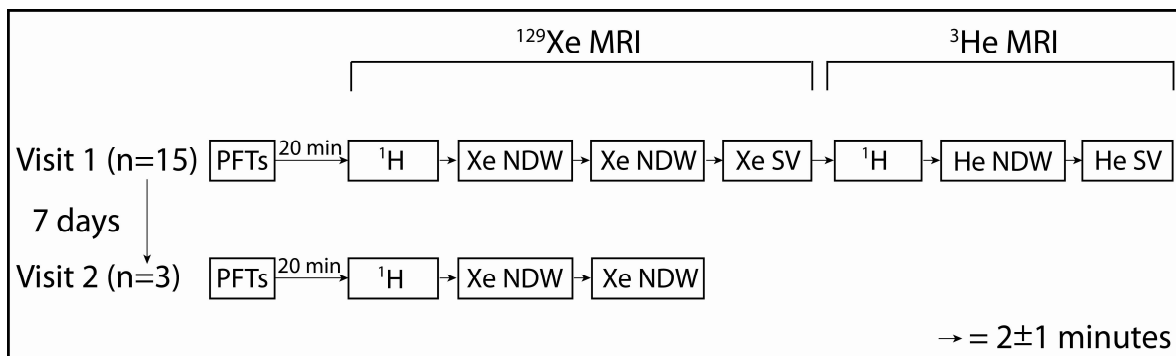


Figure 2.3 Sequence of scans acquired

¹H= proton, NDW= non-diffusion-weighted, SV= static ventilation
He= Helium-3, Xe= Xenon-129, PFTs= Pulmonary Function Tests

2.4 Image Analysis

A single expert observer analyzed the ¹²⁹Xe NDW and SV as well as the ³He NDW and SV images for regions of signal void known as ventilation defects using an in-house software developed using MATLAB R2007b (The Mathworks Inc., Natick, MA, USA) as previously described.⁶ The analysis was performed within an image visualization room with background lighting levels consistent for all image analysis sessions and the entire analysis was repeated five times (5 rounds) as shown in **Figure 2.3**. For each round of analysis, the subjects and scans were randomized to minimize the observer bias in the analysis. A period of two days was left between consecutive rounds of analysis to minimize the possibility of observer bias between rounds. To study the inter-observer reproducibility of ¹²⁹Xe MRI VDP, a second observer analyzed the repeated ¹²⁹Xe NDW and SV images once (1 round).

^{129}Xe MRI and ^3He MRI of COPD is typically characterized by heterogeneous gas distribution that is reflected in heterogeneous signal intensity for the SV and NDW images for an inspiration breath-hold scan. To compare the distribution of ^{129}Xe and ^3He gas at different time-points within the lung, segmenting the ^{129}Xe and ^3He images was based on the voxel signal intensity. A k-means clustering algorithm⁷ was used to classify the voxel intensity values into five clusters ranging from signal void (cluster 1, C1 or ventilation defect volume (VDV)) and hypo-intense (C2) to hyper-intense signal (C5). Briefly, it involved binning data points into cluster so that the data points in one cluster were as close to each other in signal intensity as possible and as far as possible from data points in other clusters. Each cluster was defined by its member objects and the centroid. The centroids were chosen and through iterations all the data points were binned into clusters so the all the pixels in a particular cluster were within a range of signal intensity values. An expert observer can usually distinguish between four visually obvious groups of signal intensities in pulmonary noble gas MRI- signal void, hypo-intense, normal intensity and hyper-intense. The static ventilation and the non-diffusion weighted images were first normalized to the range of pixel intensities 0-255. Following that the full pixel intensity range of 0-255 was divided into four equal regions: 0-63, 64-127, 128-191, 192-255 and the center of each interval was selected as a centroid. After clustering, it was noticed that the cluster representing signal void contained some pixels with hypo-intense signal. Hence, the first cluster was divided into four clusters and k-means was reapplied to it. The first two clusters of the resulting binning were classified as signal void and the other two clusters as hypo-intense signal, thus giving 5 clusters from C1-C5. C1 included the minimum signal intensity regions within the lungs as well as the background. A seeded region growing algorithm⁸ (SGRA) was used to segment out the thoracic cavity volume from the ^1H images. The clustered $^{129}\text{Xe}/^3\text{He}$ NDW and SV images were registered to the segmented thoracic cavity to exclude all the pixels in the background from C1 and only the pixels inside the thoracic cavity were included to generate C1-C5. For the purpose of analysis, the lung was divided into two regions- regions of signal void know as ventilation defect volume (VDV) or C1 and the regions of signal intensity known as ventilation volume (VV) obtained by combining C2-C5. For each $^{129}\text{Xe}/^3\text{He}$ NDW and SV image, the VDV and the VV were normalized to the thoracic cavity

volume to get a ventilation defect percent (VDP) value and the percent ventilation volume (PVV) value respectively.

For the ^1H images, before applying the SRGA a two-dimensional radially symmetric Gaussian low-pass filter was applied to reduce the effects of intrapulmonary vasculature on the thoracic cavity segmentation. A threshold based on the k-means algorithm was selected to convert the ^1H images into a thoracic cavity binary mask. Following that, initial seed points were automatically selected in both the lungs by finding columns in the binary mask containing 20 vertically adjacent pixels below the threshold and the SRGA was used to generate the thoracic mask.

For the registration process, a landmark-based affine transform consisting of rotation, translation and scaling operations was used to transform the ^1H images to register them to the $^{129}\text{Xe}/^3\text{He}$ images. Briefly, the center slices (defined as the slices that clearly showed the carina and primary bronchi) of the ^1H and $^{129}\text{Xe}/^3\text{He}$ were first displayed side-by-side and the user was prompted to select 3-7 fiducial markers on both the slices. Geometric operations consisting of rotation, scaling and translation were used to transform the ^1H image to align it with the corresponding landmarks on the $^{129}\text{Xe}/^3\text{He}$ image. The same transformation map was then applied to the rest of the slices to register all the ^1H slices to the corresponding $^{129}\text{Xe}/^3\text{He}$ slices.

The segmentation included manual steps to select the center slices for the proton and the $^{129}\text{Xe}/^3\text{He}$ images. The center slice was defined as the slice that clearly showed the trachea, carina and the main two bronchi. The other proton and $^{129}\text{Xe}/^3\text{He}$ slices were matched with each other depending on the center slices and the number of slices. The user also had to select the fiducial points for the registration step for registration of the proton and $^{129}\text{Xe}/^3\text{He}$ center slices. The same transformation was then applied to all the slices to register the proton slices to the $^{129}\text{Xe}/^3\text{He}$ slices. There was also a provision in the software for the user to manually include or exclude areas from the analysis depending on the anatomical information. The segmentation and the registration process is illustrated in **Figure 2.4**.

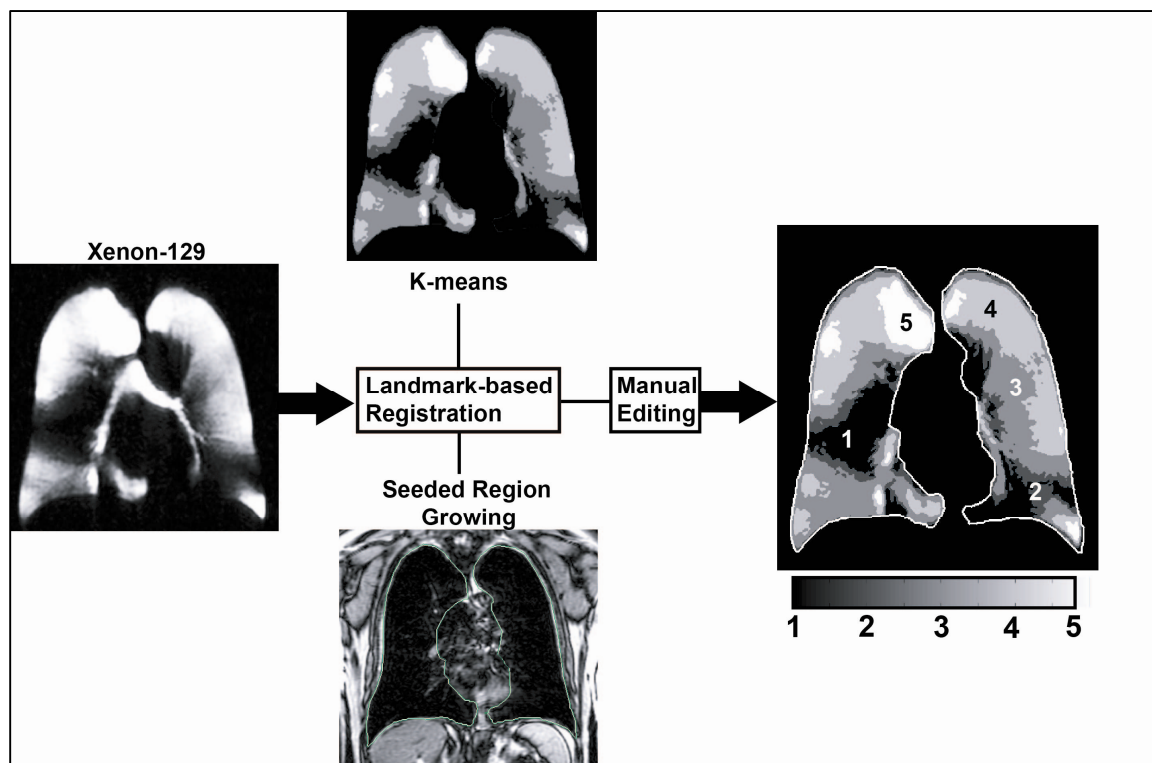


Figure 2.4 Schematic showing the semi-automated segmentation and registration process for ^{129}Xe static ventilation and ^1H images. Adapted from Kirby et.al. (2012)⁶

The signal-to-noise ratio (SNR) for all the ^{129}Xe and ^3He slices was determined by calculating the mean voxel signal value within a $5 \times 5 \text{ cm}^2$ voxel region of interest (ROI) for n representative ROIs inside the lung parenchyma, and dividing by the standard deviation of the voxel values for noise inside the same number of representative ROIs of the same dimensions in the image background where no lung structure was present. The ROIs within the lung parenchyma and the image background were selected independently and randomly for each slice.

2.5 Statistical Methods

A repeated measures analysis of variance (ANOVA) was used to determine the main effects for repeated scans for VDP using IBM SPSS Statistics 20.0 (SPSS Inc., Chicago, IL, USA). A two way mixed model intraclass correlation coefficient (ICC)⁹ analysis under absolute agreement was used to determine the degree of agreement between different visits. The ICC is a statistical analysis of agreement between two or

more measurements and the coefficient represents the agreement between those measurements. Coefficient of variation (COV) analysis was included in the study to determine the variability between repeated scans and observers. COV is a coefficient calculated as the standard deviation of the measurement as the percentage of its mean and lower COV values represent lower variability between measurements. Linear regression (r^2) and Pearson correlation coefficients (r) were used to determine the relationship between VDP values at different time-points, relationship between SNR and VDP, relationship between 2D and 3D image acquisition methods as well as the relationship between VDP and pulmonary function test measurements using GraphPad Prism version 4.00 (GraphPad Software Inc, San Diego, CA, USA). In all statistical analyses, results were considered significant when the probability of making a Type I error was less than 5% ($p<.05$).

2.6 Reference List

1. Rabe KF, Hurd S, Anzueto A *et al.* Global strategy for the diagnosis, management, and prevention of chronic obstructive pulmonary disease: GOLD executive summary. *Am. J. Respir. Crit Care Med.* **176**, 532-555 (2007).
2. Pellegrino R, Viegi G, Brusasco V *et al.* Interpretative strategies for lung function tests. *Eur. Respir. J.* **26**, 948-968 (2005).
3. Parraga G, Ouriadov A, Evans A *et al.* Hyperpolarized ^3He ventilation defects and apparent diffusion coefficients in chronic obstructive pulmonary disease: preliminary results at 3.0 Tesla. *Invest Radiol.* **42**, 384-391 (2007).
4. De ZN, Chhina N, Teh K *et al.* Asymmetric quadrature split birdcage coil for hyperpolarized ^3He lung MRI at 1.5T. *Magn Reson. Med.* **60**, 431-438 (2008).
5. Farag A, Wang J, Ouriadov A, Parraga G & Santyr G. Unshielded and Asymmetric RF Transmit Coil for Hyperpolarized ^{129}Xe Human Lung Imaging at 3.0T. Proceedings of the 20th Annual Meeting of ISMRM, Melbourne, Australia Poster# 1233.2012.2012.
Ref Type: Abstract
6. Kirby M, Heydarian M, Svenningsen S *et al.* Hyperpolarized ^3He magnetic resonance functional imaging semiautomated segmentation. *Acad. Radiol.* **19**, 141-152 (2012).
7. MacQueen J. Some methods for classification and analysis of multivariate observations. Fifth Berkeley Symposium on Mathematical Statistics and Probability; Statistical Laboratory of the University of California, Berkeley: Berkeley, Calif.: University of California Press; 281-297. 1967.
Ref Type: Abstract
8. Adams R & Bischof L. Seeded Region Growing. *IEEE Transactions on Pattern Analysis and machine Intelligence* 16(6), 641-647. 1994.
Ref Type: Abstract
9. Kenneth O.McGraw & S.P.Wong. Forming Inferences About Some Intraclass Correlation Coefficients. 1, 30-46. 1996.
Ref Type: Report
10. Hornak, J. P. *The Basics of MRI.* (2011).

CHAPTER 3: RESULTS

This chapter describes the results of the analysis described in the previous chapter. It describes the results of the reproducibility study for hyperpolarized ^{129}Xe ventilation defect percent (VDP) measurement for same day rescan (scan and 2-minute rescan) as well as 1-week rescan (scan, 2-minute rescan and 1-week rescan) for healthy volunteers and COPD subjects for intra-observer and inter-observer reproducibility. It also shows results for differences in VDP measurements for scans acquired using 2D and 3D acquisition methods. Also, we compare the reproducibility of ^{129}Xe VDP to the reproducibility of ^3He VDP.

3.1 Subject Demographics

Five healthy volunteers and ten COPD subjects (GOLD Stage I n=1; II n= 5; III n=3; IV n=1) were enrolled in the study. **Table 3.1** shows the subject demographics including the pulmonary function test results acquired at baseline (visit 1) for all the subjects. No significant differences ($p > 0.05$) were observed between the healthy group and the COPD subjects for age or body mass index (BMI). Significant differences were observed between the two groups for $\text{FEV}_{1\% \text{pred}}$ ($p < 0.001$), FEV_1/FVC ($p < 0.001$), $\text{TLC}_{\% \text{pred}}$ ($p < 0.01$), $\text{RV}_{\% \text{pred}}$ ($p < 0.01$), $\text{FRC}_{\% \text{pred}}$ ($p = 0.02$) and $\text{DL}_{\text{CO } \% \text{pred}}$ ($p = 0.01$) but not for $\text{FVC}_{\% \text{pred}}$ ($p = 0.2$), RV/TLC ($p = 0.06$) and $\text{IC}_{\% \text{pred}}$ ($p = 0.14$). There were no significant differences in the FEV_1 and FEV_1/FVC values between the two visits for the three COPD subjects that returned for the 1-week rescan. Three male HV and eight male COPD subjects were included in the study.

One COPD subject had a mild adverse effect in the 24 hour period following the study visit, but was judged not related to the imaging procedure, the details of which are reported elsewhere.¹ It resolved spontaneously, was asymptomatic (no clinical symptoms) and did not require withdrawal from the study. There were no other scanning or breath-hold related adverse effects reported in the study.

Table 3.1 Subject Demographics

Parameter	Healthy (n=5)	COPD (n=10)	P Value
Age yrs (\pm SD)	68 (12)	74 (4)	0.18
Male Sex n	3	8	-
BMI kg·m ⁻² (\pm SD)	27 (2)	25 (5)	0.5
FEV ₁ %pred (\pm SD)	105 (7)	57 (24)	0.001
FVC %pred (\pm SD)	104 (8)	91 (19)	0.2
FEV ₁ /FVC (\pm SD)	.75 (.02)	.46 (.14)	0.001
TLC %pred (\pm SD)	101 (7)	115 (8)	0.01
RV %pred (\pm SD)	100 (9)	159 (46)	0.01
RV/TLC (\pm SD)	.38 (.08)	.53 (.14)	0.06
IC %pred (\pm SD)	108 (18)	85 (31)	0.14
FRC %pred (\pm SD)	95 (14)	141 (35)	0.02
DL _{CO} %pred (\pm SD)	99 (15)	54 (32)*	0.01

SD=Standard Deviation, BMI=Body Mass Index, FEV₁= Forced Expiratory Volume in 1s, %pred=Percent Predicted, FVC= Forced Vital Capacity, TLC= Total Lung Capacity, RV= Reserve Volume, IC= Inspiratory Capacity, FRC= Functional Residual Capacity, DL_{CO}=Carbon Monoxide Diffusion Capacity of the lung *n=9 (One subject was not able to complete the DL_{CO} maneuver hence data available for nine of the ten subjects)

3.2 ¹²⁹Xe MRI Baseline Measurements

Figure 3.1 shows the center slice ventilation distribution for representative healthy volunteers and COPD subjects for ¹²⁹Xe and ³He scans and the differences in ventilation observed using the two contrast agents. Visually, elevated defects were observed for ¹²⁹Xe MRI as compared to ³He MRI for the same subjects for scans acquired within a few minutes of each other. **Table 3.2** shows the average whole lung VDP values for the 15 subjects included in the study over the 5 rounds for hyperpolarized ¹²⁹Xe and ³He baseline NDW images for observer 1. Quantitatively too, ¹²⁹Xe VDP was consistently higher than ³He VDP for all the rounds which is consistent with previously reported observations.² **Figure 3.2** shows a bar graph with mean ¹²⁹Xe VDP measurements for healthy volunteers and COPD subjects for each of the five rounds of VDP analysis for baseline NDW images. Repeated measures ANOVA failed to show any significant differences in VDP measurements over the five rounds for healthy volunteers or COPD subjects.

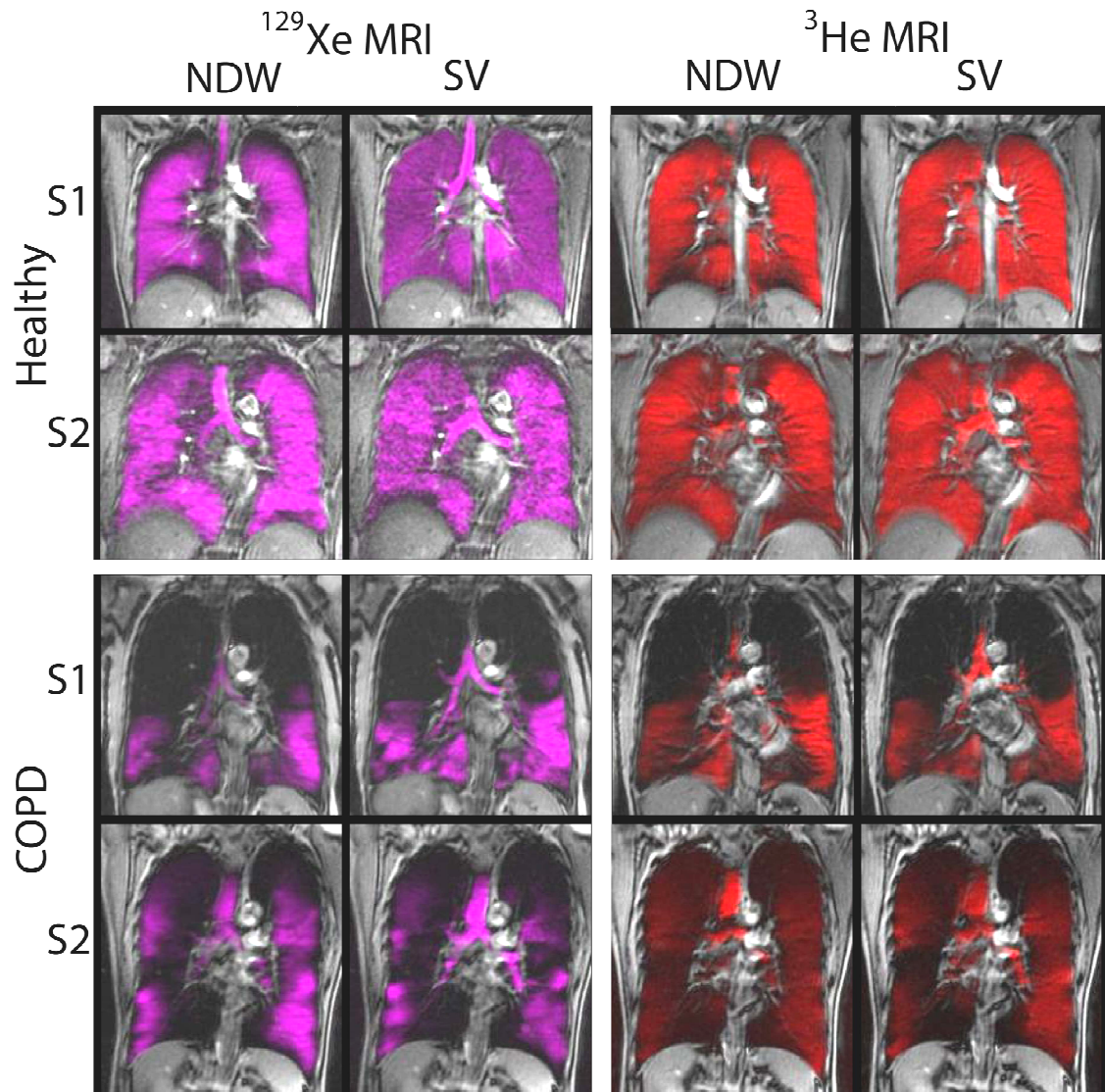


Figure 3.1 Non Diffusion Weighted (NDW) and static ventilation (SV) center slice images for ^{129}Xe and ^3He MRI for healthy volunteers and COPD subjects

Healthy subject **S1** is a 26 year old female ($\text{FEV}_{1\% \text{pred}} = 92\%$ and $\text{FEV}_1/\text{FVC} = 0.91$) and **S2** is a 69 year old male ($\text{FEV}_{1\% \text{pred}} = 101\%$ and $\text{FEV}_1/\text{FVC} = 0.75$)

COPD subject **S1** is a 77 year old female stage 3 COPD subject with $\text{FEV}_{1\% \text{pred}} = 50$ and $\text{FEV}_1/\text{FVC} = 50$, **S2** is a 79 year old male stage 2 COPD subject with $\text{FEV}_{1\% \text{pred}} = 52$ and $\text{FEV}_1/\text{FVC} = 36$

Table 3.2 Mean values for VDP for a single observer for healthy volunteers and COPD subjects for ^{129}Xe and ^3He over 5 rounds of analysis of baseline NDW images

	^{129}Xe MRI VDP (%) (n=15)	^3He MRI VDP (%) (n=15)
Round 1 Mean (\pm SD)	26 (18)	16 (14)
Round 2 Mean (\pm SD)	26 (17)	17 (14)
Round 3 Mean (\pm SD)	27 (17)	17 (13)
Round 4 Mean (\pm SD)	25 (18)	17 (14)
Round 5 Mean (\pm SD)	25 (18)	17 (14)

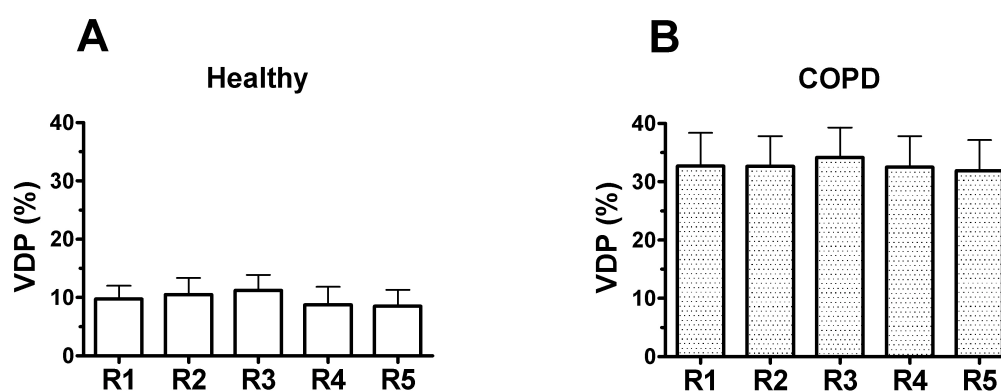


Figure 3.2 ^{129}Xe NDW VDP for Healthy Volunteers and COPD subjects
Bar graphs showing mean ^{129}Xe VDP for baseline NDW images for (A) Healthy volunteers (B) COPD subjects. No significant differences ($p > 0.05$) were observed between the 5 rounds for healthy volunteers or COPD subjects.

The ventilation defects observed using hyperpolarized noble gases have previously been shown to be spatially related to pulmonary structural abnormalities, detected using CT and histology in COPD and lung cancer patients.^{3,4} This suggests that the abnormal ventilation pattern observed in COPD subjects using hyperpolarized noble gas imaging, is due to structural abnormalities in these subjects.

We compared the ^{129}Xe MRI VDP obtained from scans acquired using a 2D FGRE pulse sequence and a 3D FGRE pulse sequence for scans done within 10 minutes of each other for the same set of subjects. We compared the VDP from NDW images obtained using a 2D FGRE sequence with VDP from SV images obtained with a 3D FGRE sequence. **Figure 3.3** shows the relationship of VDP from the NDW and the SV images. A strong and significant correlation was obtained between the two time points and repeated measures ANOVA failed to show any significant difference between scans obtained using 2D and 3D pulse sequences ($p = 0.496$). Intra-class correlation coefficient analysis showed significant and strong correlation between the 2D and 3D scans over 5 rounds of analysis ($\text{ICC} = 0.914$)

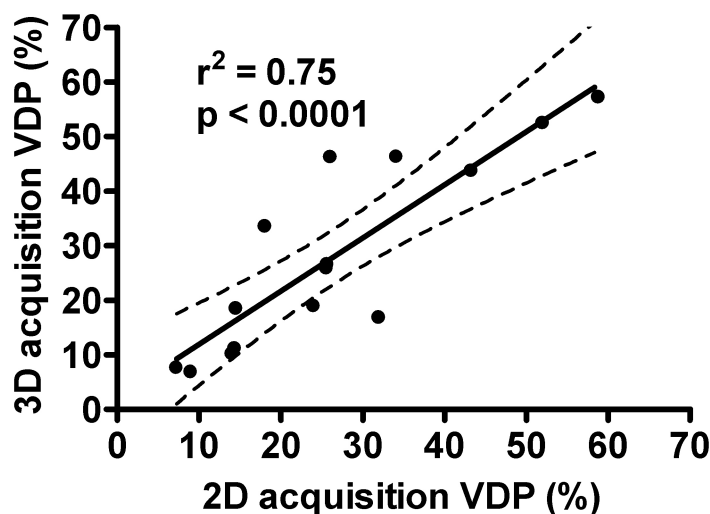


Figure 3.3 Relationship between pulse sequences for VDP
Relationship between 2D and 3D acquisition methods for ^{129}Xe MRI VDP. Solid line = mean difference, dashed line = 95% confidence intervals of regression line. 2D acquisition shows significant and positive correlation with 3D acquisition ($r^2 = 0.75$, $p < 0.0001$; $y = 0.97x + 2.17$)

We also investigated the relationship between signal to noise ratio (SNR) and VDP to see if the differences in SNR between repeated scans were responsible for differences in VDP. We found that there was no significant relationship observed between SNR and VDP ($p = 0.95$) for the 15 subjects. **Figure 3.4** shows the relationship for SNR and VDP.

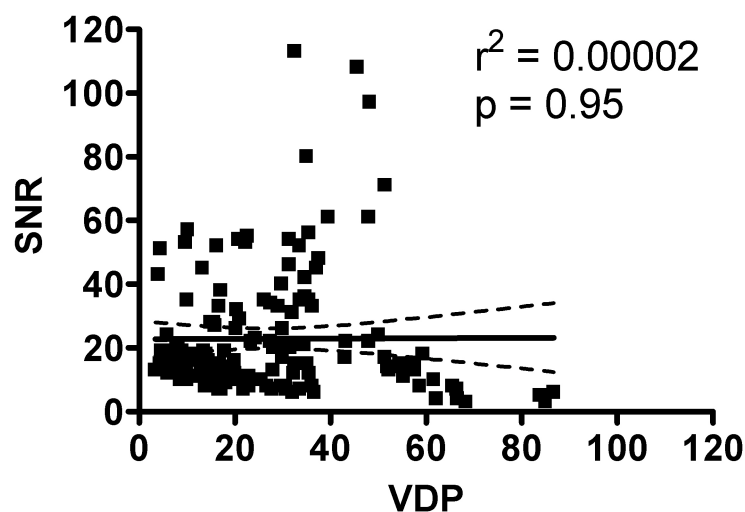


Figure 3.4 Relationship between ^{129}Xe VDP and SNR
 Relationship between SNR and VDP for ^{129}Xe MRI. Solid line = mean difference, dashed line = 95% confidence intervals of regression line. VDP shows no significant correlation with SNR ($r^2 = 0.00002$, $p = 0.95$; $y = 0.005x + 22.85$)

We analyzed the reproducibility of ^{129}Xe MRI VDP measurements over short periods of time (same day rescan and 1-week rescan) when no pulmonary physiological changes were expected to occur in the subjects. Two independent observers analyzed the NDW and SV images for VDP. Observer 1 analyzed the ^{129}Xe and ^3He NDW and SV images 5 times (5 rounds) while observer 2 analyzed the ^{129}Xe NDW images once (1 round). These data were then used to study the intra-observer and inter-observer reproducibility for ^{129}Xe MRI VDP.

3.3 Comparison of reproducibility of ^{129}Xe MRI VDP and ^3He MRI VDP

Table 3.3 shows the repeated measures ANOVA p values for ^{129}Xe MRI VDP and ^3He MRI VDP for same day rescan for observer 1 over 5 rounds of VDP analysis. The p values failed to show any significant differences between the same day rescan for ^{129}Xe or ^3He VDP. The ANOVA also failed to show any significant difference between

the 5 rounds of VDP analysis for either contrast agent. The interaction between the rounds and scans was also found to be not significant.

	^{129}Xe MRI (P value)	^3He MRI (P Value)
	Same-day (n=15)	Same-day (n=15)
Rounds	0.162	0.105
Scans	0.878	0.138
Rounds * Scans	0.404	0.108

Table 3.3 Repeated measures ANOVA for ^{129}Xe VDP and ^3He VDP for same day rescan
Same-day = Same day rescan

Table 3.4 shows ICC values for ^{129}Xe VDP same day rescan as well as ^3He MRI VDP same day rescan. Both ^{129}Xe MRI VDP and ^3He MRI VDP showed strong and significant ICC values. Table 3.4 also shows COV values for observer 1 and observer 2 for ^{129}Xe MRI VDP same day rescan and ^3He MRI VDP for observer 1 for same day rescan for all the 15 healthy volunteers and COPD subjects.

Table 3.4 ICC and COV analysis for ^{129}Xe MRI VDP and ^3He MRI VDP for same day rescan

	^{129}Xe MRI	^3He MRI
	Same-day (n=15)	Same-day (n=15)
ICC	0.949 (<.0001)	0.962 (<.0001)
COV (Obs 1) (%)	11	14
COV (Obs 2) (%)	10	-

Same-day = Same day rescan

3.4 ^{129}Xe MRI Intra-Observer Reproducibility

Figure 3.5 shows the ventilation distribution for ^{129}Xe NDW scans for three COPD subjects who had two NDW scans at visit 1 (baseline scan, 2-minute rescan) and repeated NDW scans (scan, 2-minute rescan) one week later. The center slices for the NDW ^{129}Xe MRI scans are shown in the figure for baseline scan, same day rescan and 1-week rescan. The ventilation distribution is highly heterogeneous for these COPD subjects and the location of defects is visually consistent over the three time points. The three subjects showed no significant differences in spirometry (FEV_1 , FVC or FEV_1/FVC) between the two visits separated by a period of 1 week. The repeated NDW scans were used to assess the reproducibility of hyperpolarized ^{129}Xe MRI VDP. Data from the 15 subjects who had the scan and 2-minute rescan were used to study the same day reproducibility of ^{129}Xe VDP while data from the three COPD subjects who had the scan, 2-minute rescan and 1-week rescan were used to study the 1 week reproducibility.

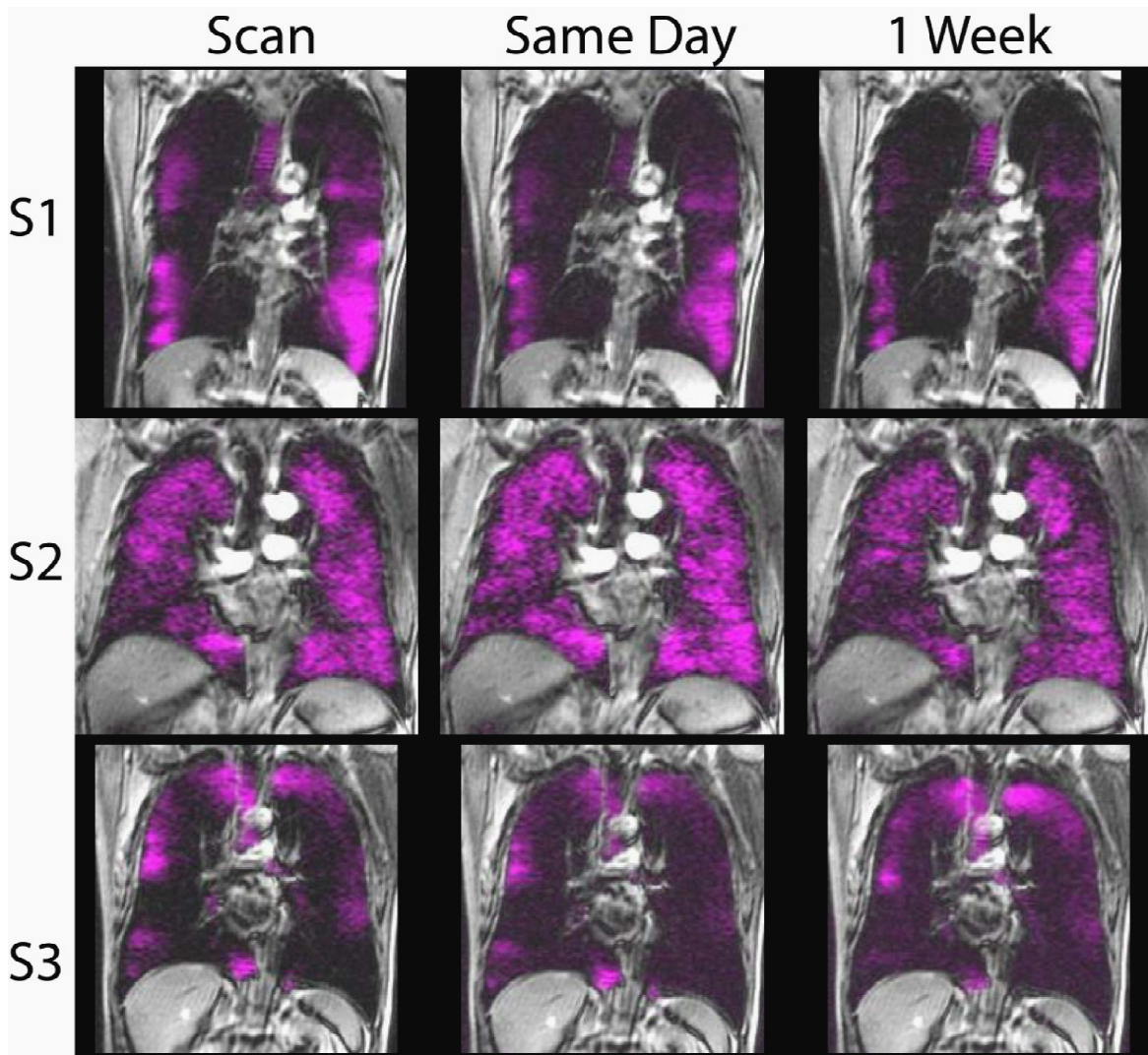


Figure 3.5 ^{129}Xe NDW images over three time points for three COPD subjects

Subject **S1** is a 79 year old male stage 2 subject with $\text{FEV}_{1\% \text{pred}} = 52$ and $\text{FEV}_1/\text{FVC} = 36$

Subject **S2** is a 76 year old male stage 2 subject with $\text{FEV}_{1\% \text{pred}} = 77$ and $\text{FEV}_1/\text{FVC} = 54$

Subject **S3** is a 73 year old male stage 4 subject with $\text{FEV}_{1\% \text{pred}} = 26$ and $\text{FEV}_1/\text{FVC} = 29$

Same day = Same day rescan, 1 Week = 1-week rescan

Table 3.5 shows repeated measures ANOVA P values for ^{129}Xe VDP for same day reproducibility (baseline NDW scan, 2-minute NDW rescan) for 15 subjects. It also shows results for 1-week reproducibility (baseline NDW scan, 2-minute NDW rescan and 1-week NDW rescan) for 3 subjects. The table shows the main effects for 5 rounds of VDP analysis by observer 1 and the main effects for repeated scans, as well as the interaction between the 5 rounds and scans. The ANOVA failed to show any significant main effects for the 5 repeated rounds of VDP analysis or the repeated scans of ^{129}Xe MRI. The interaction between the rounds and the scans was also not significant for same-day rescan or 1-week rescan.

Table 3.5 Repeated measures ANOVA for intra-observer reproducibility: ^{129}Xe VDP same day rescan and 1-week rescan

	^{129}Xe MRI (P value)	
	Same-day (n=15)	1-Week (n=3)
Rounds	0.162	0.284
Scans	0.878	0.127
Rounds * Scans	0.404	0.315

Same-day = Same day rescan, 1-Week = 1-week rescan

ICC analysis for the repeated ^{129}Xe scans is shown in **Table 3.6**. Strong and significant ICC values were observed for all the ^{129}Xe repeated scans. The 1-week rescan showed a slightly weaker correlation compared to the same day rescan although the correlation was significant and strong (ICC = 0.861). The COV analysis for ^{129}Xe VDP for the same day rescan for observer 1 and observer 2 is shown in **Table 3.6**. The table also shows the COV analysis for the 1-week rescan for both the observers.

Table 3.6 ICC and COV Analysis for intra-observer reproducibility: ^{129}Xe VDP same day rescan and 1-week rescan

	^{129}Xe MRI	
	Same-day (n=15)	1-Week (n=3)
ICC	0.949 (<.0001)	0.861 (<.0001)
COV (Obs 1) (%)	11	13
COV (Obs 2) (%)	10	13

ICC = Intra class correlation coefficient, COV = Coefficient of Variation. Numbers in parentheses are P values, Obs 1= Observer 1, Obs 2= Observer 2
Same day = Same day rescan, 1-Week = 1-week rescan

Figure 3.6 shows relationship for ^{129}Xe NDW scans over multiple time points. It shows the correlation for the baseline scan VDP with the same day rescan VDP for observer 1 over 5 rounds. Strong and significant correlation was observed for this comparison. It also shows the correlation for the baseline NDW scans with the NDW scans obtained one week later for three COPD subjects. For this comparison too, strong and significant correlation was observed.

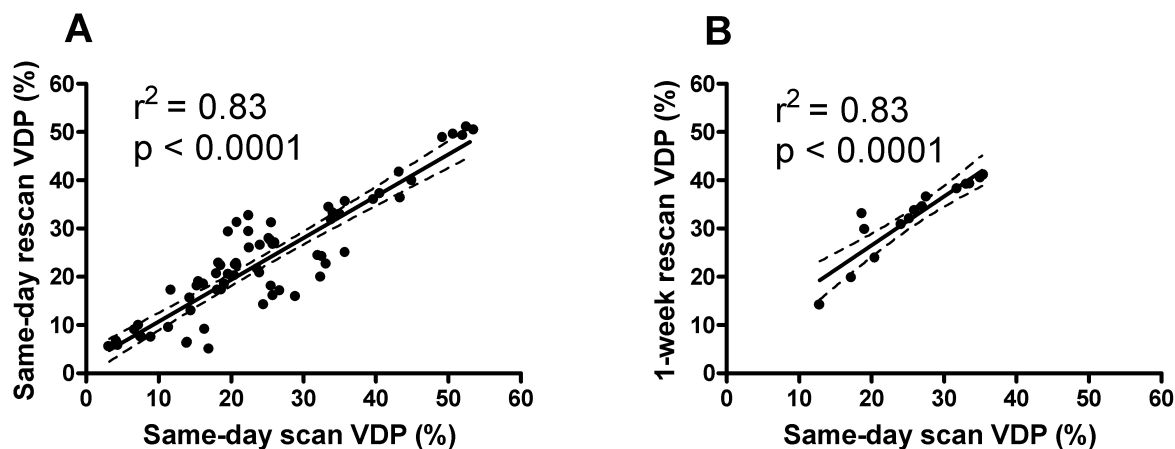


Figure 3.6 Relationship between repeated scans for VDP

Relationship between same day and 1-week repeated scans for ^{129}Xe MRI VDP. Solid line = mean difference, dashed line = 95% confidence intervals of regression line.

A) Significant and strong correlation between scan and same-day rescan ($r^2 = 0.83$, $p < 0.0001$; $y = 0.87x + 2.03$), B) Significant and strong correlation between scan and 1-week rescan ($r^2 = 0.83$, $p < 0.0001$; $y = 1.01x + 6.22$)

3.5 ^{129}Xe MRI Inter-Observer Reproducibility

To evaluate the inter-observer reproducibility for hyperpolarized ^{129}Xe MRI VDP, a second observer analyzed the repeated ^{129}Xe NDW MR images for VDP. Repeated measures ANOVA failed to show significant differences between the two observers or between repeated scans for the same day rescan or the 1-week rescan as shown by the non significant p values in **Table 3.7**. The interaction between the observers and the scans was also not significant for same day rescan or the 1-week rescan.

Table 3.7 Repeated Measures ANOVA for inter-observer reproducibility: ^{129}Xe VDP same day rescan and 1-week rescan

	^{129}Xe MRI (P value)	
	Same-day (n=15)	1-Week (n=3)
Observers	0.550	0.205
Scans	0.877	0.143
Observers * Scans	0.823	0.368

Same-day = Same day rescan, 1-Week = 1-week rescan

Table 3.8 shows the ICC and COV values for inter-observer reproducibility analysis for two observers for repeated scans for same day rescan and 1-week rescan. Significant and high ICC values were observed for both the comparisons.

Table 3.8 ICC and COV for inter-observer reproducibility: ^{129}Xe VDP same day rescan and 1-week rescan

	^{129}Xe MRI	
	Same-day (n=15)	1-Week (n=3)
ICC	0.978 (< .0001)	0.929 (< .0001)
COV (%)	11	11

ICC = Intraclass correlation coefficient, COV = Coefficient of Variation. Numbers in parentheses are P values. Same day = Same day rescan, 1-Week = 1-Week rescan

Figure 3.7 shows the inter-observer relationships for same day rescans for ^{129}Xe VDP as well as the 1-week rescans for ^{129}Xe VDP. Significant and strong correlations were observed for both the comparisons.

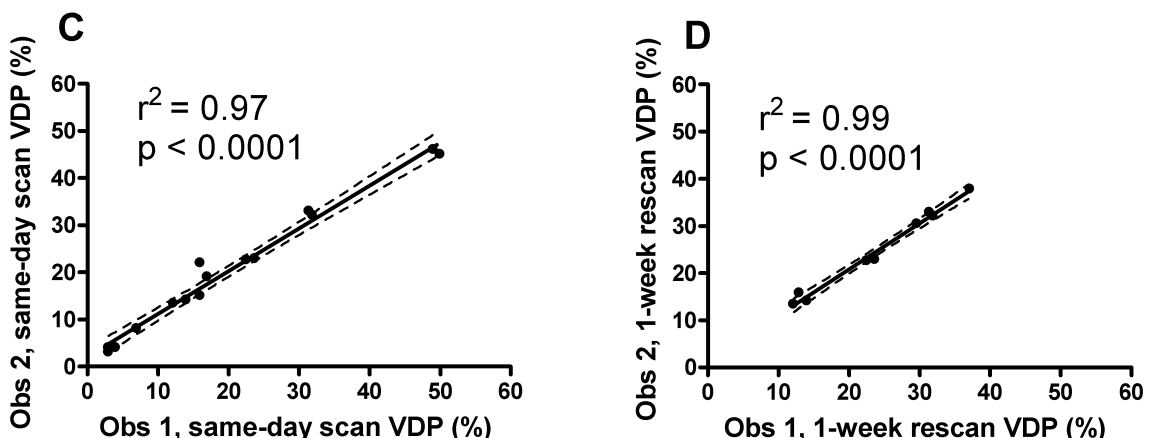


Figure 3.7 Inter-observer correlations for ^{129}Xe VDP

Obs 1 = Observer 1, Obs 2= Observer 2

Relationship between VDP analysis by two observers for ^{129}Xe MRI. Solid line = mean difference, dashed line = 95% confidence intervals of regression line. A) Significant and strong correlation between observers for same-day rescans ($r^2 = 0.98$, $p < 0.0001$; $y = 0.91x + 2.02$), B) Significant and strong correlation between observers for 1-week rescans ($r^2 = 0.99$, $p < 0.0001$; $y = 0.97x + 1.40$)

3.6 ^{129}Xe MRI VDP relationship to pulmonary function measurements

Significant and strong correlations were observed between baseline NDW ^{129}Xe VDP values and the gold standard measurements for obstructive lung disease diagnosis- $\text{FEV}_{1\% \text{pred}}$ and FEV_1/FVC as shown in **Figure 3.8**. Significant and moderate to strong correlations were also observed between VDP and lung volume measurements like RV ($r^2 = 0.91$), RV/TLC ($r^2 = 0.55$) and FRC ($r^2 = 0.80$). A significant and strong relationship was also observed between VDP and DLco ($r^2 = 0.74$). Significant and moderate correlations were observed between VDP and TLC ($r^2 = 0.59$) and IC ($r^2 = 0.52$) but not with FVC ($r^2 = 0.23$, $p = 0.07$).

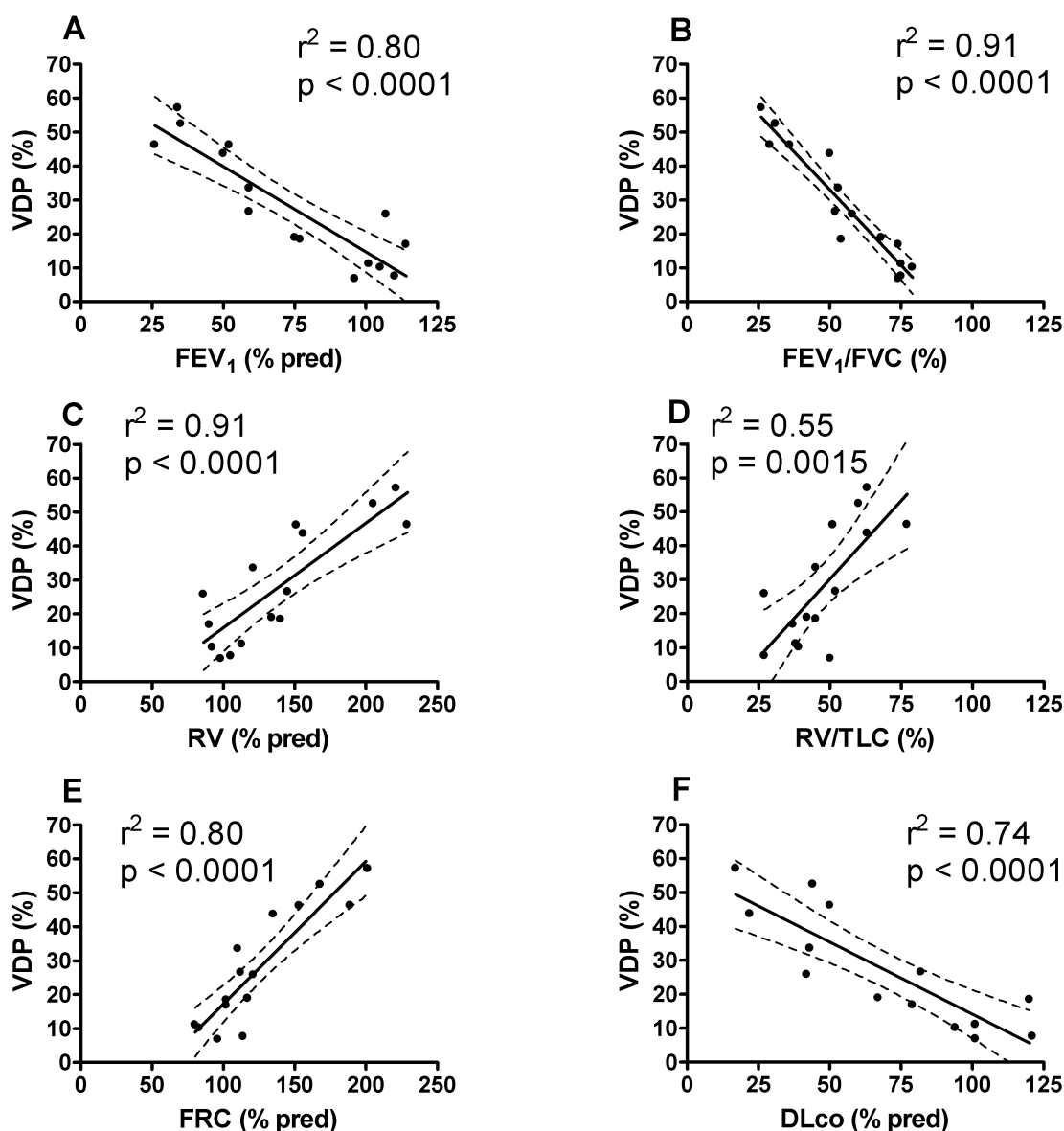


Figure 3.8 ^{129}Xe baseline NDW VDP correlations with pulmonary function tests
 Relationship between VDP and PFT measurements for all 15 subjects. Solid line = mean difference, dashed line = 95% confidence intervals of regression line. A) Significant and strong correlation between VDP and FEV_1 (% pred) ($r^2 = 0.80$, $p < 0.0001$; $y = -0.50x + 64.9$), B) Significant and strong correlation between VDP and FEV_1/FVC ($r^2 = 0.91$, $p < 0.0001$; $y = -0.89x + 77.57$), C) Significant and strong correlation between VDP and RV ($r^2 = 0.71$, $p < 0.0001$; $y = 0.31x - 14.92$), D) Significant and moderate correlation between VDP and RV /TLC ($r^2 = 0.55$, $p = 0.0015$; $y = 0.92x - 16.01$), E) Significant and strong correlation between VDP and FRC ($r^2 = 0.80$, $p < 0.0001$; $y = 0.42x - 24.72$), F) Significant and strong correlation between VDP and DL_{CO} ($r^2 = 0.74$, $p < 0.0001$; $y = -0.42x + 56.58$),

3.7 Reference List

1. Shukla Y, Wheatley A, Kirby M *et al.* Hyperpolarized ^{129}Xe magnetic resonance imaging: tolerability in healthy volunteers and subjects with pulmonary disease. *Acad. Radiol.* **19**, 941-951 (2012).
2. Kirby M, Svenningsen S, Owrangi A *et al.* Hyperpolarized ^3He and ^{129}Xe MR imaging in healthy volunteers and patients with chronic obstructive pulmonary disease. *Radiology* **265**, 600-610 (2012).
3. Mathew L, Wheatley A, Castillo R, et al. Hyperpolarized (^3He) magnetic resonance imaging: comparison with four-dimensional x-ray computed tomography imaging in lung cancer. *Acad Radiol* 2012; 19:1546-1553
4. Washko GR, Parraga G, Coxson HO. Quantitative pulmonary imaging using computed tomography and magnetic resonance imaging. *Respirology* 2012; 17:432-444

CHAPTER 4: DISCUSSION AND FUTURE WORK

In this final chapter, I will highlight all the important findings from this reproducibility study of hyperpolarized ^{129}Xe MRI VDP measurement. A discussion of the relevance of this work is presented based on the results from Chapter 3. Finally, the limitations of the study are presented followed by the future directions for this work and the conclusion for this study.

To our knowledge, this is the first study that looks at the reproducibility of hyperpolarized ^{129}Xe MRI VDP. We report: 1) No significant differences in VDP for scans acquired using a 2D FGRE pulse sequence compared to scans acquired using a 3D FGRE pulse sequence, 2) No correlation between SNR and VDP for ^{129}Xe MRI, 3) Visual and quantitative evidence of elevated defects using ^{129}Xe as a contrast agent compared to ^3He , 4) High intra-observer reproducibility for ^{129}Xe VDP and ^3He VDP for same day rescan, 5) High intra-observer reproducibility for ^{129}Xe VDP for same day and 1-week rescan, 6) High inter-observer reproducibility for ^{129}Xe VDP for same day and 1-week rescan, 7) Significant and strong correlation between ^{129}Xe VDP and pulmonary function test measurements.

4.1 ^{129}Xe MRI Baseline Measurements

For the ^{129}Xe MRI scans, I compared the VDP obtained using a 2D FGRE pulse sequence with the VDP obtained using a 3D FGRE pulse sequence, for the same subjects for scans acquired within a few minutes of each other. NDW images acquired using a 2D FGRE sequence were compared with SV images acquired using a 3D FGRE sequence. The major difference between the 2D and the 3D FGRE pulse sequence was that in the 3D acquisition, magnetic resonance data was acquired from a volume rather than a single tomographic slice. An additional phase encode pulse was applied in the 3D acquisition to image a greater thickness of tissue compared to the 2D acquisition. Repeated measures ANOVA failed to show any significant differences for ^{129}Xe VDP between 2D FGRE and 3D FGRE scans acquired within a few minutes of each other. Significant and strong ICC values were observed for the comparison of 5 rounds of NDW and SV image analysis. The ICC is a statistical analysis of agreement between two measurements, and

the coefficient represents the agreement in VDP values for observer 1 between the 2D acquisition and the 3D acquisition for same day rescan. A strong ICC value, as was observed for the NDW scan and SV same day rescan for ^{129}Xe VDP, represents a good agreement between the VDP values obtained at the two time-points using the two different pulse sequences. A significant and strong correlation was also observed between the VDP values for scans acquired using the two image acquisition methods. 3D acquisition typically provides a better SNR for imaging lung ventilation with hyperpolarized noble gases as well as better spatial resolution.¹ Therefore, 3D sequences will be useful for studies that need to accurately calculate the ventilation volume and ventilation defect volume which requires high spatial resolution in all three dimensions.

I also investigated the relationship between SNR and VDP for ^{129}Xe MRI, to see if the differences in SNR between repeated scans were responsible for differences in VDP values. It is important to investigate this relationship because typically ^{129}Xe MRI images are of a lower SNR than ^3He images due to the differences in the physical properties between the two gases. Also, repeated scans using the same contrast agent can have large variations in SNR depending on the imaging procedure used, including the scanner and pulse sequence, polarization of the gas itself and the breath-hold maneuver performed by the subject. We found that there was no significant relationship observed between SNR and VDP ($p = 0.95$) for the 15 subjects included in the study. These results suggest that the differences in SNR between repeated scans were not responsible for differences in VDP values. This is an important observation since SNR values can vary to a great degree and the reproducibility of the VDP measurement would be affected if SNR had an effect on the VDP measurement.

4.2 Comparison of reproducibility of ^{129}Xe MRI VDP and ^3He MRI VDP

We compared the reproducibility of hyperpolarized ^{129}Xe MRI VDP with the reproducibility of ^3He MRI VDP. First, both visually and quantitatively, ^{129}Xe MRI showed elevated defects as compared to ^3He MRI for the same set of subjects for scans acquired within 10 minutes of each other, which is consistent with previously reported observations.^{2,3} The differences in the physical properties of ^{129}Xe and ^3He may provide

an explanation for this observation. Kirby *et al.* reported that the lower diffusion coefficient of ^{129}Xe compared to ^3He may be responsible for slower filling of ^{129}Xe in the diseased lung regions, leading to elevated defects observed in ^{129}Xe MRI.² Previous studies have reported that ^3He MRI measurements are reproducible over short periods of time in healthy volunteers and subjects with obstructive lung disease.⁴⁻⁸ It is important to study if the differences in the physical properties of the two gases are reflected as differences in the reproducibility of ^{129}Xe MRI VDP compared to the reproducibility of ^3He MRI VDP.

For the same set of subjects, repeated measures ANOVA failed to show any significant differences in VDP values for repeated ^{129}Xe MRI scans as well as ^3He MRI scans for same day rescan (scans acquired on the same day within 2 ± 1 minutes of each other). There were no significant differences in the 5 rounds of repeated VDP analysis for ^{129}Xe or ^3He MRI indicating good intra-observer reproducibility for same day rescan for ^{129}Xe and ^3He VDP. Significant and strong ICC values were observed for same day rescan for both ^{129}Xe VDP and ^3He VDP. The ICC is a statistical analysis of agreement between two measurements, and the coefficient represents the agreement in VDP values for observer 1 between the scan and the same day rescan. A strong ICC value, as was observed for the scan and the same day rescan for both ^{129}Xe and ^3He , represents a good agreement between the VDP values obtained at the two time-points for both the contrast agents. The COV values for observer 1 and observer 2 were 11% and 10% respectively for ^{129}Xe VDP, and that for ^3He was 14% for observer 1. Observer 2 did not analyze the ^3He images and hence a COV value for observer 2 was not available. COV is a measurement of the standard deviation as a percentage of the mean and lower COV values for ^{129}Xe VDP compared to ^3He VDP suggest that there is lower variation in ^{129}Xe VDP same day rescan compared to ^3He VDP same day rescan. However, this interpretation should be made with caution using COV analysis as there are major limitations for this statistical method. For one, COV is the ratio of standard deviation over mean. The mean values for VDP were observed to be significantly lower for ^3He compared to ^{129}Xe and hence the COV might not accurately reflect the difference in variation between the two contrast agents. Secondly, our subject cohort included healthy volunteers who have low mean VDP values and hence push the COV values up. All

factors considered, this analysis suggests that the intra-observer reproducibility of ^{129}Xe MRI VDP and ^3He MRI VDP is high for same day rescan for healthy volunteers and subjects with COPD.

4.3 ^{129}Xe MRI Intra-Observer Reproducibility

We analyzed the intra-observer reproducibility of ^{129}Xe VDP for same day rescan (scan, 2- minute rescan) and 1-week rescan (scan, 2-minute rescan and 1 week rescan) for 5 rounds of VDP analysis. For the same day rescan, a repeated measures ANOVA failed to show any significant differences between the VDP values for repeated scans for the cohort of 15 subjects, which included healthy and COPD subjects. There are several sources of variation for scans acquired within 2 minutes of each other, such as 1) subject compliance (breath-hold, motion), 2) polarization of the gas and gas delivery methods, 3) observer dependence in the semi-automated segmentation software. We tried to minimize the variation in repeat scans due to subject compliance by giving the subjects extensive coaching regarding inhalation of the contrast agent and the breath-hold requirements. The observer variation in the segmentation and registration steps was minimized by giving the observers extensive training regarding the use of the semi-automated segmentation software. These results suggest that the ^{129}Xe VDP measurement is robust to variations between scans acquired over short periods of time. The ANOVA also failed to show any significant difference between the 5 rounds of VDP analysis for the single observer for same day rescan. This suggests high intra-observer reproducibility for the VDP measurement for same day rescan of ^{129}Xe MRI. The ICC value for same day rescan for ^{129}Xe VDP was significant and strong indicating good agreement between the VDP values for the repeated scans. The COV values for same day rescan were 11% and 10% for the two observers. The COV values were higher than previously reported COV values for ^3He VDV for COPD subjects.⁹ However, this subject cohort included healthy subjects along with COPD subjects, who on account of their lower mean VDP values push the COV values higher. The COV values observed for ^{129}Xe VDP for same day rescan were lower than those for ^3He VDP same day rescan for the same subject cohort. These results suggest that ^{129}Xe MRI VDP is highly reproducible for same day rescan when no physiological pulmonary changes are expected

to occur. The measurement is robust to variations in subject compliance, polarization of the gas as well as the observer error in the semi-automated segmentation method for scans acquired within a few minutes of each other.

For the 1-week rescan reproducibility, the ANOVA failed to show any significant differences between the scan, 2 minute rescan and 1-week rescan for the three COPD subjects that had the 1-week repeat scan. Visually too, the defects appeared consistent over the three repeated scans. There are several sources of variation for scans acquired 1-week from each other, such as 1) subject compliance (breath-hold, motion), 2) polarization of the gas and gas delivery methods, 3) scanner 4) position of the coil within the bore of the MRI 5) observer dependence in the semi-automated segmentation software, 6) potential physiological changes. An effort was made to keep the variation in the position of the coil inside the bore of the scanner to a minimum between the scans. The three COPD subjects showed no significant differences in spirometry (FEV₁, FVC or FEV₁/FVC) between the two visits separated by a period of 1-week suggesting that no significant global change in respiratory function had taken place over the one week period. These results suggest that the ¹²⁹Xe MRI VDP measurement is robust to variations in scans over a period of one week. This implies that the ¹²⁹Xe MRI VDP measurement is reproducible over longer periods of time and can cope with variations arising from various sources like the patient, scanner, contrast agent as well as the observer analyzing the images. The repeated measures ANOVA failed to show any significant differences in the 5 repeated rounds of VDP analysis for the 1-week rescan. This suggests that ¹²⁹Xe MRI VDP shows good intra-observer reproducibility for 1-week repeated scan. Significant and strong ICC values were observed for the 1-week rescan for ¹²⁹Xe VDP indicating good agreement between the VDP values for the three repeated scans. The COV for the 1 week rescan was 13% for both the observers who analyzed the ¹²⁹Xe repeated scans. Significant and strong correlation values were observed for same day rescan and 1-week rescan.

In order to be confident about the physiological changes and biological phenomenon observed in the subject, we should be confident that the source of the variation in the measurement is from the subject (physiological change) and not from any stage of the imaging procedure. The results for the intra-observer reproducibility suggest

that ^{129}Xe MRI VDP is a highly reproducible measurement over same day rescans as well as over 1-week rescans and can be used as a reliable measurement for pulmonary imaging studies.

4.4 ^{129}Xe MRI Inter-Observer Reproducibility

Two independent observers analyzed the ^{129}Xe same day and 1-week repeated scans for evaluation of inter-observer reproducibility of VDP measurement. For the same day rescan, a repeated measures ANOVA failed to show any significant differences in VDP measurement between the two observers. Also, the ANOVA failed to show any significant differences between the repeated scans for the same day rescan for either observer. For the 1-week rescan too, it failed to show any significant differences in VDP between the two observers. As well as the scan, the same day rescan and the 1-week rescan. The segmentation software used for the calculation of VDP is semi-automated with the observer providing input regarding which areas of the lung are classified as defects and also has to select fiducials for the registration step. These results suggest that the inter-observer variability in this process is not significant between observers and different observers analyze the images in a consistent way, when properly trained to use the software. This suggests that the VDP measurement can be reliably used in multi-observer or even multi-center research studies if the observers are properly trained. The ICC value showed a significant and strong agreement between the two observers for the scan and same day scan as well as the scan, same day rescan and 1-week rescan. The COV was observed to be 11% between the two observers for both the scan and same day rescan as well as the scan, same day rescan and 1-week rescan. Although this COV value seems high, it has to be considered that the subject cohort contains healthy volunteers who push the COV value up because of their low mean VDP. The correlation coefficient between the two observers for VDP measurement was found to be significant and strong for the scan and same day rescan and the scan, same day rescan and 1-week rescan. These results suggest that the inter-observer reproducibility for ^{129}Xe VDP is high and the measurement can be reliably used in multi-observer and multi-center studies.

4.5 ¹²⁹Xe MRI VDP relationship to Pulmonary Function Measurements

We evaluated the relationship between VDP and all the pulmonary function test measurements. There was a strong and significant inverse correlation between VDP and the gold standard measurement for obstructive lung disease diagnosis – FEV₁/FVC. Significant and strong inverse correlation was also observed between VDP and FEV_{1%pred} but a significant relationship was not observed between VDP and FVC%_{pred}. Subjects with obstructive lung disease have a reduced FEV₁/FVC ratio because of airway narrowing caused by a lot of factors including thickening and obliteration of airways and small airways disease. FEV₁/FVC reduction in obstructive lung disease has been reported to be sensitive to airway narrowing and bronchoconstriction.¹⁰ The significant and strong correlation of VDP with FEV₁/FVC suggests that VDP can be a very useful tool for studying the different airway and parenchymal abnormalities in obstructive lung disease. FEV_{1%pred} value is used for the classification of COPD subjects into different stages, depending on the severity of the disease.¹¹ A significant and strong correlation between ¹²⁹Xe VDP and FEV_{1%pred} suggests that VDP can be used to classify subjects into stages depending on the ventilation abnormalities and VDP values. Similar relationships between ventilation defects and spirometric measurements have been previously reported in obstructive lung disease using ³He and ¹²⁹Xe MRI measurements.^{2,12,13} We also observed a significant and strong positive correlation between ¹²⁹Xe VDP and RV. In COPD patients, the RV values increases markedly due to “gas trapping” in the alveoli. Gas trapping is caused by the decrease in the elastic recoil of the lungs due to fibrosis as well as the collapse of the bronchioles during expiration leading to large amounts of air being trapped in the alveoli. The significant and strong correlation between ¹²⁹Xe VDP and RV suggests that VDP might be a good tool for diagnosis of gas trapping in patients suffering from COPD. There was also a significant and strong inverse correlation between VDP and DL_{CO} observed. DL_{CO} is a surrogate measurement for the diffusion of oxygen across the alveolar membrane into the blood. The strong correlation suggests that VDP might be a good indicator of emphysema in subjects suffering from COPD. The strong correlations observed between ¹²⁹Xe MRI VDP and the pulmonary function test

measurements suggest that VDP might be a useful tool for obstructive lung disease diagnosis, monitoring disease progression and evaluating response to treatment.

4.6 Study Limitations

We acknowledge that this work was limited due to the small number of subjects included in the study, especially for the 1-week rescans. Since we had a small subject size, caution should be exercised when extrapolating these results to the general COPD population and other obstructive and restrictive lung disease populations. We did not evaluate the reproducibility of ^{129}Xe MRI VDP in other obstructive and restrictive lung diseases other than COPD. For the COPD subjects who returned for the 1-week rescans, we did not acquire proton scans at the 1-week rescans and had to use proton scans from the baseline visit. Although the shape and size of the thoracic cavity is not expected to change significantly over a one week period, this could potentially be a source of error for the 1-week rescans VDP. Another limitation of the study is that we did not acquire repeated ^3He MRI scans for 1-week rescans for the three COPD subjects and hence a direct comparison between ^{129}Xe VDP and ^3He VDP for 1-week rescans reproducibility could not be made.

4.7 Future Work

The results and discussions presented in this thesis provide some important insights in the intra-observer and inter-observer reproducibility of hyperpolarized ^{129}Xe MRI VDP measurement and provide the foundation for future work. The reproducibility of ^{129}Xe VDP measurement needs to be evaluated in other pulmonary diseases like asthma, CF and RILI. The reproducibility of ^{129}Xe MRI ADC measurement, used to probe the lung microstructure, needs to be evaluated for obstructive and restrictive lung diseases.

Over the last two decades, there has been tremendous progress made in understanding structural and functional changes in pulmonary diseases using hyperpolarized ^3He MRI. However, due to the limited availability and high cost of ^3He , its clinical translation has not been possible. ^{129}Xe is more abundant and cheaper and hence is a much more realistic option as a contrast agent in clinical applications.

However, due to the differences in the physical properties between ^{129}Xe and ^3He , many of the studies and work performed using ^3He will have to be reproduced using ^{129}Xe . While recently there have been studies performed comparing ^{129}Xe and ^3He MRI measurements in healthy volunteers and subjects with pulmonary diseases,^{2,3,14} there is a need to perform more studies using ^{129}Xe MRI probing the effects of the differences in the physical properties of ^{129}Xe in comparison to ^3He on pulmonary imaging measurements.

4.8 Conclusion

The development of pulmonary imaging techniques has led to advancements in our understanding of pulmonary structural and functional changes associated with pulmonary disease. Spirometry and plethysmography, which provide gold standards measurements for obstructive lung disease diagnosis, are limited because they provide only a global measurement of lung function in regionally highly heterogeneous diseases like COPD and asthma and are insensitive to early stages of the disease. CT, the gold standard for pulmonary lung structure evaluation, is limited by its high radiation dose and its inability to provide regional functional information in pulmonary disease. Hyperpolarized noble gas magnetic resonance imaging (MRI) has emerged as a non-invasive, non-radiation based sensitive tool for visualizing the regional lung structure and function. ^{129}Xe is one of the contrast agents that can be used for hyperpolarized gas pulmonary imaging. However, the reproducibility of hyperpolarized ^{129}Xe MRI measurements had not yet been studied or determined. Hence, the aim of this thesis was to evaluate the reproducibility of hyperpolarized ^{129}Xe MRI measurements over short periods of time. Our results show that hyperpolarized ^{129}Xe MRI VDP has high intra-observer and inter-observer reproducibility for scans acquired on the same day as well as after a period of 1-week. ^{129}Xe MRI VDP also showed strong and significant correlations with pulmonary function test measurements. These results suggest that hyperpolarized ^{129}Xe MRI VDP is reproducible over short periods of time and can be used as a reliable measurement to study pulmonary function in imaging studies. Hyperpolarized ^{129}Xe MRI is able to provide pulmonary structural and functional information and has emerged as a very important tool in pulmonary imaging research studies.

4.9 Reference List

1. Wild JM, Woodhouse N, Paley MN *et al.* Comparison between 2D and 3D gradient-echo sequences for MRI of human lung ventilation with hyperpolarized ³He. *Magn Reson. Med.* **52**, 673-678 (2004).
2. Kirby M, Svenningsen S, Owringi A *et al.* Hyperpolarized ³He and ¹²⁹Xe MR imaging in healthy volunteers and patients with chronic obstructive pulmonary disease. *Radiology* **265**, 600-610 (2012).
3. Kirby M, Svenningsen S, Kanhere N *et al.* Pulmonary ventilation visualized using hyperpolarized helium-3 and xenon-129 magnetic resonance imaging: differences in COPD and relationship to emphysema. *J. Appl. Physiol* **114**, 707-715 (2013).
4. Diaz S, Casselbrant I, Piitulainen E *et al.* Hyperpolarized ³He apparent diffusion coefficient MRI of the lung: reproducibility and volume dependency in healthy volunteers and patients with emphysema. *J. Magn Reson. Imaging* **27**, 763-770 (2008).
5. Mathew L, Evans A, Ouriadov A *et al.* Hyperpolarized ³He magnetic resonance imaging of chronic obstructive pulmonary disease: reproducibility at 3.0 tesla. *Acad. Radiol.* **15**, 1298-1311 (2008).
6. Niles DJ, Kruger SJ, Dardzinski BJ *et al.* Exercise-induced bronchoconstriction: reproducibility of hyperpolarized ³He MR imaging. *Radiology* **266**, 618-625 (2013).
7. Parraga G, Ouriadov A, Evans A *et al.* Hyperpolarized ³He ventilation defects and apparent diffusion coefficients in chronic obstructive pulmonary disease: preliminary results at 3.0 Tesla. *Invest Radiol.* **42**, 384-391 (2007).
8. Parraga G, Mathew L, Etemad-Rezai R, McCormack DG & Santyr GE Hyperpolarized ³He magnetic resonance imaging of ventilation defects in healthy elderly volunteers: initial findings at 3.0 Tesla. *Acad. Radiol.* **15**, 776-785 (2008).
9. Kirby M, Heydarian M, Svenningsen S *et al.* Hyperpolarized ³He magnetic resonance functional imaging semiautomated segmentation. *Acad. Radiol.* **19**, 141-152 (2012).
10. Gibbons WJ, Sharma A, Loughheed D & Macklem PT Detection of excessive bronchoconstriction in asthma. *Am. J. Respir. Crit Care Med.* **153**, 582-589 (1996).
11. Rabe KF, Hurd S, Anzueto A *et al.* Global strategy for the diagnosis, management, and prevention of chronic obstructive pulmonary disease: GOLD executive summary. *Am. J. Respir. Crit Care Med.* **176**, 532-555 (2007).

12. de Lange EE, Altes TA, Patrie JT *et al.* Evaluation of asthma with hyperpolarized helium-3 MRI: correlation with clinical severity and spirometry. *Chest* **130**, 1055-1062 (2006).
13. Fain SB, Gonzalez-Fernandez G, Peterson ET *et al.* Evaluation of structure-function relationships in asthma using multidetector CT and hyperpolarized He-3 MRI. *Acad. Radiol.* **15**, 753-762 (2008).
14. Mugler JP, III & Altes TA Hyperpolarized ^{129}Xe MRI of the human lung. *J. Magn Reson. Imaging* **37**, 313-331 (2013).

APPENDICES

Appendix A: Health Science Research Ethics Board Approval Notices



Use of Human Participants - Ethics Approval Notice

Principal Investigator: Dr. Grace Parraga
Review Number: 18131
Review Level: Full Board
Approved Local Adult Participants: 50
Approved Local Minor Participants: 0
Protocol Title: Xenon-129 Magnetic Resonance Imaging of Healthy Subjects: Hardware and Software Development and Reproducibility
Department & Institution: Imaging, Robarts Research Institute
Sponsor: Canadian Institutes of Health Research

Ethics Approval Date: August 12, 2011

Expiry Date: August 31, 2016

Documents Reviewed & Approved & Documents Received for Information:

Document Name	Comments	Version Date
UWO Protocol		
Letter of Information & Consent		2011/07/13
Protocol	Received for information only	2011/06/22
Advertisement		2011/07/13

This is to notify you that the University of Western Ontario Health Sciences Research Ethics Board (HSREB) which is organized and operates according to the Tri-Council Policy Statement: Ethical Conduct of Research Involving Humans and the Health Canada/ICH Good Clinical Practice Practices: Consolidated Guidelines; and the applicable laws and regulations of Ontario has reviewed and granted approval to the above referenced study on the approval date noted above. The membership of this HSREB also complies with the membership requirements for REB's as defined in Division 5 of the Food and Drug Regulations.

The ethics approval for this study shall remain valid until the expiry date noted above assuming timely and acceptable responses to the HSREB's periodic requests for surveillance and monitoring information. If you require an updated approval notice prior to that time you must request it using the UWO Updated Approval Request form.

Member of the HSREB that are named as investigators in research studies, or declare a conflict of interest, do not participate in discussions related to, nor vote on, such studies when they are presented to the HSREB.



Use of Human Participants - Ethics Approval Notice

Principal Investigator: Dr. Grace Parraga
Review Number: 18130
Review Level: Full Board
Approved Local Adult Participants: 100
Approved Local Minor Participants: 0
Protocol Title: A Single-center Study Evaluating Hyperpolarized 129Xenon Magnetic Resonance Imaging in Subjects with Chronic Lung Disease
Department & Institution: Imaging, Robarts Research Institute
Sponsor: Canadian Institutes of Health Research

Ethics Approval Date: August 12, 2011

Expiry Date: August 31, 2016

Documents Reviewed & Approved & Documents Received for Information:

Document Name	Comments	Version Date
UWO Protocol		
Letter of Information & Consent		2011/07/13
Advertisement		2011/07/13
Protocol	Received for information only	2011/06/22

This is to notify you that the University of Western Ontario Health Sciences Research Ethics Board (HSREB) which is organized and operates according to the Tri-Council Policy Statement: Ethical Conduct of Research Involving Humans and the Health Canada/ICH Good Clinical Practice Practices: Consolidated Guidelines; and the applicable laws and regulations of Ontario has reviewed and granted approval to the above referenced study on the approval date noted above. The membership of this HSREB also complies with the membership requirements for REB's as defined in Division 5 of the Food and Drug Regulations.

The ethics approval for this study shall remain valid until the expiry date noted above assuming timely and acceptable responses to the HSREB's periodic requests for surveillance and monitoring information. If you require an updated approval notice prior to that time you must request it using the UWO Updated Approval Request form.

Member of the HSREB that are named as investigators in research studies, or declare a conflict of interest, do not participate in discussions related to, nor vote on, such studies when they are presented to the HSREB.

Appendix B: Copyrighted Material and Permissions



RightsLink®

[Home](#)
[Account Info](#)
[Help](#)



Title: Hyperpolarized 3He diffusion MRI and histology in pulmonary emphysema

Author: Jason C. Woods,Cliff K. Choong,Dmitriy A. Yablonskiy,John Bentley,Jonathan Wong,John A. Pierce,Joel D. Cooper,Peter T. Macklem,Mark S. Conradi,James C. Hogg

Publication: Magnetic Resonance in Medicine

Publisher: John Wiley and Sons

Date: Oct 20, 2006

Copyright © 2006 Wiley-Liss, Inc.

Logged in as:
Nikhil Kanhere

LOGOUT

Order Completed

Thank you very much for your order.

This is a License Agreement between Nikhil Kanhere ("You") and John Wiley and Sons ("John Wiley and Sons"). The license consists of your order details, the terms and conditions provided by John Wiley and Sons, and the [payment terms and conditions](#).

[Get the printable license.](#)

License Number	3140840032865
License date	May 02, 2013
Licensed content publisher	John Wiley and Sons
Licensed content publication	Magnetic Resonance in Medicine
Licensed content title	Hyperpolarized 3He diffusion MRI and histology in pulmonary emphysema
Licensed copyright line	Copyright © 2006 Wiley-Liss, Inc.
Licensed content author	Jason C. Woods,Cliff K. Choong,Dmitriy A. Yablonskiy,John Bentley,Jonathan Wong,John A. Pierce,Joel D. Cooper,Peter T. Macklem,Mark S. Conradi,James C. Hogg
Licensed content date	Oct 20, 2006
Start page	1293
End page	1300
Type of use	Dissertation/Thesis
Requestor type	University/Academic
Format	Print and electronic
Portion	Figure/table
Number of figures/tables	1
Original Wiley figure/table number(s)	Figure 2
Will you be translating?	No
Total	0.00 USD

[ORDER MORE...](#)
[CLOSE WINDOW](#)

Copyright © 2013 Copyright Clearance Center, Inc. All Rights Reserved. [Privacy statement](#). Comments? We would like to hear from you. E-mail us at customercare@copyright.com

Appendix C: Curriculum Vitae

Nikhil Kanhere (B.E.)**Education and Work Experience:**

- 2011- M.E.Sc. Candidate, Graduate Program in Biomedical Engineering,
Western University, London, Ontario, Canada
Supervisor: Dr. Grace Parraga
- 2010 - 2011 Research Intern at Krishna Institute of Medical Sciences,
Karad, India
Supervisor: Dr. Asha Pratinidhi
- 2006 - 2010 Bachelor of Computer Engineering (B.E),
University of Pune, Pune, India
Passed with Distinction
Supervisor: Prof. Kiran Patil

Research, Publications and Scholarly Activities:**M.E.Sc Thesis:**

- Reproducibility of inhaled contrast agent hyperpolarized Xenon-129 Magnetic Resonance Imaging in Chronic obstructive pulmonary disease and never-smokers
Supervisor: Dr. Grace Parraga

Publications and Presentations:**A. Refereed Journal Manuscripts**

- Kirby M, Svenningsen S, **Kanhere N**, Owrangi A, Wheatley A, Coxson HO, Santyr GE, Paterson NA, McCormack DG, Parraga G. Pulmonary Ventilation Visualized using Hyperpolarized Helium-3 and Xenon-129 Magnetic Resonance

Imaging: Differences in COPD and Relationship to Emphysema. J Appl Physiol. PMID: 23239874 [Epub ahead of print Dec 13 2012]

- Kirby M, **Kanhere N**, Etemad-Rezai R, McCormack DG and Parraga G. Hyperpolarized Helium-3 Magnetic Resonance Imaging of Chronic Obstructive Pulmonary Disease Exacerbation: Case Report. JMRI doi: 10.1002/jmri.23896

B. Peer Reviewed Poster Presentations

- M. Kirby, D. Pike, S. Svenningsen, **N. Kanhere**, A. Wheatley, N.A. Paterson, D.G. McCormack, H.O. Coxson and G. Parraga. (2013) Hyperpolarized Helium-3 Magnetic Resonance Imaging Phenotypes of Chronic Obstructive Pulmonary Disease: Relationship to Exacerbations. American Thoracic Society, Philadelphia, Pennsylvania, USA May 13, 2013
- **N. Kanhere**, M. Kirby, A. Wheatley, G.E. Santyr, D.G. McCormack, G.B. Rodrigues, G. Parraga and L. Mathew. (2012) Hyperpolarized ^3He and ^{129}Xe Magnetic Resonance Imaging of Radiation-induced Lung Injury. American Thoracic Society, San Francisco, California, USA. May 21, 2012
- **N. Kanhere**, M. Kirby, A. Wheatley, A. Ouriadov, G.E. Santyr, D.G. McCormack, and G. Parraga. (2012) Reproducibility of Hyperpolarized ^{129}Xe Magnetic Resonance Functional Imaging of Chronic Obstructive Pulmonary Disease. International Society for Magnetic Resonance in Medicine, Melbourne, Australia. May 8, 2012
- **N. Kanhere**, M. Kirby, A. Wheatley, A. Ouriadov, G.E. Santyr, D.G. McCormack, and G. Parraga. (2012) Reproducibility of Hyperpolarized ^{129}Xe Magnetic Resonance Functional Imaging of Chronic Obstructive Pulmonary Disease. 10th Imaging Network Ontario Symposium Toronto, Canada. February 13,14 2012
- **N. Kanhere**, M. Kirby, A. Wheatley, A. Ouriadov, G.E. Santyr, D.G. McCormack, and G. Parraga. (2012) Reproducibility of Hyperpolarized ^{129}Xe Magnetic Resonance Functional Imaging of Chronic Obstructive Pulmonary Disease. London Health Research Day, London, Canada. March 20, 2012
- **N. Kanhere**, M. Kirby, A. Wheatley, A. Ouriadov, G.E. Santyr, D.G. McCormack, and G. Parraga. (2012) Reproducibility of Hyperpolarized ^{129}Xe Magnetic Resonance Functional Imaging of Chronic Obstructive Pulmonary Disease. 7th Annual London Imaging Discovery Day, London, Canada, June 27,2012

- **N. Kanhere**, S. Ingle, A. Bhatewara, K. Patil. (2010) Number plate recognition using Artificial Neural Networks. Sinhgad Institute of Technology, Pune, India. April 12, 2010

C. Invited Presentations

- M. Kirby, D. Pike, S. Svenningsen, **N. Kanhere**, A. Wheatley, N.A. Paterson, D.G. McCormack, H.O. Coxson and G. Parraga. (2013) Hyperpolarized Helium-3 Magnetic Resonance Imaging Phenotypes of Chronic Obstructive Pulmonary Disease: Relationship to Exacerbations. American Thoracic Society, Philadelphia, Pennsylvania, USA May 13, 2013

Honours and Awards:

- Queen Elizabeth II Graduate Scholarship in Science and Technology (QEIGSST) May 2012 - April 2013
\$15,000 CAD over three semesters of Graduate school
- ISMRM (International Society for Magnetic Resonance in Medicine) Trainee (Educational) Stipend for the 2012 meeting in Melbourne, Australia. May 4-11, 2012
Awarded to support the attendance of students, postdoctoral and clinical trainees to present abstracts at the scientific meeting
\$540 USD
- Western Graduate Research Scholarship- Full tuition waiver (\$6725/year) for two years, Western University, Canada, September 2011
Awarded to graduate students entering the program with an average more than 78%
- “Best Research and Development Project” in a competition held at Vishwakarma Institute of Information Technology, Pune, India for the final year engineering project, March 2010
Chosen as the best project from among 80 projects
 - Only group from the class to receive direct funding from the University of Pune, India for our final year project. Equivalent to \$1000 for one year, August 2009